Nuclear Factor Dynamics: Regulation of Gene Expression by Nuclear Targeting of P-TEFb

Lana Bosanac

▶ **To cite this version:**

Lana Bosanac. Nuclear Factor Dynamics: Regulation of Gene Expression by Nuclear Targeting of P-TEFb. Biophysics. Ecole Normale Supérieure de Paris - ENS Paris, 2010. English. NNT : . tel-00699906

HAL Id: tel-00699906
https://theses.hal.science/tel-00699906

Submitted on 22 May 2012

HAL is a multi-disciplinary open access archive for the deposit and dissemination of scientific research documents, whether they are published or not. The documents may come from teaching and research institutions in France or abroad, or from public or private research centers.

L'archive ouverte pluridisciplinaire **HAL**, est destinée au dépôt et à la diffusion de documents scientifiques de niveau recherche, publiés ou non, émanant des établissements d'enseignement et de recherche français ou étrangers, des laboratoires publics ou privés.

Preface

This manuscript has been written to document my research work as a doctoral candidate in the Functional Imaging of Transcription team at the Laboratory of Molecular Biology at the Ecole Normale Superiore in Paris, during the period from October 2007 to October 2010.
The teams research activities are the investigating of transcriptional processes by live cell microscopy.
The research presented in this thesis concerns the an interdisciplinary field that requires joint efforts of scientists with backgrounds in biology, physics and mathematics. The objective of the project is to explore the nature of dynamics of general transcription factor P-TEFb with respect to its distribution and target search. Challenges involve theoretical, experimental, and technical aspects.
Financial support for the duration of the thesis was insured by CNRS on the basis of funding provided by the French Ministry of Research.

Acknowledgements

I would like to express my gratitude to everyone at the Laboratory of Molecular Genetics at ENS for welcoming me and having me here for the last three years. A special thanks to Francois Taddei, Ariel Lindner and all staff and members of my doctoral school, the Frontieres du Vivant, for making the uttermost efforts in interdisciplinarity and being more than a doctoral school.
I wish to express my deepest and sincere gratitude to my supervisor Xavier Darzacq. for his contagious enthusiasm and inspiration, and never failing interest in discussing and commenting on research directions. Also, a big thank you to Olivier Bensaude for endless optimism, his invaluable advice and support throughout the thesis. I extend my gratitude to Robert Tjian for external tutorship and making it possible to present my work at the Janelia Farm research campus on several occasions.
I would like to thank the examiners, Bernard Vandenbunder and Arnaud Poterzman for reading my manuscript in such a short notice. I sincerely thank Olivier Bensaude, Francois Taddei, Robert Tjian and Raphael Voiturier for kindly accepting to be jury members at my thesis defense.
A special thanks also to Brigitte Arnaud, Martine Duponchelle, Laura Ciriani and Marline Francis for their help with solving the maze of French administration.
I thank my colleagues and friends at the lab, for providing a positive and stimulating work environment; and making me look forward to each day in the lab: Sebastien Causse, Ibrahim Cisse, Lydia Boudarene, Benjamin Mathieu, Thibault Moresee, Ignacio Izzeddin, Davide Normanno, Nina Verstraete, Claire Darzacq, Adrien Senecal, Emilie Lagoutte, Olivier Collin, Vera Ruda, Vincent Recamier and Florence Proux. Especially to Seb, Ibra, for mentoring me on science and human relations within, and to Benjamin and Lydia for their unselfish help. A special thanks to Claire Darzacq for the crash course on Western blots; to Corentin Spriet and Laurent Helliot for the workshop on FLIM. A thanks to Maxime Dahan and his lab who welcomed me at the beginning of my stay. I also wish to thank all members of the Janelia Farm Consortium for eye-opening discussions. Thank you all again. It has been a pleasure.

A big thanks to the very special people outside the lab: Maja Petković, Katlin Silm and Milan Djilas. Thank you for the comradeship and friendship.

Lastly, and most importantly, I would like to thank to my family, my father Miroslav, my mother Zdravka and my sister Rosana for their excessive love and support. To them I dedicate this thesis.

Abstract

Proteins engaged in macromolecular complexes interacting with chromatin move throughout the nucleus by diffusive processes, transiently and repetitively contacting their target sites. Diffusion and interactions play important roles in gene expression by defining the target gene search time.
In the work presented in this thesis we monitored the mobility of the Positive Transcription Elongation factor b (P-TEFb) responsible for the phosphorylation of the RNA polymerase II C-terminal domain and showed that its relatively high mobility is regulated by the 7SK small nuclear ribonucleoprotein complex (7SK snRNP). Without the 7SK regulating complex, transient interactions of the P-TEFb cycline T1 component with RNA polymerase II prevent the nuclear distribution of the elongation factor therefore restricting its activity to sites of high polymerase concentration and limiting its recruitment to new sites. This observation demonstrates that the fast mobility of proteins required for the stochastic assembly of nuclear molecular machines is not only a physical property of macromolecules but a biophysical parameter tightly controlled by cellular regulators.

Contents

I Introduction **1**

II Nuclear Dynamics **4**

1 Live Cell Imaging and Fluorescence Microscopy **4**
1.1 Quenching and Photobleaching 6
1.2 FRET: Fluorescent Resonance Energy Transfer 6
1.2.1 FLIM: Fluorescence Lifetime Imaging Microscopy 8

2 FRAP : Fluorescence Recovery After Photobleaching **9**
2.1 FRAP Analysis 10
2.1.1 Diffusion-uncoupled FRAP recoveries 14
2.1.2 Diffusion-coupled FRAP recoveries 14
2.1.3 Addressing Binding: Gene Arrays 17
2.1.4 Modelling of FRAP Recoveries by Differential Equations 19
2.2 FLIP: Fluorescence Loss in Photobleaching 23

3 Single Molecule Dynamics **24**
3.1 Localization of Single Molecules 24
3.2 STORM and PALM 27
3.3 Single Molecule Tracking 28

4 Kinetic Analysis **32**
4.0.1 Kinetic imaging techniques 32
4.0.2 Compact vs. non-Compact modes of movement 33

III P-TEFb **38**

5 The P-TEFb Complex **38**
5.1 Sequestering in the large complex 39
5.2 P-TEFb - PolII interaction 43

6 The biochemistry of P-TEFb role in transcription elongation **44**
6.1 Promoter-proximal Pausing of the RNA Pol II: the essence of gene regulation for most protein-transcribing genes 45
6.2 Role of P-TEFb in RNA Processing 47

7 Physiological modulations of P-TEFb activity **48**
7.1 Phosphorylation 49
7.2 Acetylation 49

7.3 P-TEFb specificity . . . 50
7.4 P-TEFb regulation in cell cycle . . . 51

8 Inhibition of P-TEFb activity: Concentration speculations 53
8.1 Flavopiridol . . . 53

9 Brd4 recruits P-TEFb to cellular genes 53

10 Clinical Implications of P-TEFb as a target molecule 54
10.1 Oncology . . . 55
10.2 Virology . . . 56
10.3 Tat recruits P-TEFb to the TAR element in HIV transcription . . . 57
10.4 Cardiology . . . 58

IV Nuclear Targeting of P-TEFb: Results and Discussion 60

11 The mobility of P-TEFb ensemble molecules 62
11.1 Fluorescence Recovery After Photobleaching . . . 62
11.1.1 Quantifying the FRAP . . . 63
11.2 Addressing Binding . . . 64
11.3 Fluorescence Loss in Photobleaching . . . 67
11.3.1 Saturation of System . . . 71

12 Probing Interaction Partner RNA Pol II 73
12.1 Probing the interaction by FLIM . . . 76
12.2 Eliminating the Substrate . . . 79
12.3 Testing of binding-defective mutants . . . 80

13 P-TEFb Single Molecule Dynamics 82
13.1 Single Molecule Analysis . . . 83
13.2 Error Calculations . . . 86

V Modelling of the Biological System 87

14 Differential Equations 87

15 Compact vs. Non-Compact Modes of Movement 89
15.1 Finding the diffusion constant of P-TEFb . . . 90

VI Summary and Discussion 95

16 Controlled Diffusion Mechanisms 95

17 P-TEFb's interaction with PolII **98**

18 Parameterization of Dynamics **99**

19 Conclusions, Considerations and Perspectives **100**

VII Materials and Methods **102**

20 Cell Culture **102**
20.1 Splitting cells . . . 102
20.1.1 Splitting cells on coverslips . . . 102
20.2 Transfections . . . 102
20.2.1 Transient . . . 102
20.2.2 Stable Cell lines . . . 103
20.2.3 RNA Interference . . . 103
20.2.4 Freezing Cells . . . 104
20.2.5 Defreezing Cells . . . 104

21 Bench works **104**
21.1 Fixing Cells . . . 104
21.2 Immunofluorescence . . . 104
21.3 Western Blot . . . 105
21.4 Midi-preps . . . 106

22 Technical setup **107**
22.1 FRAP setup . . . 107
22.2 PALM setup . . . 107
22.3 FLIM Imaging . . . 108

23 Data Analysis **109**

VIII Bibliography **110**

IX Appendix **124**

24 FLIP Imaging, Normalization and Background **124**
24.1 Method of Accumulation Factor Measurement . . . 124

25 Controls **124**
25.1 Overexpression Cell lines without DRB . . . 125
25.2 Truncation CycT1 FLIP Experiments with out DRB . . . 125

26 Error Estimations **125**

27 Artefacts **128**

Part I

Introduction

A systemic definition of life is that living things are self-organizing and autopoietic (i.e. self-producing). An oversimplification of what life really is, for both of these functions, as well as for the sake of capacity to build more complex and robust systems, it is necessary to have a process that enables the storage of information as well as its readout. The storing of information is effectively made by DNA which uses the combination of 4 different bases to code for different amino acids that are then able to produce proteins to fulfill all necessary cellular functions for survival. Storing of information is useless unless this information can be actively used to fullfill necessary functions of the living entity. This readout of the stored information is called transcription. Specifically, transcription is the process by which DNA is read out into template RNA molecules, which then are transported out into the cytoplasm and used to produce proteins by the process of translation.

As the kernel of all living things, the study of the genome on molecular basis gives rise to immense complexity when attempting to describe a final living organism by in its terms. Therefore, [BRENNER2010] proposes the cell as the correct level of abstraction for "the solving of forward problems of computing the behavior of the system from its components and their interactions." Considering the cell as the object for the study of living things, the topic of gene expression seems central. Gene expression determines a cell's survival, growth, division, differentiation or apoptosis. Gene expression is highly organized and controlled process which gives the cell the capacity to control it's fate. Whether the protein will be transcribed and its quantity is actively controlled by the cell at several steps. Evolutionary theories suggest that expression levels of proteins are calibrated to maximize fitness [ELENA2003, ORR2005, IBARRA2002, HARTWELL1999, ROSEN1967, SAVAGEAU1976, HARTL1997, HEINRICH1996, MAYNARD1997, HARTL1984 AND LIEBERMEISTER2004]. [ALON2005] showed in a simple E.Coli Lac system that protein expression is indeed a result of cost-benefit optimization, (while mutations allow rapid tuning by evolution to function optimally in new environments). Even though this is a simplified system, one can assume same trends of cost-benefit behaviour with more complex organisms. Specifically, a robust and precise system needs extensive transcriptional control that will precisely calibrate the production of each single protein coded for on a temporal and quantitative basis. This gene regulation gives cells the ability to respond to extra and intracellular stimuli participating in cell cycle, growth, differentiation and survival; and is tightly regulated by transcription factors.

Since the discovery of the first transcription factor, the field of gene regulation gained a lot of popularity, being of central importance to all living organisms for function and development. Whether the cell submits to differentiation or guards its pluripotency depends on the transcription of the genes in question. Likewise, falsely regulated tran-

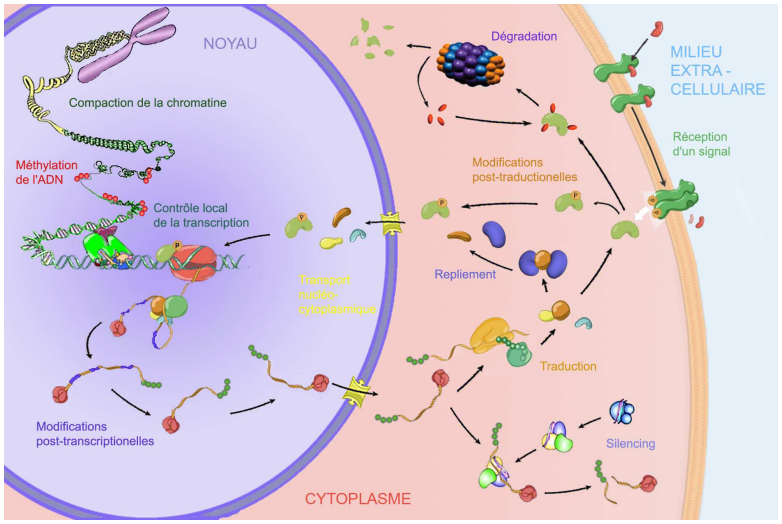

Figure 1: **Transcription Processes in the Cell**Diagram portraying transcriptional mechanisms, from local controls of transcription to modification of the genomic environment, post-transcriptional modifications of RNA and translational control by silencing and degradation. Source unknown.

scriptional processes lead to developmental faults, autoimmune diseases, cancers, and disfunctions of the organism.

Historically, the study of gene regulation was initiated late 1950s/early 1960s by Francois Jacob and Jacques Monod on lactose metabolism genes. Providing E.Coli with lactose causes induction of three proteins not present in the bacterial cell under usual conditions. This demonstrated the plasticity of gene expression as a mode of survival for the organism and highlighted its importance for survival.

Discovery of general and specific transcription factors led to queries of mechanisms of target search, complex biochemical cascades etc. In eukaryotes, gene regulation occurs at the level of transcription of specific mRNAs by RNA PolII in several phases: pre-initiation, initiation, promoter clearance, elongation, RNA processing and termination [MARGARITIS2008, SAUNDERS2006, SIMS2004]. The transcription of eukaryotic genes finds its critical control mechanism at the elongation step [SAUNDERS2006, NECHAEV2008, PRICE2008]. The elongation step itself is initiated and controlled by phosphorylation of the C-terminal domain (CTD) at the Rpb1 subunit of RNA Pol II, performed by the positive transcription elongation factor b (P-TEFb), which thereby poses as the hallmark of elongation.

Biochemical essays continue to give insight into gene regulation by conducting experiments in vitro. Although yielding useful information about reaction mechanisms and interactions between molecules running transcriptional processes, the test tube environment differs with a high degree from the environment in vivo, and the results obtained herewith are to be taken into account with reserve. With the technology today, we are able to probe transcriptional mechanisms in vivo by direct observation in the live cell. Live cell imaging provides us with methods to probe spatial organizations,

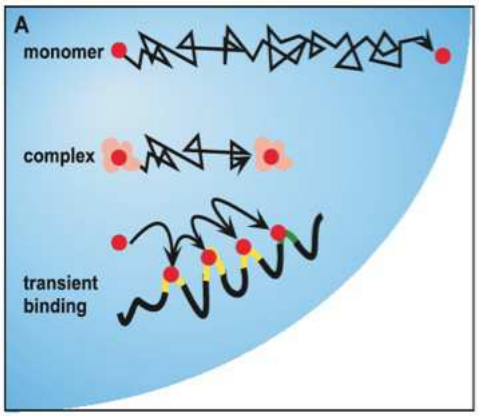

Figure 2: **Nuclear dynamics** A nuclear protein modifies it's mobility by sequestering into complexes and binding with intrinsically high turnover rates [MISTELLI2001]

colocalizations, interactions, and most importantly dynamics of the processes underlying transcription.
Transcription factors move throughout the nucleus by the simple process of diffusion. Diffusive properties of molecules are modified by their sequestering into complexes or binding to substrates. These processes macroscopically seem to have a stochastic nature, since there is no directionality in the movement, ad weak and transient interactions are ubiquitous. Considering this stochasticity and the perpetually dynamic environment of the nucleus, in the present thesis we pose the query of distribution and target search of the general and crucial transcription factor P-TEFb.

We use the methods of fluorescent microscopy to address questions of localization, interaction and mobility of the transcription factor in its natural environment. By manipulation with drugs, and binding defective mutants, we are able to take conclusions about the substrates of P-TEFb, it's motion profiles, and most importantly, develop a theory by which it is able to control gene expression by modification of its diffusive properties.

Part II

Nuclear Dynamics

The nucleus is a dynamically organized perpetually changing ensemble of molecular interactions that are always in exchange. Proteins move in the nucleus by passive diffusion and molecular interactions have characteristically high turnover rates. Nuclear compartments are stable, dynamic steady-state protein aggregates which are held together and organized by association and dissociation of the residents of the nucleoplasmic space. Immobile fractions are low.
In this scenario, naturally the mobility rates of single proteins plays a key role in determining the search time required for it to reach its target amid a spectrum of other binding sites. A key problematics set to a general transcription factor in the nucleus is maintenance of it's ubiquitousness which enables replenishment, or activation of new target sites - but at the same time it's efficient docking and function at these.
Modern live cell imaging has opened a new era of cellular biology, providing us with the possibility of addressing this question. Using fluorescent microscopy in combination with transfected fluorescent proteins, it is possible to study localization of specific molecules inside the cell, visualize cellular structures and their movements in real time. Most importantly, it is possible to determine the properties of transcription, the kinetics of transcription factor movement, their binding and residence times at target sites in the nucleoplasm.
With new advances, it has become feasible to analyze and identify component processes that make up transcription, and even assign rate constants to the underlying processes. disassembly this data, one can find the life times of complexes and determine the efficiency of the process they take part in.
Nuclear dynamics by fluorescent microscopy contributes with information that is not obtainable by chromatin immunoprecipitation, microarray studies, or other bulk assays - this one can resolve events in single cells. Different approaches of live cell imaging are numerous, and include FRAP, FCS, FRET and single molecule tracking.
The following sections will provide an insight in the listed live cell imaging methods and their advantages, present the model system of artificial gene arrays and give insight into the analysis of imaging data.

1 Live Cell Imaging and Fluorescence Microscopy

The nucleus is governed by short residence times, stochastic formation of complexes, anomalous diffusion and continuous assembly and disassembly of transcription factors. This sets high requirements to the imaging machinery. Indeed, real-time visualization and quantification of transcription and other cellular processes has become possible only in the last decade. Some of the advances that made this possible are the

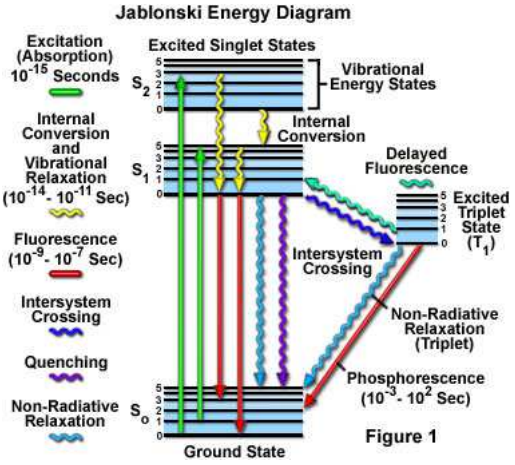

Figure 3: **Fluorescence Mechanisms** Jablonski energy diagram portraying mechanisms of fluorescence excitation and emission [www.olympusfluoview.com]

shift from film to digital photography, the increase in speed of computers and their storage capacity (which enable recording at speeds comparable to biological trafficking events, as well as speedy deconvolution algorithms and 3D reconstruction of images by PSF fitting); tunable filters allowing readout of entire spectral bandwidths; enabling the combinatorial use of many more dyes/fluorophores, EMCCDs with extremely sensitive signal detection and STORM which enabled imaging with resolution below the diffraction limit [SHAV-TAL2004]. The borders of both temporal and spatial resolution are being pushed consistently, and techniques such as photo-activation, photo-conversion and Stroboscopic illumination, promise real-time single -molecule measurements of nuclear kinetics.

An essential point in live cell imaging is knowing how to isolate the molecule of study in order to observe it. This has been done before by radioactive labeling of the molecules of interest, microinjection of proteins on quantum dots, etc.. Imaging of biological processes in vivo has been revolutionized with the discovery of fluorescent tags.

Fluorescence is the property of some atoms and molecules to absorb light at a particular wavelength and to subsequently emit light of longer wavelength after a brief interval, termed the fluorescence lifetime. The manifestation of the interaction between light and matter forms the basis for the expansive field technique of fluorescence microscopy which is rapidly becoming an important tool in genetics and cell biology.

The breakthrough in single cell studies came with the discovery of green fluorescent protein, a protein composed of 238 amino acids (26.9kDa), which exhibits bright green fluorescence when exposed to blue light. GFP was initially isolated from the jellyfish Aequorea victoria. Its use in cell research led to the awarding of the Nobel Prize in Chemistry 2008 to Martin Chalfie, Osamu Shimomura, and Roger Y. Tsien. By knowing the genetic sequence of GFP, one is able to construct combinatory DNA plasmids which upon transfection use the cell's transcriptional machinery to produce fluorescent fusion

proteins and thereby enable visualization of the molecule in vivo [SHANER2005].
Observations from time-lapse studies with fluorophores typically show the steady-state distribution of a protein. In image sampling, long exposure times enable the acquisition of images which enable differentiation between stationary and moving molecules by differences in sampling. Tracking of individual molecules is possible using stroboscopic excitation. However, this technique does not directly provide information about kinetic properties of the system. Two characteristics of fluorophores are photobleaching and energy transfer under certain conditions, both of which can be used as an advantage in controlled experiments to analyze the kinetics and interactions respectively of the system under study.

1.1 Quenching and Photobleaching

Excessive or prolonged exposure of a fluorophore to irradiation leads to an effective reduction in its amount of emission. This is exposed by either the process of quenching or photobleaching. The first is often reversible whereas the latter is not. The average number of excitation and emission cycles that occur for a particular fluorophore before photobleaching is dependent upon the molecular structure and the local environment. Some fluorophores bleach quickly after emitting only a few photons, while others that are more robust can undergo thousands or millions of cycles before bleaching.
Photobleaching is usually a negative connotation, and efforts are made to reduce it by limiting the exposure time or lowering excitation energies, both of which also reduce the signal to noise ratio. However, under certain circumstances photobleaching can be utilized to obtain information about the system as in the method of fluorescence recovery after photobleaching (FRAP) where a targeted area inside a fluorophore field is intentionally bleached using excessive levels of irradiation. After the bleach, surrounding fluorophores diffuse back into the targeted area, which recovery can be quantitatively measured, yielding diffusion rates of the fluorophore.

1.2 FRET: Fluorescent Resonance Energy Transfer

A fluorophore in the excited state can lose excitation energy by conversion to light (fluorescence), through thermal equilibration (vibrational relaxation) or by transfer of energy to another molecule through collision or complex formation (non-radiative dissipation and quenching). When forming a complex or colliding with a solvent molecule, energy is transferred by the coupling of electronic orbitals between the fluorophore and colliding molecule.
In the case of resonance energy transfer, a fluorophore in the excited state (the donor) may transfer its excitation energy to a neighboring chromophore (the acceptor) nonradiatively through the long range dipole-dipole interactions over nanometer distances. The theory behind resonance energy transfer assumes the donor fluorophore acts as an

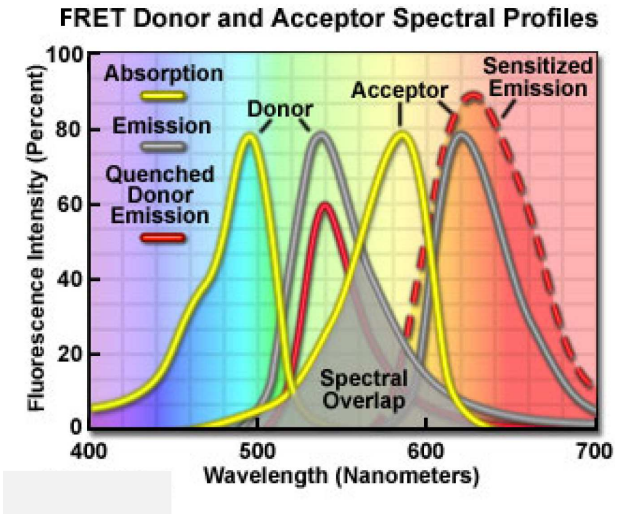

Figure 4: **Fluorescent Resonance Energy Transfer** FRET diagram showing donor and acceptor spectral profiles: Overlap (grey area) between the donor emission (central gray curve) and acceptor absorption spectra (central yellow curve) is required for the process to occur. When this overlap is present, and the donor and acceptor are separated by less than 10 nanometers, donor excitation energy can be transferred non-radiatively to the acceptor. The net result is quenching of the donor fluorescence emission (red curve) and an increase in the emission intensity of the acceptor (sensitized emission, red dashed curve). [http://micro.magnet.fsu.edu]

oscillating dipole that transfers energy to a similar dipole at a particular resonance frequency in a manner analogous to the behaviour of coupled oscillators.
FRET is possible whenever the emission spectrum of the donor overlaps the absorption spectrum of the acceptor (which itself might not be fluorescent). The transfer of energy manifests itself by quenching the donor emission in the presence of the acceptor and increased (sensitized) emission of acceptor fluorescence.

Efficiency of resonance energy transfer varies with the degree of spectral overlap, but most importantly as the inverse of the sixth power of the distance separating the donor and acceptor chromophores. Energy transfer to the acceptor requires the distance between the chromophores to be relatively close, within the limiting boundaries of 1-10 nanometers. The phenomenon can be detected by exciting a labeled specimen with illumination wavelengths corresponding to the absorption (excitation) maximum of the donor and detecting fluorescence emission in the peak emission wavelength region of the acceptor. Alternatively, the fluorescence lifetime of the donor can be measured in the presence and absence of the acceptor. The dependence of energy transfer efficiency on the separation distance between the donor and acceptor provides the basis for the utility of resonance energy transfer in the study of cell biology. This facet of resonance energy transfer enables the technique to be used as a spectroscopic ruler to study and quantify interactions between cellular components, as well as conformational changes within individual macromolecules, at the molecular level.
Branches of FRET, such as FLIM, exist, which render better quantification of interactions in live cells by measuring their differences in lifetime.

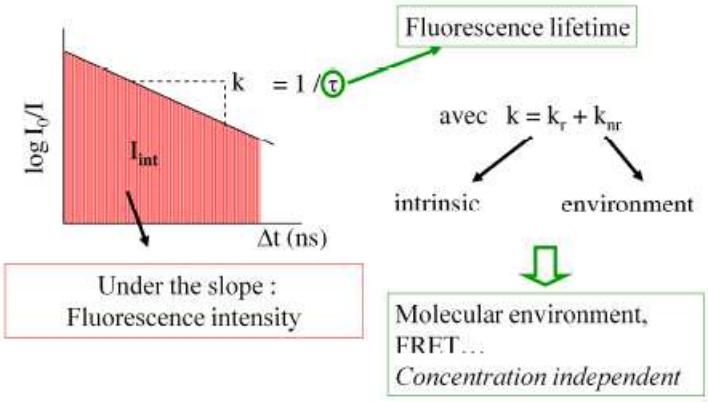

Figure 5: **FLIM Measurement** The area under the slope gives the total photon number corresponding to the intensity. From the slope itself, the fluorescence lifetime can be extracted. It is composed of several elements: the first is an intrinsic parameter of the fluorophore. This value can be altered by the local environment such as ion concentration or a FRET event, resulting in a decrease of the total fluorescence lifetime. Courtesy of Corentin Spriet.

1.2.1 FLIM: Fluorescence Lifetime Imaging Microscopy

All fluorophores have their own characteristic lifetimes in the excited state. Differences in lifetime can be used to distinguish colors of fluorophores, and identify autofluorescence. Ordinary fluorophores have lifetimes of the nanosecond order. The factors affecting the fluorescence lifetime include ion intensity, hydrophobic properties, oxygen concentration, molecular binding, and molecular interaction by energy transfer when two proteins approach each other. Lifetime is, independent of fluorophore concentration, photobleaching, light scattering and excitation light intensity. Therefore, fluorescence lifetime imaging allows accurate ion concentration measurements and FRET analysis.
The general method of FLIM (fluorescence lifetime imaging) involves the measurement of the lifetime in nanoseconds by a laser with a pulse duration of a few hundred picoseconds and a nanosecond level shutter. In some cases of delay after excitation by a pulse laser, the fluorescence image can be obtained by the gate operation of the image intensifier or by measuring while varying the delay time until a gate opens.
Probing interactions of a fluorophore, one uses the fact that a donor has shorter excitation/emission wavelengths that provide energy to an acceptor. The lifetime of the excitation state of the donor is variable depending on whether or not the acceptor interaction exists. Measurement based on lifetime permits better quantification because it is not necessary to consider the overlap of fluorescence during detection.
A theoretical FLIM measurement is shown in (Figure 5). The recorded graph of intensity vs. time for the decay of fluorescence can be used to obtain the total number of photons emitted corresponding to the intensity under the slope. The slope of the graph itself is used to measure the fluorescence lifetime by fitting to exponentials.

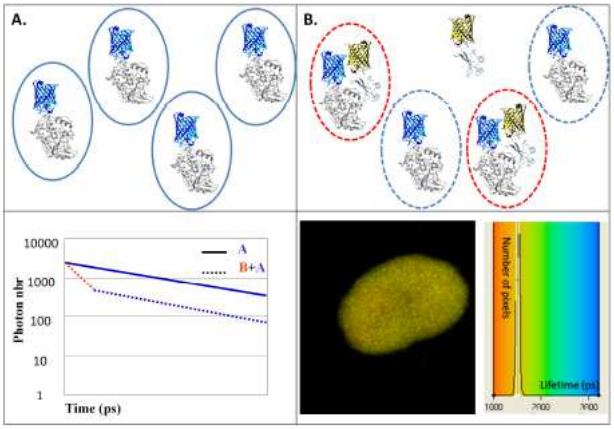

Figure 6: **Lifetime applied to FRET measurements** In (A), one gets only single species corresponding in the easiest cases on a mono-exponential decay. If there is a mix of interacting and noninteracting molecules, the same slope as in A plus shorter lifetime will be obtained (shown in red). This measurement can be performed on a whole image. It is then possible to measure a mean lifetime for each pixel and obtain a map of short lifetime components. In the example shown, corresponding to Jun/Fos interaction studies, the lifetime of the donor alone was measured to be 2.5ns. Here a lifetime of 1.5ns is obtained in the whole nucleus, corresponding to a strong and homogeneous interaction of the two molecules. In this case, the longer the wavelength, the shorter the lifetime of the complex, - the stronger the interaction Courtesy of Corentin Spriet.

2 FRAP : Fluorescence Recovery After Photobleaching

Although photobleaching usually is considered a disadvantage of fluorophores setting finalizement on the length of acquisition time and illumination strength for higher signal, intentional photobleaching in a carefully planned experiment can yield information about the kinetics of the system under study. With photobleaching techniques, it is possible today not only to investigate the localization and accumulation of fluorescently tagged molecules and their dynamic intracellular localization (e.g. using confocal time-lapse imaging) but also investigate their dynamics in living cells to obtain quantitative information.

FRAP [POO1974, LIEBMAN1974, EDIDIN1976, AXELROD1976] is used to measure the temporal dynamics of fluorescently tagged molecules. In this technique, a small spot is photo-bleached by a brief exposure to an intense focused laser beam, causing the permanent loss of fluorescence of the molecules affected. The technique was developed in the 1970s by Axelrod and colleagues [AXELROD1976] in order to measure rates of lateral transport of proteins and lipids in cell membranes [POO1974, PETERS1974, EDIDIN1976, ZAGYANSKY1976, JACOBSON1976, SCHLESSINGER1976]; and has since then made great progress with the discovery of GFP. Today, FRAP can be conducted with a confocal as well as wide-field microscope and yield information on three mobility parameters: the diffusion coefficient, immobile fractionS, and the residence times of the molecule spent in the immobile state.

With the assumption of elementary binding kinetics, the size of the immobile fraction and the duration of immobilization can be determined by the on and off-rates of the

fusion protein to and from relatively immobile complexes or DNA. In the case where the system is diffusion unlimited, a diffusion coefficient and the immobile fraction, as well as a residence time in the immobile state can be derived from the recovery curves. Likewise, it is possible to describe the dynamic binding and release from immobile complexes in terms of immobilization rate k_{on} and release rate k_{off} [VAN ROYEN2008]. Then,

$$\frac{k_{on}}{k_{off}} = \frac{mobile_fraction}{immobile_fraction}$$

and the residence time is given by:

$$\tau_r = \frac{1}{k_{off}}$$

Variations of FRAP can be employed each according to its own advantages in the experimental conditions. There are several different variants of FRAP: spot FRAP, strip FRAP, FLIP and inverse FRAP. Each has their own advantages as shown in (Table 1).
Initial FRAP studies of nuclear proteins found unexpectedly high mobilities of many

Table 1: Types of FRAP experiments

FRAP type	**Conditions/Advantages**
spot FRAP	classic
strip FRAP	increased resolution at low transfection
half cell bleach	additional binding sensitivity
inverse FRAP	monitoring export from area of interest
FLIP	monitoring fluorescence dynamics in areas other than within FRAP bleach

nuclear factors, (i.e. the glucocorticoid receptor, [MCNALLY2000]). Since, many studies revealed the kinetics of nuclear factors to be governed by diffusion. This enables the analysis of FRAP curves with differential equations, as shown in the section below.

2.1 FRAP Analysis

The significance of FRAP data can be estimated by a qualitative analysis, summed up in the following points:

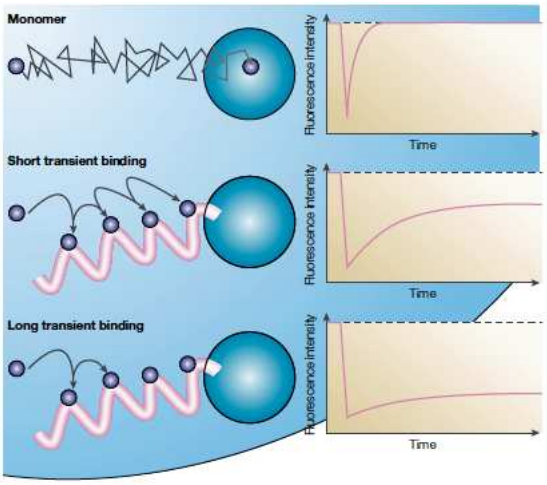

Figure 7: **FRAP Recoveries resulting from diffusion and binding** Cartoon depicting FRAP recovery curves in different scenarios of freely diffusing fluorophores, transient binding and long-term immobilization [PHAIR2001]

- Intensities can be expressed relative to the average of a sufficient number of measurements before bleaching:

$$I(prebleach) : I(norm, t) = (I(t) - I(bkg))/(I(prebleach) - I(bkg))$$

- $$I(norm, t) = (I(t) - I(0))/(I(pre) - I(0))$$

  ; this way of normalization enables the quick visual estimation of the size of a potentially present immobilized fraction

- - intensity values relative to fluorescence after complete recovery $(I(inf))$ and the intensity directly after bleaching $(I(0))$:

$$I(norm, t) = (I(t) - I(0))/(I(inf) - I(0))$$

- Combined flipfrap data can be analyzed by first calculating the fluorescence intensity difference between the flip region and the frap region:

$$I(flipraf p) = I(fliproi) - I(fraproi)$$

However, precise determination of the physical parameters governing the system under analysis is possible through a more elaborate quantitative analysis of the FRAP recovery curves. This analysis can involve both fitting experimental data to models from

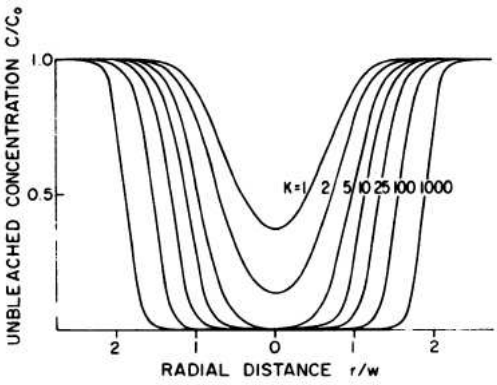

Figure 8: **Measurement of the laser profile** Normalized initial post-bleach florophore concentration $C(r,0)/C_0$ with a Gaussian beam of radius w at e^{-2} intensity for various values of the bleaching parameter K proportional to the bleach pulse energy [AXELROD1976]

1D diffusion [HOUSTMULLER1999, ELLENBERG1997] to 3D models incorporating many aspects of FRAP experiment [BLONK1993, BRAGA2004, 2007, SPRAGUE2005, 2004, BRAECKMANS2003, CARRERO2003], or a Monte Carlo simulation of diffusion of individual molecules; which takes time but is simple mathematically.
In order to apply the prior to a 2D diffusion, [AXELROD1976] applies the assumption of a Gaussian intensity profile laser beam. Then, for a one way bleach. i.e. concentration of bleached fluorophore; having a first order reaction with rate constant $\alpha I(r)$:

$$dC(r,t)/dt = -\alpha I(r)C(r,t)$$

where $I(r)$ is the bleaching intensity. For small bleaching pulse T, at $t = 0$,

$$C(r,0) = C_0 exp[-\alpha T I(r)]$$

where C_0 is the initial uniform fluorophore concentration. The amount of bleaching induced in time T is expressed by parameter $K = \alpha T I_0$.
For a Gaussian intensity profile, I(r) is given by

$$I(r) = (2P_0/\pi w^2) exp(-2r^2/w^2)$$

where w is the half width at e^-2 height, and P_0 is the total laser power. The differential equation for lateral transport of a single speices of fluorophore by diffusion with diffusion coefficient D is :

$$\delta C(r,t)/\delta t = D\nabla^2 C(r,t)$$

where the boundary condition is $C(\inf, t) = C_0$, and the initial condition $C(r,0)$ is given by the initial concentration of the fluorophore.
The fluorescence $F_K(t)$ observed at time $t >= 0$ is given by:

$$F_K(t) = (q/A) \int I(r) C_K(r,t) d^2 r$$

where $C_K(r,t)$ is the solution for the differential equation given for the K-dependent initial condition given by $C(r,0)$, parameter q the product of all the quantum efficiencies of light absorption, emission and detection and A is the attenuation factor of the beam during observation of recovery. Before the beginning of bleach,

$$F_K = qP_0C_0/A$$

The initial fluorescence $F_K(0)$ after bleaching depends on beam profile but not the mode of recovery:

$$F_K(0) = (qP_0C_0/A)K^{-1}(1-e^{-K})$$

for a Gaussian beam. Thus, the K value can be determined uniquely from its t=0 point. A convenient way of displaying fluorescence recovery curves is in fractional form f_K:

$$f_K(t) = [F_K(t) - F_K(0)]/[F_K(\inf)F_K(0)]]$$

The closed form solution is thus:

$$F_K(t) = (qP_0C_0/A)vK^{-v}\Gamma(v)P(2K|2v)$$

where $v = (1+2t/\theta_D)^{-1}$, $\theta_D = w^2/4D$, the "characteristic" diffusion time; and $\Gamma(v)$ is the gamma function. The χ^2-probability distribution P(2K—2v) is tabulated. This equation can be simplified into solutions for varying values of K.

- For large K ($K >= 4$ and $t/\tau_D >= 0.25$): $P(2K|2v)$ approaches one, such that this equation reduces to:

$$F_K(t) \sim rox(qP_0C_0/A)vK^{-v}\Gamma(v)$$

- A series solution for $F_K(t)$ valid for all K and t is:

$$F_K(t) = (qP_0C_0/A)\Sigma_{n=0}^{\inf}[(-K)^n/n!][1+n(1+2t/\tau_D)^{-1}]$$

- For $K << 1$, this assumes the simple form:

$$F_{K<<1}(t) = (P_0C_0/A)[1-K/2(1+t/\tau_D)]$$

The approach developed by [AXELROD1976] for simplified procedure for routine analyses of FRAP recoveries involves a three-point fit of the data, and is especially useful when the nature of transport and $F_K(\inf)$ are known. Here F and f represent an experimental recovery curve in arbitary units and in fractional form, respectively. $F_K(-)$ is the fluorescence before bleaching.

1. Determine time $\tau_{1/2}$ for which $f_K(\tau_{1/2}) = 1/2$
2. Assuming a Gaussian beam shape, determine $F_K(0)/F_K(-)$ and use the equation for $F_K(0)$ to calculate the bleaching parameter K

3. Calculate the mobility rate by the:

$$D = (w^2/4\tau_{1/2})\gamma_D)$$

where $\gamma_D = \tau_{1/2}/\tau_D$

Naturally, this case of analysis is also applicable for FRAP recoveries in the nucleus. However, the nucleus is dense with a lot of specific and unspecific interactions, attenuating diffusion. One can determine the strength of binding upon the comparison of the recovery curves of GFP-nls and the fusion protein. It is optimal to use same size proteins here, since size-dependent effects can arise such as temporary trapping of random movements of freely diffusing molecules [WACHSMUTH2000, ARRIO-DUPONT2000, SEKSEK1997]. Whether diffusion can be ignored depends on the relative magnitude of the diffusion time (time required for molecule to diffuse across bleach spot in absence of binding) and association rate (the on-rate of binding multiplied by the concentration of available bInding sites at equilibrium. $(1/k_{on})$ is the inverse of time required to begin binding. The relative magnitudes of these two parameters reflect the potential interplay between diffusion and binding and thus whether a FRAP recovery is diffusion coupled or uncoupled.

2.1.1 Diffusion-uncoupled FRAP recoveries

Here, diffusion time ¡¡ time to begin binding. Consequently recovery due to diffusion occurs first and due to binding follows later, resulting in a FRAP curve that is separable into two phases: the initial diffusive phase, then exchange at binding sites leading to the recovery of fluorescence due to bound molecules. The rate of recovery reflects the strength of binding, whereby slower recoveries correspond to tighter binding.
In the simplest case, diffusion uncoupled FRAP can be modelled as the inverse of an exponential decay, namely $1-Ae^{k_{off}t}$ [SPRAGUE2004, BELGAREH2001, BULINSKI2001], where A can be used to calculate the association rate [SPRAGUE2004].
The next simplest case is the one with two independent binding states, in which case two exponential terms are employed, and an association and dissociation rate for both can be determined [SPRAGUE2004]. However, one needs to be careful here since it is possible to fit two exponentials to many diffusion coupled frap recoveries. A more complex situation arises with multiple binding states with interdependent binding. In this case, a set of ordinary differential equations describes the binding interactions and can be solved numerically [PRESLEY2002, DUNDR2002] and fitted to FRAP data by various techniques [PHAIR2004, SLEPCHENKO2003].

2.1.2 Diffusion-coupled FRAP recoveries

In diffusion-coupled FRAP recoveries, the diffusion time is either slower or comparable to the time for the molecule to associate with a binding site. Since diffusion and

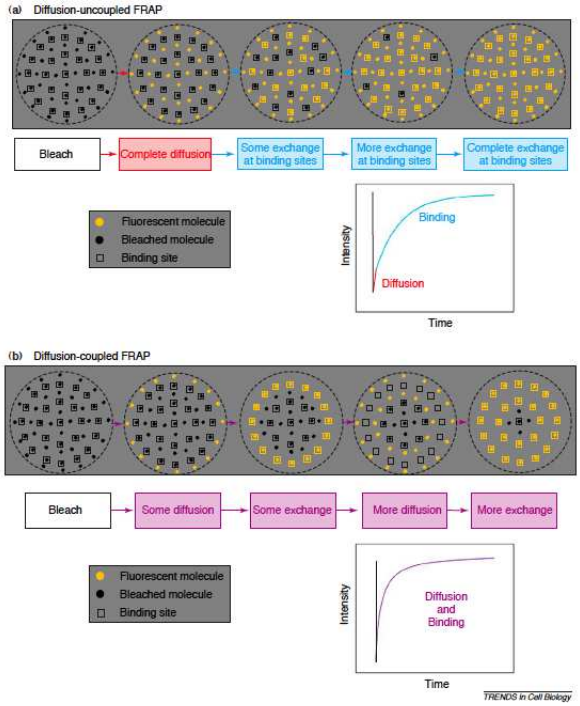

Figure 9: **Cartoon explaining diffusion coupled and diffusion uncoupled FRAP behaviour** [SPRAGUE2005]

binding are intermixed, the recovery cannot be separated into two phases. The time for complete recovery in a diffusion-coupled scheme is determined by both the association rate and the off-rate at each binding step. Based on estimates of cellular binding and diffusion rates, it seems that diffusion coupled FRAP is likely to be more common than currently appreciated [SPRAGUE2004].
Analysis of diffusion-coupled recoveries is made by estimation of diffusive behaviour of the molecule and superimposing the binding interactions subsequently. The diffusive behaviour is estimated by solving differential equations for FRAP recoveries as in the case of [AXELROD1976].
Several other factors that influence the diffusion of molecules into the bleached zone become important in the diffusion coupled FRAP. Assumptions have to be taken into account:

- Instantaneous bleach leading cylindrical bleach pattern
- Homogeneous distribution of binding sites that are immobile during recovery
- Bleach at a reasonable distance from cellular boundaries [SPRAGUE2005]

An important simplification can arise that enables direct fitting of the recovery curves: when the time to associate with a binding site is much faster than the time required to diffuse, then a diffusion coupled frap recovery exactly mimics diffusion but at a slower rate determined by the strength of binding [SPRAGUE2004, CRANK1975, ELSON1979, KAUFMAN1990]. In this case, the recovery can be fitted by just the diffusion equation and [AXELROD1976] theory applies.
These solutions yield an effective diffusion constant, D_{eff}, which is smaller than the cellular D. Thus, binding parameters could be determined by computing $D/D_{eff} - 1$. This type of diffusion is estimated to occur in one third of biological FRAP experiments where binding interactions are present [SPRAGUE2004]. It can be distinguished from pure diffusion because the FRAP recovery curve will be noticeable slower than that of unconjugated GRP, but will still be fitted by a pure diffusion model. Two important constraints to consider when applying the effective diffusion model is that it does not permit independent estimates of the association and dissociation rates, but only their ratio. Also, it is impossible to determine the number of binding states since the same FRAP curve arises from one, two, three or more binding states as long as the sum of the ratios of the individual association rates to dissociation rates is the same. I.e. FRAP fitted to effective diffusion yields a predicted ratio of association rates to dissociation rates that might reflect either a single binding state or the sum of several states.
A more complicated diffusion-coupled scheme arises when the diffusion time is comparable to the association time. Predicted FRAP recoveries for this type of situation have been calculated for circular [SPRAGUE2004] bleach spots. These equations can be used when the effective diffusion method fails.
To distinguish between the diffusion coupled and uncoupled systems, [PHAIR2004] suggest the approach of measuring recovery in various areas of the bleached zone.

If the time for diffusion throughout the bleached zone is much faster than the association rate, then the recovery will be independent of position in the bleached zones and diffusion-uncoupled behaviour is indicated. An alternative approach is to use different spot sizes for bleaching and to determine whether the FRAP recovery changes [SPRAGUE2004]. This strategy is based on the fact that diffusion, but not the reaction kinetics depends on the spatial scale. Thus, in the diffusion-uncoupled mode, there is almost no change in the recovery with bleach spot size because diffusion occurs instantaneously and occupies a miniscule initial portion of the curve that is often not even recorded. By contrast, in the diffusion coupled mode, there is a detectable change in recovery with bleach spot size, because diffusion and binding are intertwined throughout the measured recovery phase.

2.1.3 Addressing Binding: Gene Arrays

Artificial gene arrays, made up of multiple copies of the same gene that is in a tandem repeat integrated in the chromosome, can be a useful tool in visualizing the activity of genes and mechanisms of transcription by amplification of the biological signal. Naturally, this is an ensemble measurement that will swallow the stochastic nature of a single gene being transcribed. Nevertheless, information about the extent of binding, rate of transcription, rate of mRNA export etc. can be estimated using this tool.
In the case of bleaching a multiple gene array to obtain quantifications of elongation kinetics, this constrainment is set experimentally by including all of the gene array in the bleaching spot. F.ex. in the cases of MS2 and PolII XFP fusion proteins, have a sufficiently high freely diffusive population [KIMURA2002], the system can be considered reaction-dominant and the recovery may be separated into two phases: the initial fast diffusive phase, followed by the slow phase which underlies exchange at the binding sites. [DARZACQ2007] found that the binding of PolII indeed are numerous and consecutive, but not interdependent, making it possible to fit the recoveries to sums of exponentials.
An elegant way of labeling specific chromatin regions uses arrays of the Lac operator (LacO) DNA sequence that are inserted into the DNA sequence of interest ,and the expression of a fluorescent-protein -Lac repressor (LacI) fusion protein, which will bind to these DNA repeats [ROBINETT1996].
RNA molecules can be followed by inserting a series of RNA aptamers (stem-loops) into the transcript of interest and the RNA is then tagged by the expression of fusion protein that comprises a fluorescent protein fused to MS2 (a bacteriophage coat protein) that forms specific and stable interactions with these secondary structures and enables the following of the mRNA export to the nucleus [SHAV-TAL2004].
So far, three cases of amplified genes have been studied: the polytene salivary gland chromosomes in Drosophila [YAO2006], the ribosomal DNA nucleolar clusters [GORSKI2008], and artificially developed mammalian gene arrays [RAFALASKA-METCALF2007].
Initially, the purpose of the artificial array created by Tsukamoto et al. [TSUKAMOTO2000]

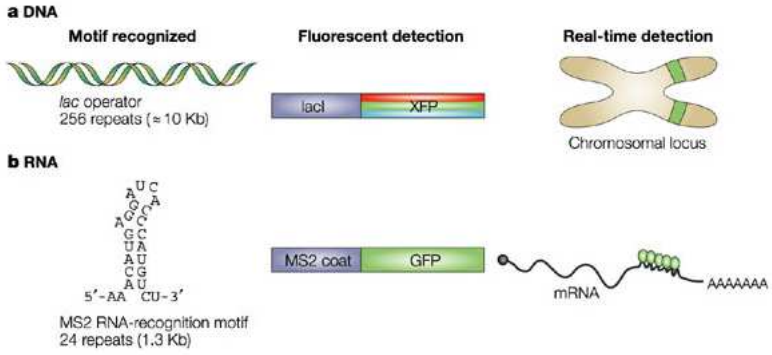

Figure 10: **Fluorescent labeling of DNA and RNA** [SHAV-TAL2004]

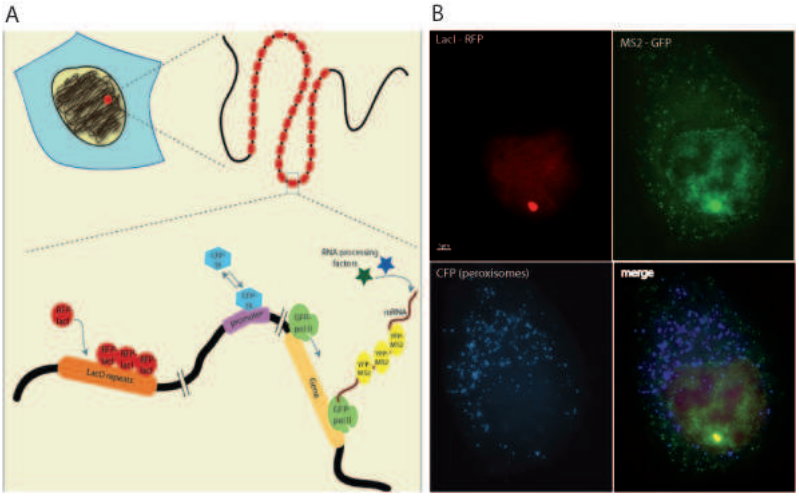

Figure 11: **The gene array of SJ cell line** (A) cartoon of the construct; (B) images of the fluorescently tagged active transcription sites [DARZACQ2007]

was used to study chromatin remodeling upon gene activation by inserting a Tet-inducible reporter gene containing Lac operator sites in large arrays. This system was then improved by Janicki et al. [JEANG1999] who inserted 24 repeats of the MS2 bacteriophage replicase translational operator which allowed visualization of mRNA. In the following works, this system was used to estimate various kinetic steps of transcription [DARZACQ2007].

Majority of the fluorescence at the gene array is due to interacting molecules, increasing the resolution on binding events reflecting catalytic activity. This enables a scenario in which one can investigate binding kinetics. [BOSISIO2006] for example, used a gene array in combination with inverse FRAP to measure the dissociation rate of NF-κB. [SPRAGUE2006] created models of axial and radial binding in order to include not

only the global distribution over the nucleus but also a superimposed specific binding cluster site, boundarized both axially an radially in the cell. They showed that the global binding model indeed gives binding parameters off by an order of magnitude; confirming that a heterogenous distribution of binding sites kinetically behaves very different from a homogeneous.

2.1.4 Modelling of FRAP Recoveries by Differential Equations

Considering only diffusion as in AXELROD1976 et al., one can say that since local temperature is hardly affected by bleaching and the viscosity of the nucleus is relatively constant, D is determined mainly by the hydrodynamic radius of the particle. But in reality, other factors affect diffusion in living cells such as specific and nonspecific interactions, hindrance by mobile and imobile obstacles [REITS2001].
behaviour A lot of things can go wrong when modelling FRAP behaviours. For example many models presume just one binding state, but some have postulated two or three distinct binding states [DUNDR2002, PHAIR2004, DARZACQ2007, SPRAGUE2006]. Some have allowed diffusion in addition to binding, [SPRAGUE2004, CARRERO2003, HINOW2006, BEAUDOUIN2006] and some have presumed it can be neglected [DUNDR2002, PHAIR2004, DARZACQ2007 GORSKI2008] (appropriate if time to diffuse across bleach spot is faster than time to bind to chromatin). These assumptions are then translated into a mathematical/computational model [SPRAGUE2004, DUNDR2002, PHAIR2004, DARZACQ2007, SPRAGUE2006, CARRERO2003, HINOW2006, BEAUDOUIN2006, GORSKI2008, MUELLER2008] that describes binding and diffusion by parameters and can be fitted. FRAP recovery time sets an upper bound on the residence time, but an accurate kinetic model is able to estimate the actual residence time [MUELLER2010].

The general equation of diffusion and binding equation:

$$F + S \rightleftharpoons_{k_{on}}^{k_{off}} C$$

the most general case is a set of three coupled reaction -diffusion equations:
$f = [F]$, $s = [S]$ and $c = [C]$.

$$\delta f/\delta f = D_f \nabla^2 f - k_{on} f s + k_{off} c$$

$$\delta f/\delta s = D_s \nabla^2 s - k_{on} f s + k_{off} c$$

$$\delta f/\delta c = D_c \nabla^2 c - k_{on} f s - k_{off} c$$

Here ∇^2 is the LaPlacian operator. The assumptions are:

1. The biological system has reached equilibrium before photo-bleach. The number of free binding sites doesn't change, eliminating the second equation. Thus, the pseudo-1st order rate constant can be defined: $k_{on} S_{eq} = k_{on}^*$.

2. Binding sites are part of a large relatively immobile complex: $D_c = 0$; such that:

$$\delta f/\delta t = D_f \nabla^2 f - k^*_{on} f s + k_{off} c$$

$$\delta c/\delta t = k^*_{on} f - k_{off} c$$

(above: [SPRAGUE2005] for 2D, [BEAUDOUIN2005] for 3D)
Before the bleach, the system is at equilibrium and F and C have achieved steady-state values, F_{eq} and C_{eq} are such that the ratio of free/bound molecules is determined by:

$$df/dt = dc/dt = 0 \longrightarrow$$

$$k^*_{on} F_{eq} = k_{off} C_{eq} or F_{eq}/C_{eq} = k_{off}/k^*_{on}$$

Total equilibrium is not altered by photobleaching, but the equilibrium for bleached $\rightleftharpoons$ unbleached molecules is disturbed. I.e. f and c are concentrations of fluorescent molecules at time of photo-bleach t = 0. Measured FRAP recovery data is the sum of free and bound fluorescence, averaged over bleach spot:

$$frap(t) = avg(f(t)) + avg(c(t))$$

Final height of the FRAP recovery equals the sum of equilibrium concentrations F_{eq} and C_{eq}; i.e after normalizing to 1, and assuming that the bleach spot is small relative to the total cell volume:

$$F_{eq} = k_{off}/(k^*_{on} + k_{off})$$

and

$$C_{eq} = k^*_{on}/(k^*_{on} + k_{off})$$

ANALYSIS OF THE FULL REACTION-DIFFUSION EQUATION

To solve the equations of coupled reaction-diffusion, La Place transform is performed. By analogy with the heat conduction problem between two concentric cylinders, a solution involving Bessel functions can be devised. The general solution for the FRAP recovery within a circular bleach spot: the average of La Place transform of fluorescent intensity within the bleach spot:

$$\overline{frap}(p) = 1/p - F_{eq}/p(1 - 2K_1(qw)I_1(qw)) \times (1 + k^*_{on}/(p + k_{off})) - C_{eq}/(p + k_{off})$$

q depends on k^*_{on}, k_{off} and D_f. w is the radius of the bleach spot. I_1 and K_1 are modified Bessel functions of first and second kind. p is the Laplace variable that inverts to yield time. I.e. inverse transform of previous equation can compute numerically to yield the predicted FRAP recovery as a function of time, by matlab routine *invlap.m* [HOLLENBECK1998]. This permits ready evaluation of how the predicted recovery depends on each of the parameters associated with the FRAP model. This full model

describes all possible behaviors of a FRAP recovery for a single binding reaction in the presence of diffusion.
Three simplified cases of the full model solution have been considered for following behaviours:

- **Pure-Diffusion Dominant**
  The equation here reduces to :

  $$\delta f/\delta t = D_f \nabla^2 f$$

  Analyzed by [AXELROD1976]. A closed form solution exists involving modified Bessel function [SOUMPASIS1983]:

  $$frap(t) = f(t) = exp(-\tau D/2t)[I_0(\tau_D/2t) + I_t(\tau_D/2t)]$$

  where $\tau_D = w^2/D_f$. When binding is almost nonexistent and molecules are free, the FRAP recovery curve should be fit by one parameter τ_D, thereby determining D_f. Note that here, $k_{off}/k^*_{on} \ll 1$.

- **Effective Diffusion**
  In the case where the reaction process is much faster than diffusion, then at any location within the bleach spot the binding reaction rapidly achieves a local equilibrium. Under these conditions, [CRANK1975] showed that reaction =diffusion equations reduce to a simple diffusion equation but with a different effective diffusion constant D_{eff}:

  $$D_{eff} = D_f/(1 + (k^*_{on}/k_{off}))$$

  D_f can be determined by first measuring FRAP recoveries for GFP, then correcting for the fusion protein and allowing for its extra mass relative to GFP alone using $D \propto M^{-1/3}$ for simplicity. [SPRAGUE2004]. Since effective diffusion is governed by the standard diffusion equation, D_{eff} can be determined by fitting the FRAP recovery curve with the diffusion model. The fit will yield a value: $\tau_D = w^2/D_{eff}$, giving an estimate for D_{eff} and hence the ratio k^*_{on}/k_{off}. In this case, $k^*_{on}w^2/D_f \gg 1$.

- **Reaction Dominant**
  In the case where diffusion is very fast compared to both binding and the time scale of the FRAP measurement: free molecules equilibrate instantly. A full solution has not been developed, but [BULINSKY2001] demonstrated analytically that the rate constant for FRAP recovery is identical to the dissociation rate constant k_{off}.
  Here, the total fluorescence recovery over time is:

  $$frap(t) = 1 - C_{eq} exp(-k_{off} t)$$

  C_{eq} depends only on off- and on-pseudo rates so the fit to the FRAP recovery in the reaction-dominant case yields k^*_{on} and k_{off}. The rate of FRAP recovery

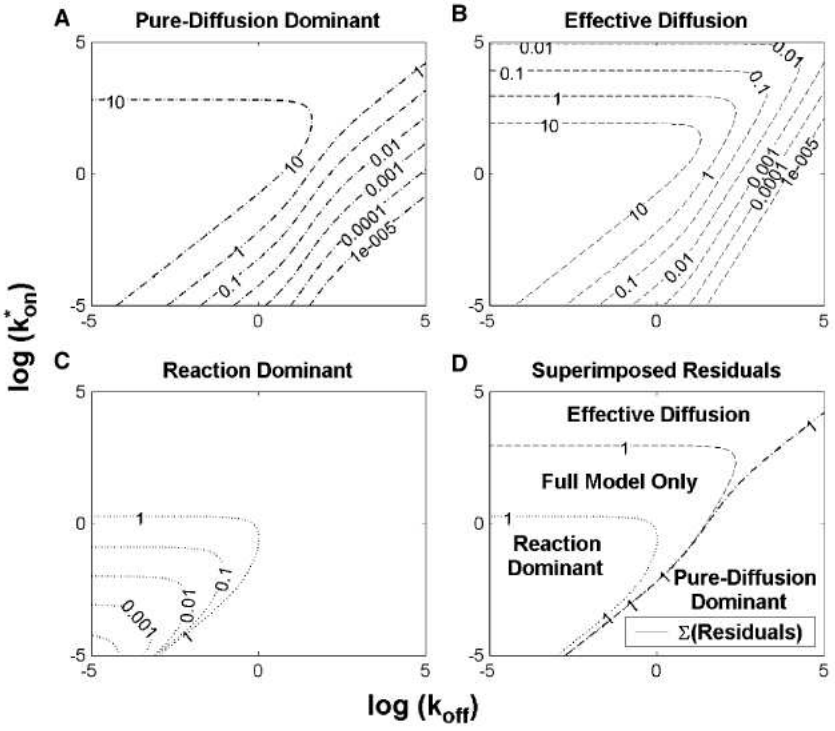

Figure 12: **Field graph of reaction constants of the full equation model describing recovery of fluorescence** Regime bound graph of natural logs of association and dissociation rates plotted against each other. field lines represent regimes at which approximation scan be applicable in order to simplify the full model of FRAP [SPRAGUE2004]

depends only on the off-rate. In all cases, the pseudo-on rate disappears from the exponential term for FRAP recovery because of the well-mixed assumption. $k^*_{on}w^2/D_f \ll 1$ and C_{eq} is significantly large $k_{off}/k^*_{on} \leq 1$

The speed of of redistribution of fluorophores does not reflect the length of interactions, but their affinity. In such cases, the reaction -diffusion model of can be simplified since interactions are considered instantaneous: for homogeneously distributed binding sites, it has been shown that the model then becomes effectively diffusive, and also for an inhomogeneous case, one can rewrite the model to [BEAUDOUIN2005]:

$$\frac{\delta i(\overrightarrow{r},t)}{\delta t} = D * Free * i^{st}_{average}\Delta(\frac{i(\overrightarrow{r},t)}{i^{st}(\overrightarrow{r})})$$

with $i(\overrightarrow{r},t)$ the local fluorescence intensity. For relatively homogeneous distributions of binding sites, the equation for this is approximately a diffusive equation with an effective diffusion coefficient equal to the product of the diffusion coefficient with the percentage of free proteins D*Free. Thus, the speed of redistribution depends only

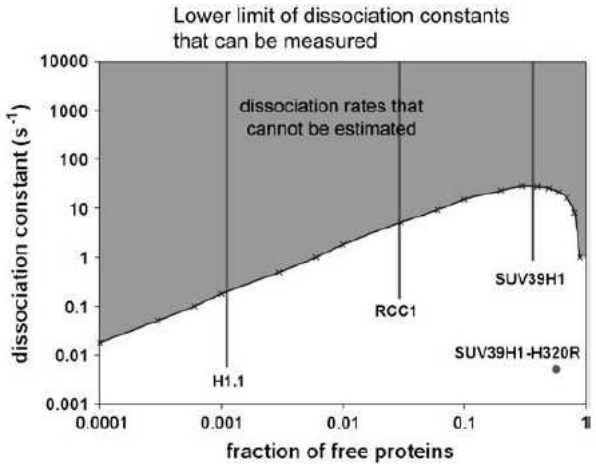

Figure 13: **Estimation of dissociation rates: experimental and theoretical limits** Positions of the different constructs on the diagram of fraction of free proteins versus dissociation rates. The curve between the shaded and the unshaded regions corresponds to the limit of dissociation rates that can be estimated, with a tolerance of 5%, determined from the comparison between reaction-diffusion and instantaneous reaction models. The shaded region corresponds to the space where the dissociation rate cannot be estimated. [BEAUDOUIN2005]

on the diffusion coefficient and the percentage of protein available for diffusion in the steady state, but not on the kinetics of the interactions [BEAUDOUIN2005].
The binding reaction can appear instantaneous in FRAP/PA experiments and that only a lower k_{off} can be determined from such experiments. Yet, the dependence of the ability to identify the dissociation rate on the percentage of free protein which reflects the affinity of the interaction in the steady state is possible.

2.2 FLIP: Fluorescence Loss in Photobleaching

A variance of FRAP is FLIP, in which a specified cell area is repeatedly bleached and the loss of fluorescence of surrounding areas are monitored. This technique enables determination of dissociation kinetics from nuclear compartments away from the bleaching area by depletion of mobile fluorophores. Whereas FRAP is able to yield information about the mobility of fluorophores at short distances close to the bleaching spot, FLIP is able to amplify differences coming from the spatial aspect of movement of these molecules. By using a small bleach spot to deplete fluorescence periodically, the surrounding fluorophores are bound to have a time at which they will pass through the small bleach spot and get bleached.
Considering the sensitivity at the spatial aspect, FLIP gives a more exact way to analyze the mobility of a protein which is likewise involved in binding. [KIMURA2002, FROMAGET2007] in this way efficiently revealed differences in mobility of RNA Pol II upon treatment with different transcriptional inhibitors.

3 Single Molecule Dynamics

The methods described previously give the method of observing ensembles of molecules and their dynamics. However, the underlying kinetics of individual molecules can give signatures that can provide us with precious information about the behaviour of the system.
New developments in optics, use of high-intensity laser light sources and high-sensitivity charge-coupled devices aided by digital image analysis makes it possible today to observe and track single fluorescent molecules. Super resolution techniques have come a long way, such as near field scanning optical microscopy (NSOM) [BETZIG1992, POHL1993], stimulated emission depletion (STED) [HELL2003, WILLIG2006], structured illumination [GUSTAFSSON2000, 2005], reversible saturable optical fluorescence transitions microscopy [HOFFMAN2005], multiphoton fluorescence [ZIPFEL2003], and saturated structured-illumination microscopy (SSIM) [GUSTAFSSON2005]. They all have achieved lateral resolution of tens of nanometers, each with their own limitations: NSOM difficult to operate in a noninvasive mode and low imaging depth. Multiphoton, STED and SSIM are based on nonlinear optical effects and typically require the use of high-intensity pulsed lasers which can induce sample damage.
The major prerequisite for optical detection of single fluorophores is the reduction of background signals. Background fluorescence mainly arises from autofluorescence, out of focus fluorescence and impurity fluorescence [NIE and ZARE1997, XIE and TRAUTMAN1998]. Reducing background fluorescence has been achieved by reducing the depth of probed volume by TIRF, near-field illumination, multiphoton or confocal imaging.

3.1 Localization of Single Molecules

The resolution of a visible light microscope is commonly about $1/2\lambda$, i.e. $\sim 250nm$ [JAMES1976], Objects of smaller sizes appear as diffraction limited spots, so-called Airy disks. Although the size of these objects is limited by the resolution of the microscope, their center of localization can be determined precisely, given a sufficient number of photons (N) in the spot [BOBROFF1986]. For shot noise, precision of localization scales as $N^{-1/2}$, whereas for background noise the precision will scale as N^{-1}.
Generally, when imaging single particles in two dimensions, the PSF can be approximated by a 2D Gaussian of the form:

$$f(x,y) = Aexp[-\frac{(x-x_c)^2 + (y-y_c)^2}{2\sigma_{xy}^2}]$$

Achievable localization accuracy depends on the respective SNR, defined as:

$$SNR = \frac{I_0}{\sqrt{\sigma_{bg}^2 + \sigma_{I_0}^2}}$$

where I_0 designates the maximum signal intensity above background, σ_{bg}^2 the variance of the background intensity values, and $\sigma_{I_0}^2$ the true variance of the maximum signal intensity above the background; determined as in [KUBITSCHECK2000]. Then, single molecules can be tracked and their diffusion coefficient found by the relation to the mean square distance in 2D:

$$< \Delta x^2 + \Delta y^2 >= 4Dt$$

In 2002, [THOMPSON2002] developed a Gaussian mask fitting algorithm based on least-squares analysis, intermediate in complexity between the simple centroid based algorithm an a full nonlinear squares fit. Considering a 1D pixel array where i and j are indices, S_{ij} is the signal value of the pixel, and N_{ij} the expected value from a Gaussian distribution with a width s and centered at x_0, y_0 defined in dimensions of pixels. Then the sum χ^2 sum for a Gaussian fit is minimized, resulting in the equations:

$$0 = \frac{d}{dx_0}\Sigma(S_{ij} - N_{ij})^2 = \Sigma S_{ij}(i - x_0)N_{ij} - \Sigma(i - x_0)N_{ij}^2$$

where

$$N_{ij} = exp(-\frac{(i - x_0)^2}{2s^2} - \frac{(j - y_0)^2}{2s^2})$$

The sum in the equation is approximately zero by symetry, resulting in the implicit equation:

$$x_0 = \frac{\Sigma i S_{ij} N_{ij}}{S_{ij} N_{ij}}$$

for the position of the paticle. Thus x_0 is the average of the pixel coordinates weighted by the number of photons in each pixel but with mask N_i that is smooth instead of binary and equal to the point spread function of the imaging apparatus. After the location of the particle was found, the estimated total number of photons i the spot N was calculated according to:

$$N = \frac{\Sigma S_{ij} N_{ij}}{\Sigma N_{ij} N_{ij}}$$

and the spot discarded as an artifact in the case where $N < 25$pixels.
The uncertainties in this method are given by the common statistics for the standard error of the mean,pixelisation noise (by size of pixel), photon counting noise and background. Localization of spots with fewer numbers of photons is dominated by background noise, and higher by photon counting noise. The optimal image magnification depends on the expected number of photons and background noise, but for most cases of interest, the pixel size should be about equal to the standard deviation of the point spread function [THOMPSON2002].

The localization accuracy of a specific estimation method is defined as the standard deviation of the estimated locations of the single molecule assuming repeated experiments [BOBROFF1968, SCHUTZ1998, THOMPSON2002]. [ABRAHAM2009] showed that the maximum likelihood estimator, although computationally more demanding,

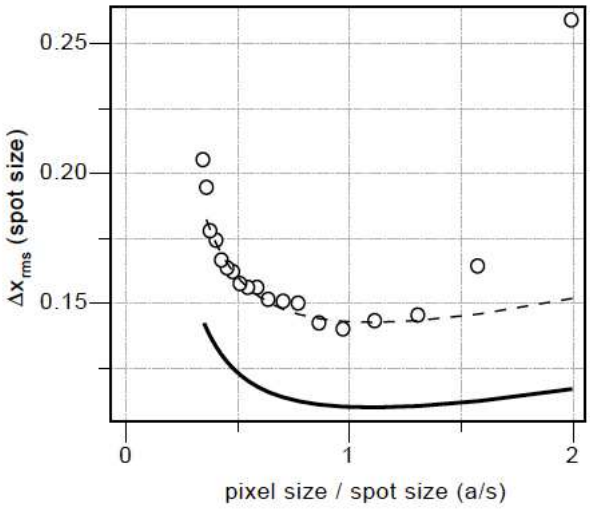

Figure 14: **Choosing the optimal pixel size** Localization uncertainty increases for small pixel sizes a due to increased background noise and for large pixel size due to pixelization noise, predicting an optimal pixel size.[THOMPSON2002]

are more accurate than the nonlinear least squares estimators. This was done by fitting Gaussians to Airy profiles. At high noise levels, they were found to be the same. To further investigate estimation methods, [OBER2004] calculated the Fisher information matrix for the underlying stochastic data generation process. [1] By this, they showed that the limit of localization of accuracy of a single molecule is given by:

$$\delta_v = \lambda_{em}/2\pi n_a(\gamma A t)^{1/2}$$

where λ_{em}, n_a, γ A and t denote the emission wavelength of the single molecule, the numerical aperture of the objective, the efficiency of the optical system, the emission rate of the single molecule and the acquisition time respectively [OBER2004].
Indeed, the position of a single emitter can be determined to almost arbitrarily high accuracy with the sufficient number of photons. Based on this, fluorescence imaging with one-nanometer accuracy (FIONA) has been demonstrated [YILDIZ2003]. but the localization accuracy of FIONA does not directly translate into imaging resolution as multiple emitters in close proximity will still be difficult to resolve. This issue was adressed in part by taking advantage of photobleaching of single dyes or photo-blinking of quan-

[1] The Fisher information matrix $I(\theta)$plays a central role in the analysis of estimation algorithms. Its inverse provides, through the classical Cramer-Rao lower bound, a lower bound for the variance $var(\theta)$ of any unbiased estimator θ (estimation procedure whose mean produces the correct result), specifically:

$$var(\theta) >= I^{-1}(\theta)$$

tum dots to distinguish their individual signals. These approaches had been used to resolve 2-5 fluorophores within a diffraction limited spot, but extending these techniques to more than a few fluorophores remains a challenge.

3.2 STORM and PALM

The essence of any fluorescent super-resolution technique is to spatially isolate signals of densely packed single molecules by either spectral [CHURCHMAN2005, OIJEN1999] or temporal means, the latter exploiting the photobleaching [QU2004, GORDON2004] or blinking of emitters [LIDKE2005]; in order to be able to localize each of the molecules by determining its center of fluorescence, implement a statistical fit of the ideal PSF to its measured photon distribution. In these techniques however, the number of emitters isolated per region (2-5) has been too small to give resolution comparable to existing super-resolution techniques. These distinguishing optical characteristics were utilized by stochastic activation and photobleaching of photoactivable fluorescent proteins (PALM) [BETZIG2006] and cyclic activation of different colors of fluorescent dyes (STORM) [RUST2006], solving the number of emitters isolated by reconstruction and serial activation.
PALM (photo-activated localization microscopy) succeeded in the isolation of single molecules at high densities (up to $10^5/\mu m^2$) based on serial photo-activation and subsequent bleaching of numerous sparse subsets of photoactivable fluorescent protein molecules [PATTERSON2002, ANDO2004, WIEDENMANN2004, ANDO2004 II, TSUTSUI2005, LUKYANOV2005 in BETZIG2006]. To minimize both autofluorescence and detector noise, [BETZIG2006] imaged his sample by total internal reflection fluorescence (TIRF) microscopy onto an EMCCD camera that can detect single photons. When necessary excitation and thus bleaching was maintained until such sparse fields were obtained. Additional image frames were then captured until single-molecule bleaching resulted in a mean molecular separation considerably larger than that required for isolation (figure principle behind palm). This method is capable of resolving the most precisely localized molecules at separations of a few nanometers. A trade-off exists wrt. PALM: including fewer but brighter molecules results in higher localization and crisper images, but at a reduced molecular density giving less complete information about the spatial distribution of the target protein.

Stochastic optical reconstruction microscopy (STORM) is an imaging technique in which a fluorescence image is constructed from high-accuracy localization of individual fluorescent molecules that are switched on and off using light of different colors. STORM consists of a series of imaging cycles. In each cycle, only a fraction of the fluorophores in the field of view are switched on such that each of the active fluorophores is optically resolvable from the rest and their images are not overlapping. Imaging resolution of 20nm was demonstrated using a simple TIRF microscope, low-power continuous wave lasers and a photo-switchable cyanine dye [RUST2006]. The resolution of STORM is limited by the accuracy with which individual switches can be localized dur-

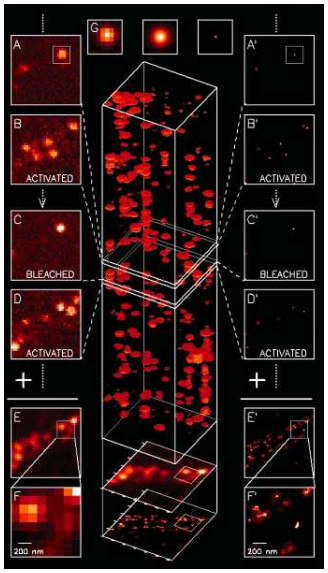

Figure 15: **The principle behind PALM** Cycles of activation, bleach and reconstruction: the fluorophores are activated, localized within nanometer range, then bleached. The cycles are repeated to reconstruct a superresolution image [BETZIG2006]

ing a switching cycle. Bates et al. [BATES2007] introduced a family of photo-switchable fluorescent probes and demonstrated multicolor STORM by photo-switchable reporter fluorophores that can cycle between fluorescent and dark states, whose combinatorial pairing of reporters and activators allows the creation of probes with many distinct colors. Color specific iterative activation allowed their localization with nanometer accuracy.

3.3 Single Molecule Tracking

Having in hand the imaging methods of stationary single molecules, one can proceed to the analysis of their dynamics.
First imaging of the kinetics of fluorophores was demonstrated by [KUBITSCHECK2000] of single molecules of GFP in gels and viscous solutions at depths of up to $\sim 10\mu m$ from the interface. The 2D localization accuracy was determined to be $\sim 30nm$, and up to nine images were possible at the frame rate of $\sim 80Hz$. Analysis of mean square distances extracted from single molecule tracking data (SMT) in aqueous solution of GFP by fluorescence video microscopy yielded same diffusion constants as obtained from FCS [GRUNWALD2006], confirming the system parameters.
The following year, the same group [KUES2001] published a paper on the visualization and tracking of single protein molecules in the cell nucleus of permeabilized 3T3 cells by labeling a recombinant E.C. β-galactosidase protein P4K with an average of ALEXA488 chromophores per tetramer. A large tracer protein molecule was selected

to carry several fluorophores homogenous in size, hydrophil and inert in nucleus. After import via the NPC, single protein trajectories could be observed in the cell nuclei with a time resolution of 10ms and with a lateral localization accuracy of $\sim 35nm$. A naturally occuring U1 snRNP in the nucleus was likewise tracked. In contrast with the previous case, freely diffusing U1 snRNP was observed rarely. Speckles were found to represent and be surrounded by binding sites for U1 snRNPs. At these the splicing factors were found attach for an average time of 60ms, and rearrange rapidly between binding sites with an effective diffusion constant of $3\mu m^2/s$ [KUES2001 II].
Hence, the tracking of single GFP molecules was possible due to their low concentration in solution, while the reduction in the fluorescence signal inside the nucleus because of the refractive index mismatch [HELL1993 in KUES2001] was compensated for by high signal of multimeres of ALEXA488.
In theory, good fluorophores can yield on average as many as 10^5 photons before photobleaching, a single fluorophore could theoretically be tracked to a precision of 65nm over 100frames, or 20nm over 10 frames in the absence of background noise. use of high numerical aperture objectives is essential both to decrease the spot size and to maximize the number of collected photons. However, tracking single molecules in cell nuclei gives rise to several limitations to be taken into account before pulling deterministic conclusions about the system.
Using a wide-field epi-fluorescence microscope, only a slice of the vertical axis in the nucleus is imaged, having it's center in the focal plane and extending $\sim 1\mu m$ in the direction of the optical axis. By imaging only a slice of a finite depth, there is a risk of the fastest population escaping imaging by moving out of the focal plane too fast. [KUES2001] conducted a Monte-Carlo simulation in the entire nucleus by fixing the diffusion constant at a value and subsequently recording only the trajectories in the observation slice. The fit to MSD yielded the correct diffusion constant in their case of $2.5\mu m^2/s$ and confirms validity of experimental approach. One has to however be careful in the case of two or more populations of differently diffusing fluorophores: the slower one will inevitably dominate in quantity without this being necessarily realistically the case.
Another method [ANDERSON1992, WILSON1996, SMITH1999 in KUES2001] was based on analyzing probability distribution of absolute molecular displacement as a function of t_{lag}. The probability distribution indicates whether fractions of molecules with different modes of motion are present. this approach allows conclusions from relatively short trajectories, because the data from all observed trajectories are gathered. $p(r,t)dr$ is defined as the probability that a particle starting at the origin will be found at time t within a shell of radius r and a width dr. For random diffusion in two dimensions:

$$p(r,t)dr = \frac{1}{4\pi Dt} exp(-r^2/4Dt) 2\pi r dr$$

The frequency distribution $p(r,t)dr$ is constructed by counting the number of displacements within the interval $[r, r+dr]$ for each value of t_{lag} from all observed trajectories. This was made for the observation slice. The frequency distributions of jump distances were recorded on the bases of five trajectories with 10^4 single steps at lag times of 18, 54,

90 and 126ms corresponding to those the experimental stacks. The diffusion constants fit, but they get less exact with larger lag times.
The jump distance probability distribution of immobile molecules is described by the time-independent probability distribution:

$$p_{im}(r)dr = \frac{N_{im}}{\sigma_{acc}^2} exp(\frac{-t^2}{2\sigma_{acc}^2})rdr$$

For intracellular transport the diffusion coefficients depended on the lag time, in contrast to free diffusion. This indicates that diffusion in the nucleus is restricted. Such restriction can be brought about by physical and chemical parameters (barriers, assoc/dissoc reactions). At such conditions the dependence of the diffusion coefficient on the lag time can be described by:

$$D = \frac{\Gamma}{4} t^{\alpha-1}$$

where Γ designates the transport coefficient and α the factor quantifying the time dependence of the diffusion coefficient.
Naturally, there are detection limits for diffusion coefficients that are measurable. The upper limit of diffusion constants is defined by the mean square distance that the molecules move during the image integration time δt. This value must be smaller than the area of the Airy disk of the utilized objective lens. then the movement of the molecule during the image integration time would not notably blur the image reducing SNR and localization precision. The upper limit for the measurable diffusion coefficient, D_{max} can be estimated by:

$$D_{max} <= \frac{\lambda^2}{NA^2 \delta t}$$

where NA denotes the numerical aperture, λ the wavelength of the fluorescence emission. the minimum image acquisition time δt is determined by the fluorescence signal of the probe and the given noise sources. In praxis, this results in a limit of D of about $10\mu m^2/s$ (diffusion of protein with 3nm radius). In case this limit for D is exceeded, fluorescence spots are obtained that are integrals over the convolutions of the PSFs.
A lower detection limit for the diffusion coefficient is given by the condition, that the particles must move beyond the localization precision during the total observation time δt_{obs}:

$$D_{min} <= \frac{\sigma^2}{4\delta t_{obs}}$$

Theoretically, observation time can be prolonged as required: only stability of experimental setup and photobleaching of fluorophores pose an upper limit.
Recently, stroboscopic laser excitation was used with stochastic photo-activation and super-resolution fluorescence imaging [ENGLISH2010] in order to record diffusion trajectories of small protein molecules in bacterial cells with milisecond time resolution and sub-diffraction limited spatial precision. Current imaging technology allows for

observation of slow processes and it potentially biases the observed distribution toward slower sub-populations; while fast milisecond dynamics may be completely overlooked. This limitation is circumvented by combining this imaging technique with stroboscopic illumination [YU2006, ELF2007 in ENGLISH2010]. The duration of the excitation pulse is a critical parameter for obtaining distinct fluorescence spots from rapidly moving single molecules. The optimal value is a trade-off between collecting the large numbers of photons needed to determine the position of the molecule accurately and the broadening of the spot due to diffusion of the molecule during the excitation pulse (under their experimental conditions, 0.4 - 1ms) [ENGLISH2010]. The fitting precision of stroboscopic illumination is proportional to the square root of the number of detected photons [THOMPSON2002]. Any movement could easily be frozen within a diffraction-limited spot using pulses shorter than 200microsec. but precise localization is not possible given the poor photo-physical properties of mEOS2 and hence higher pulse durations were utilized. also frames are recorded at the highest read out speed of our EMCCD camera (4ms for 28pixel lines).
In a system without spatial confinement, the MSD of a diffusing particle is proportional to time to the power of α, i.e. $< \Delta x^2 > \propto t^\alpha$ where α is unity for normal diffusion. Experimental analysis of MSD must be complemented by simulations of diffusion in the given geometry of each cell [DEICH2004, NIU and YU2008 in ENGLISH2010]. Nonuniformity in the spatial distribution of diffusion coefficients is fully described by confinement effects since identical patterns emerge when simulated [ENGLISH2010]. Another standard approach is to calculate the cumulative distribution functions (CDFs) of displacements, getting diffusion coefficients by fitting them to an exponential function corresponding to 2D Brownian motion [SCHUTZ1997, VRLJIC2002].

4 Kinetic Analysis

Simple diffusion has been shown as the process driving transport of transcription factors around the nucleus. Short residence times at substrates and dynamic complex lifetimes, as well as the dynamic self-organization of the nucleus have been established. Putting physical parameters to this system enables determination of the nature of the diffusions that occur, strengths of binding and complex lifetimes which can yield useful information about the kinetics of the system.
Kinetical models are characterized by physical parameters such as diffusion, binding and release constants, residence times. By fitting to experimental data, quantitative information about the system can be obtained. For cell processes, often differential equations are adopted as templates for a model since they have previously shown to effectively describe several cellular processes such as biochemical kinetics, membrane transport and binding events.
The types of mathematical models implemented are curve fitting, statistics, phenomenological laws, enzyme kinetics and logic models [PHAIR2001].
Transcription factors generally exhibit sub-diffusive properties caused by unspecific interactions and obstacles encountered within the nucleus [PHAIR2000]. Furthermore, a transcription factor can exhibit more than one apparent diffusion constant due to complex formation.

4.0.1 Kinetic imaging techniques

Imaging techniques widely used today: FRAP, FLIP, FCS, and FRET provide insights into the dynamics of transcription factors. The methods have been explained in the previous sections. The kinetic information from each of these is presented in Table(1).

FLIP

Whereas FRAP modelling has been established using both diffusion [AXELROD1976] and binding mechanisms combined for homogeneous and heterogenous distributions of binding sites [SPRAGUE2004,2006]; the modelling of FLIP is more complex and does not have a universal protocol. [PHAIR2000, supl.mat.] performed a quantitative analysis of FLIP on SF_2/ASF and fibrillarin. This was done by constrainment of nucleoplasmic diffusion coefficients by values obtained in FRAP analysis in order to extract information about the system's binding coefficients, residence times and steady-state distributions. The latter were calculated from the matrix of rate constants assuming an average protein degradation rate constant corresponding to a half life of 12h, and were used to initialize the protein content of each compartment at the start of the FLIP protocol. These distributions combined with estimates of molecular abundances permitted estimation of the number of molecules in each compartment as well as intercompartmental fluxes.

Table 2: Imaging techniques and measured parameters

FRAP	(effective) diffusion
FLIP	diffusion, mean residence times, steady state distributions in compartments, inter-compartmental fluxes
FCS	fluorophore concentration, size, diffusion
FRET/FLIM	environmental conditions of fluorophore, fluorophore interactions
Single molecule dynamics	diffusion, residence times

However, this FLIP analysis is assuming compartments of a measurable size and constant distribution of factors in other parts of the nucleoplasm. Additionally, a diffusion unlimited system is assumed, where binding constants are measureable. In cases where the system exhibits effective diffusion, such analysis is not appropriate.

FRET and FLIM

In FLIM data, FRET shows up as a dramatical decrease of the donor lifetime [LAKOWICZ1999, ELANGOVAN2002, BECKER2001,2002,2003]. The fluorescence decay functions contain the fluorescence of quenched and of unquenched donor intensity and are therefore double-exponential (Figure(16)). Fitting of double exponentials delivers the lifetimes τ_0 and τ_{FRET} and the intensity factors, a and b of the two decay components [BECKER2001,2002,2003]. The ratio of quenched vs. unquenched molecules is given by b/a while the average coupling efficiency of FRET pairs is given by τ_0/τ_{FRET}. In principle, both of these can be derived from a single donor lifetime measurement [BERG].

4.0.2 Compact vs. non-Compact modes of movement

How long does it take a random walker to reach its target site? This quantity has been defined as the first-passage-time (FPT), a key quantity for the kinetics of transport-limited reactions [YUSTE1995, RICE1985]. FTP has been extensively investigated in confined domains in homogeneous environments [REDNER2001]. However, when addressing this problematics in nucleus, there is a requirement to take into account its heterogenous nature. [CONDAMIN2007] developed a general theory that is able to accurately evaluate mean FPT in complex media. They consider a finite space made up

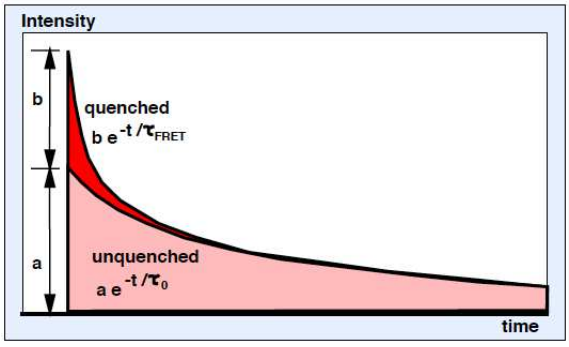

Figure 16: **Fluorescent Resonance Energy Transfer: the donor intensity decay** Scheme portraying the double exponential fluorescence decay functions of quenched and unquenched donor intensity. The ratio b/a gives their proportions, whilst the average coupling efficiency of FRET pairs is given by τ_0/τ_{FRET} [source unknown]

of a lattice of nodes, which can be arbitrarily regular, diordered or hierarchical, or can also assume some configuration such as that of a scale-free network. The scale-free case consists of nodes with many different degrees of connctedness, and the likelihood of that a node has a certain number of links declines as a power law with that number: many networks of nodes will have a small number of connections, but few have a large number [SHLESINGER2007].
Three cases for the mean FPT between an arbitrary source and a designated target at a distance r have been found. To a good approximation, this time always grows linearly with the number of nodes N, but also depends either on r raised to a certain power or in a special case, the logarithm of r. Montroll et al. [MONTROLL1969] approximated no linear dependence of FTP on N, but since he did not take into account the role of the source-target separation, results of [CONDAMIN2007] seem more fundamental. Herewith, the mean FPT is parametrized in terms of two characteristic 'dimensions'. These dimensions are derived from scaling relationships between the variables that are inherent in the problem:

- fractal dimension d_f which characterizes the density of nodes in the lattice (in a 2D lattice, the number of enclosed nodes will scale as some power of the circle's radius. in a constant density of nodes, in 2D $d_f = 2$; whereas for fractal shapes in the plane such as a Sierpinski gasket or percolation cluster which have a hierarchy of self-similar node groupings that only sparsely filll the plane, $d_f < 2$).

- walk dimension d_w which characterizes the ease with which the walker can move though the lattice. Mathematically, it enters the expression for the mean-square displacement from the source as a function of number of moves, n, which is written to scale as n^{2/d_w} (in a regular 2D lattice, $d_w = 2$, meaning that MSD grows linearly with number of moves made, the diffusive case. But on a lattice with many bottle-necks and dead ends, the walk can be severely impeded, producing a d_w of greater than 2, and a process slower than diffusion).

There is three cases for the mean first passage time between an arbitrary source and a designated target at distance r; given by the difference between the fractal dimension and the walk dimension $d_f - d_w$:

1. In cases where $d_f > d_w$, if the walker is significantly impeded or latice is sparse, a compact, local exploration arises. There is a strong positive dependence of the mean FPT on the initial source target separation, of the form $< T > \sim N(A - Br^{d_w - d_f})$.

2. In the opposite case, where $d_f < d_w$, this characterizes a non-compact exploration in which a random walker leaves a region with many sites unvisited. The Levy flight is an example of non-compact exploration. This random walk performs jumps of many sizes, making its starting point irrelevant. The formula for FPT also shows a dependence of the form $< T > \sim N(A + Br^{d_w - d_f})$ but because the exponent is negative by definition, this dependence disappears at large values of r, leaving the mean FPT dependent on the number of nodes alone.

3. Finally in the third case $< T > \sim N(A - Blnr)$, there is a weak, logarithmic dependence of the mean FPT on the separation.

Here A is related to the small scale properties of the walk, B can be written solely in terms of Π which is the infinite space scaling function. These expressions thus unveil a universal scaling dependence on the MFJPT o the geometrical parameters N and r, i.e. both the volume of the confining domain and the source - target distance. The results were successfully tested on the PIN yeast length-scale invariant network simulation [CONDAMIN2007].
Most functions of a living cell are regulated by coordinated chemical reactions that involve low concentrations of reactants that are limited by transport. This is why understanding the origin of anomalous transport in cells and its impact on reaction kinetics is an important issue. Calculations were conducted on transport observables (first-passage observables) by [CONDAMIN2008] with efforts to discriminate between the continuous time random walks (CTRW) [REDNER2001, HOLCMAN2007] and the other relying on spatial inhomogeneities as exemplified by diffusion in deterministic or random fractals such as critical percolation clusters [NOH2004, BARTON1989, CONDAMIN2005].

FPT observables make it possible to distinguish between the two. The FPT has a finite mean and exponential tale for the fractal model, and a infinite mean and power law tail in a CTRW model. Analyzing the tail of the distribution of the FPT therefore provides a first tool to distinguish them. Since experimental data is limited in time, truncated means need to be implemented to define MFPT for CTRW. In this case, the scaling of the MFPT for CTRW with the source-target distance is the same for a simple random walk, and can be distinguished from the scaling of the MFPT on random fractals: the se two scalings are strikingly different for d = 3: the CTRW performs aera non-compact exploration of space ($d_w = 2 < 3 = d$) leading to a finite limit of the MFPT at large source-target distance, whereas exploration is compact for a random walker

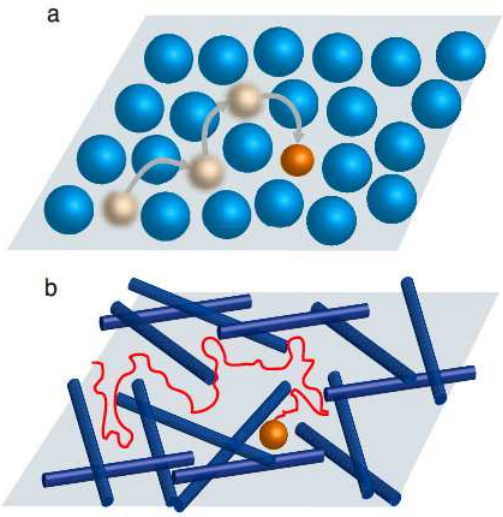

Figure 17: **Two scenarios of sub-diffusion for a tracer particle in crowded environments (CTRW and fractal environment)** (A) Random walk in a a dynamic crowded environment. The tracer particle evolves in a cage whose typical lifetime diverges with density. This situation can be modeled by a CTRW with power-law distributed wiating times. (B) Random walk with static obstacles. This situation can be modeled by a a random walk on a percolation cluster. [CONDAMIN2008]

on the percolation cluster ($d_w > d_f$) leading to a scaling $\propto r^{d_w - d_f}$ of the MFPT [CONDAMIN2008].
1917 Marian Smoluchowski [SMOLUCHOWSKI1917] calculated the relationship between rates of chemical reactions and the diffusion coefficient of the participating molecules, thus setting the diffusion limit of reaction rates. However, experimental observations showed much faster reaction rates than calculated, indicative of intrinsic mechanisms to speed up diffusions. One of these is known to be the reduction in dimension (f.ex. the 3D diffusion followed by 1D scanning [RICHTER1974, BERG1981, COPPEY2004, HALFORD2004, HU2006, SLUTSKY2004, WANG2006, ELF2007.]), another is active transport mechanisms that speed up target each for particles larger than 10nm [LOVERDO2008]. Considering crowded environments of complex architectures of cell structures such as the nucleus, it is not surprising that a modification of an idealized system with homogeneous and random distributions of molecules with at least linearly increasing exploration volume over time will also pose a difference in terms of the efficiency of target search. Mathematically, it is known that the exploration volume $V(t)$ increases asymptotically as $t^{1/2}$ in one dimension, whereas in three dimensions it increases linearly.

This distinguishes between diffusion in 'compact' exploration spaces with zero escape probability and a sub-linear V(t), and in non-compact exploration spaces with finite escape probability and a linear V(t). Most fractal topologies are compact, and the resulting non-classical reaction kinetics have been termed fractal-like reaction kinetics. Considering a distribution, it turns out that fractal-like reaction kinetics are also accompanied by non-random reactant distributions in space, even with initial random

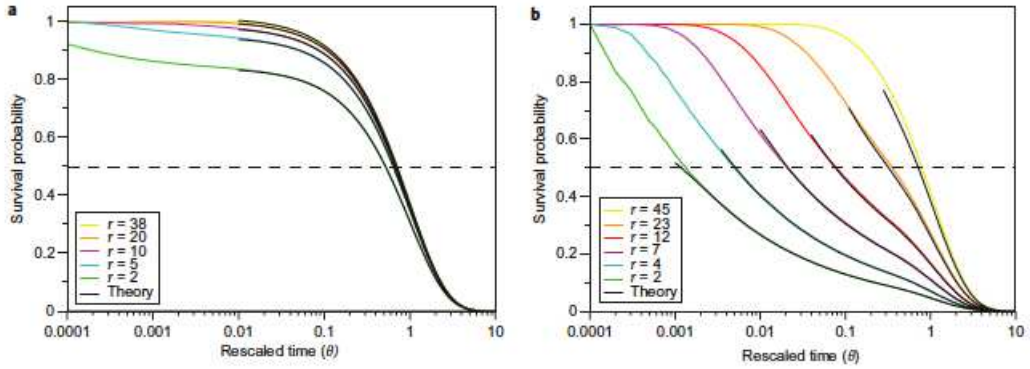

Figure 18: **Geometrical kinetics and the first passage time dependence on initial position** Survival probabilities plotted for different source-target distances r. (A) depicts the non-compact case exemplified by 3D diffusion and (B) the diffusion on a Sierpinski gasket. They typical reaction time depends weakly on the initial position of the reactant in the non-compact case, while the compact case the reaction time runs over several orders of magnitude. [BENICHOU2010]

distribution [KOPELMAN2010]. [BENICHOU2010] posed the question of how the FPT distribution depends on the volume of the confining domain and the initial position of the diffusing molecule; and whether these factors potentially could be used to control the kinetics.
The general derivation uses a random walker in a fractal medium with a fractal dimension and the dynamics characterized by the dimension of the walk. The results differ significantly depending on the relative size of these dimensions:

- in non-compact exploreation, when the fractal dimension is larger and $V(t) \propto t$ it is the mean of the FPT that characterizes the kinetics, as in the simple case of regular 3D diffusion. The initial position has little effect on kinetics.
- in compact exploration, (sub-linear rise with time of exploreation volume), the full distribution of the FPT is required and not just the mean, and the kinetics depend strongly on the original distance beteen the initial starting position and the target.

These show that geometrically controlled kinetics describes such situations and it is typical of certain important reactions inside biological cells. Further more, [BENICHOU2010] show that 100nm colocalization in the nucleus may speed up the transcription kinetics by three orders of magnitude, illustrating the importance of correct treatment of such chemical reactions, and opening the possibility that geometry of cellular environments was evolutionary fitted to optimize i.e. facilitate and control the chemical reactions within them.

Part III

P-TEFb

P-TEFb is a general transcription factor that facilitates the production of full-length mRNAs of protein-coding genes (with the exception of certain short intronless genes [MEDLIN2005]). In transcription, RNA Polymerase II C-terminal domain (CTD) is hypophosphorylated when initially recruited to genes. Followingly, it undergoes sequential phosphorylation at Ser5 by CDK7 and enters a pause at the promoter proximity. The release from this paused state and thereby switch to productive elongation requires phoshorylation by P-TEFb at Ser2 residues of CTD [PRICE2000], NELF and DSIF [SAUNDERS2006]. This is accompanied by mRNA capping and loss of NELF [BRES2008].
Apart from enabling the onset of transcription elongation, P-TEFb influences multiple factors of gene expression, such as co-transcriptional control of mRNA processing (integration of mRNA synthesis with histone modification), pre-MRNA processing and export of mature mRNA to promote translation in the cytoplasm.
Also, P-TEFb stimulates the Pol II mediated synthesis of human immunodeficiency virus (HIV) transcripts from the 5'long terminal repeat of the integrated proviral genome and it's importance of regulation has been indicated in many cancers and other pathological states.
By the importance of its actions, it is expectable/obvious that P-TEFb should be a molecule physiologically highly controlling its activity and effectively responsive with a broad spectrum of interaction profiles. Indeed, the activity of P-TEFb is tightly controlled by sequestering into complexes, chemical modification of the molecule, etc. Following subsections will give a broad overview of P-TEFb characteristics, its function and the importance of it's regulation in the cell.

5 The P-TEFb Complex

The P-TEFb molecule consists of a CDK9(cyclin-dependent-kinase) subunit along with its associated cycline, CycT1 (T, because of its involvement in transcription [PENG1998]). CycT1 and two splicing isoforms of CycT2a and T2b constitute the family of C-type cyclins. 80% of CDK9 is sequestered endogenously with CycT1 [CHO2009], 20% of it co-exists with other cyclins (T2a, T2b, K)[PENG1998(genes)]. In its active form, P-TEFb is made up of a cycline and cyclin-dependent-kinase (CDK9) subunit. The kinase CDK9 is activated by forming non-covalent complexes with cyclins.
All cyclins bear two prototypical cyclin boxes at the N-terminus, histidine rich region, providing binding to CTD of RNA Pol II and proline-serine rich C-terminus [KOHOUTEK2009]. CycT1, in contrast to T2a/b, contains TAR recognition motif (TRM)

next to cyclin boxes, which is important for formation of ternary complex between Tat/Tar/P-TEFb and initiation of HIV transcription [WEI1998, WIMMER1999].
CycT1 is a predominant nuclear protein, while CDK9 can shuttle between nucleus and cytoplasm. Enforced expression of CycT1 mediates the nuclear accumulation of CDK9. This ability of CycT1 to mediate the nuclear accumulation of CDK9 requires the cycline homology box [NAPOLITANO2002]. By control of nuclear accumulation of CDK9, CycT1 is recognized as the limiting factor of abundancy of P-TEFb in the nucleus. Indeed, the expression of CycT1/2 has to be tightly regulated at the transcription level, at the level of RNA stability, translation and ubiquitination [LIOU2006, MARSHALL2005].
Likewise, in the cell, there are two forms of CDK9: 42-kDa form and 55-kDa form, resulting from a 117 residue amino-terminal extension that is not present in the previous. [SHORE2003]. CycT2 and CycK molecules are present at much lower concentrations than CycT1 in many cell types [PENG1999, FU1999]. Therefore, the most abundant classic form of P-TEFb consists of the 42kDa CDK9 and CycT1.

5.1 Sequestering in the large complex

P-TEFb activity is regulated by its sequestering into a larger complex: P-TEFb exists in two forms, alone and sequestered in the 7SKsnRNP complex, in which its kinase activity is inhibited. These two, often annotated the small and the large complex respectively, are in a dynamic equilibrium with each other: upon addition and removal of DRB in presence of cycloheximide, which blocks protein synthesis, the large complex recovered, indicating that the two are in dynamic exchange.[NGUYEN2001]
Proportions in the abundance of the two complexes varies with cell types and states. For example in HeLa cells, approximately half of P-TEFb exists sequestered in the large complex, while the other half is an active complex containing the bromodomain protein Brd4 [JANG2005,YANG2005]
Studies suggest that shifts in this equilibrium may underlie alternative pathways toward unrestricted growth or terminal division/differentiation [HE2006, SANO2002, TURANO2006].

Analysis of the large inactive P-TEFb complex indicates that it contains one 7SK molecule, a dimer of Hexim1 or Hexim2, and two P-TEFb molecules containing Cdk9 phosphorylated at threonine 186. This oligomerization of P-TEFb incorporation into a homo-or hetero-dimer of Hexim is mediated through the basic region within the central part with bound 7SK snRNA and its coiled-coil region in the C-terminal domain [BLAZEK2005, LI2005].
However, the exploration of P-TEFb associating partners in the large complex is not complete: two additional proteins participating in the formation of the LC were recently identified : MEPCE (7SK snRNA methyl-phosphate capping enzyme) [JERONIMO2007] and Larp7 which stabilizes 7SK snRNA by binding to its 3'- UUUU-OH tail and thus protecting it from degradation by exonucleases [HE2008]. Both are stably associated with 7SK snRNA after release of P-TEFb in contrast to Hexim1 which

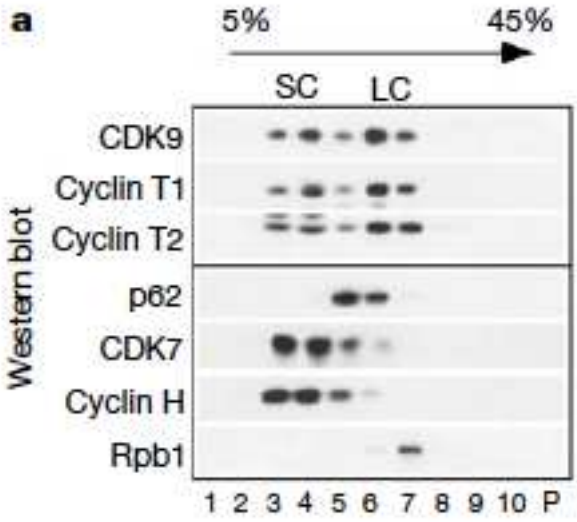

Figure 19: **Structural and functional characterization of human CDK9, cyclin T1 and cyclinT2 complexes** Fractionation of an HeLa cell extract by ultracentrifugation on a glycerol gradient. Distribution of CDK9, cyclin T1 and cyclin T2 in the gradient fractions and pellet (P) was monitored by western blot using specifc antibodies. The same blots were probed for Rpb1, p62 (a TFIIH-specifc subunit), CDK7 and cyclin H (subunits of both TFIIH and CAK complexes). (SC, small complexes; LC, large complexes.) [NGUYEN2001]

is displaced after the disruption [BARBORIC2009, HE2008, KRUEGER2008, DIRIBARNE2009, MARKERT2008].
It was shown that stable and simultaneous knockdowns of 7SK and Larp7 molecules failed to decrease cell viability [HE2008], which suggests that these are not required for cell survival. Rather, they contribute to the suppression of growth and transformation. This opens the topic of the tightly regulated equilibrium between the small and the large P-TEFb complex.
Disruption of the large complex and thereby the functional P-TEFb equilibrium between the two complexes plays an extremely important role in globally regulating transcription and could therefore be detrimental to many key cellular functions. The ratio of these two P-TEFb populations is likely to be different among different cell lines or tissues and moreover, the P-TEFb distribution in a given cell type may also change according to its growth and differentiation status.
The breakdown of the P-TEFb/HEXIM/7SK complex is triggered by all treatments that inhibit transcription. Arrest in mitosis is one exception perhaps because transcription is then arrested at both initiation and elongation steps whereas drugs and UV act mainly at the elongation step [BARRANDON2007].
A very good example of the tight control of the P-TEFb functional equilibrium is found by analyzing the effects of haexamethylene bisacetamide (HMBA), a hybrid bipolar compound, two issues of both P-TEFb activity and growth of human HeLa and erythroleukemia cells (MELC) were addressed. Whereas HMBA retarded HeLa cell growth

only weakly and transiently, it is by far the best-characterized suppressor of growth and inducer of terminal differentiation of MELC. An efficient, albeit temporary disruption of the 7SK snRNP and activation of P-TEFb dependent transcription were observed during the initial phase of the treatment. The peak 7SK snRNP disruption occurred app. 2h after the treatment commenced. Interestingly, a prolonged incubation with the drug actually led to a gradual recovery of the 7SK snRNP [HE2006]. HMBA induces HEXIM1 expression in a P-TEFb dependent manner. 6-12h after the HMBA treatment started, the HEXIM1 expression began to increase significantly and its nuclear concentration remained four to five times higher than the pre - treatment level for at least 72h [HE2006], pushing the equilibrium back. All this data strongly supports the notion that the functional P-TEFb equilibrium is tightly and dynamically regulated to reflect and accommodate the intracellular transcriptional demand as well as the proliferative or differentiated states of cells.
The tight regulation of the functional equilibrium points to P-TEFb as a common target for the global control of cell growth and differentiation by its associated regulators [ZHOUandYIK2006].
The following subsections give a summup of the most important components of the large complex and their roles in the functional equilibrium..

7SK

Human 7SK RNA is an abundant 331nt nuclear transcript generated by RNA polymerase III. Upon P-TEFb activation, 7SK RNA is released and associates a subset of heterogeneous nuclear ribonucleoproteins (hnRNP). 7SK RNA hs been evolutionary conserved in vertebrates and homologues are found in annelid, mollusc and insect genomes. 7SK RNA folds into several hairpins that serve as specific platforms for binding proteins. It is stabilized by monomethylation of its 5'-triphosphate group and binding of a specific La-Related protein, LARP7 at its 3' end. 7SK RNA is localized in the nucleoplasm and efficiently knocked down by RNA interference [ROBB2005]. The gamma phosphate of the 5' triphosphate group on 7SK first nucleotide is monomethylated. Such 5'-mono-methyl cap protects U6 and 7SK RNA against degradation but is incompatible with translation of mRNAs.
HnRNPs associate 7SK released from disrupted complexes following an arrest in transcription [VAN HERREWEGHE2007, HOGG2007, BARRANDON2007] HnRNPS are generally thought to chaperone nascent transcripts. Thus, hnRNPs no longer bind neotranscripts in transcription-arrested cells, the concentration of hnRNP devoid of RNA increases markedly and reaches an order of magnitude excess over that of 7SK RNA. Hence, it is proposed that hnRNPs released from nascent transcripts trap 7SK RNA thereby preventing it to reassemble with HEXIM1 and P-TEFb [MICHELS2008].
This model is supported by following observations:
(a) removal of hairpin 3, the hnRNP-binding motif in 7SK RNA, prevents LC disruption in response to an arrest in transcription [VAN HERREWEGHE2007]
(b) siRNA knock-down of hnRNP K increases the proportion of P-TEFb associated with

7SK RNA [HOGG2007]
(c) knock-down of A-type hnRNP attenuates LC disruption in response to inhibition of transcription.
This regulation forms a positive feedback capable of fine tuning transcription activity.

Hexim1

Hexim1 has been demonstrated to specifically bind to 7SK snRNA via a stretch of 18 basic amino acids reminiscent of the arginine rich RNA recognition motif present in many RNA binding proteins [MICHELS2004, YIK2003]. Reversible phosphorylation of CDK9, most probably at the conserved Thr-186 in the Tloop is required for in vitro association of P-TEFb and 7SK RNA. [CHEN2004]
The elements crucial for P-TEFb binding are contained in the two terminal hairpins of human 7SK. The distal part of 5′ terminal hairpin of 7SK directs HEXIM1 binding. The HEXIM1 and P-TEFb binding element of 7SK show strong evolutionary conservation in vertebrates.[EGLOFF2005]
Only about 20% of total nuclear HEXIM1 is actually in association with P-TEFb in log-phase HeLa cells [MICHELS2003 YIK2005] When the total cellular level of HEXIM1 is being gradually reduced by RNAi the population of free Hexim is the first to dissapear, 7SK/P-TEFb being minimally affected. This indicates strict control of equilibrium LC-SC. To avoid preturbation of the P-TEFb equilibrium, homologue HEXIM2 is also increasingly recruited to the LC when Hexim1 siRNA is conducted [BYERS2005, YIK2005].

Larp7

Larp7 binds and stabilizes nearly all nuclear 7SK via 3′-UUU-OH, leading to the sequestration and inactivation of P-TEFb. (A recent study [JERONIMO2007] demonstrates that the 5'end of this RNA is also protected in 7SK snRNP by a specific methylphosphate capping enzyme called BCDIN3.) This function requires its La domain and intact C terminus. The latter is frequently deleted i human tumors due to micro-satellite instability-associated mutations. Larp is homologous to human La protein, a 3′-UUU-OH sequence-specific RNA-binding protein that associates with nascent PolIII transcripts and protects them from degradation by 3′-exonucleases. Larp7 knockdown shifts the P-TEFb equilibrium toward the active Brd-4 bound state and causes P-TEFb dependent malignant transformation and activation of key tumor-related genes. Together, these observations link the Larp7-dependent modulation of P-TEFb activity to the global control of cell growth and tumorigenesis [HE2008]. The unique C-terminal region of Larp7 is frequently deleted in human cancers and absent in hLa. In support, Larp7 mutants lacking the C-terminal region were unable to bind 7SK and enter 7SK snRNP, which would lead to a loss in tumor suppressor activity. On the other hand, mutant Larp7 may also acquire a gain-of -function in promoting tumorigenesis in a manner reminiscent of that of activated oncogenes [HE2008].

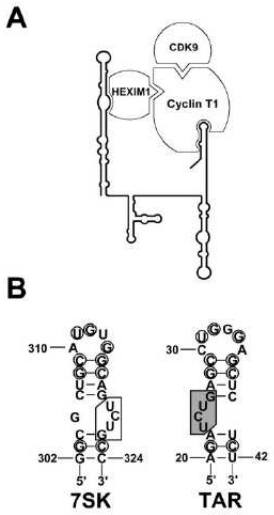

Figure 20: **7SK-dependent regulation of the CTD kinase activity of P-TEFb** (A) Structural organization of the kinase-inactive 7SK/HEXIM1/P-TEFb complex. The schematic structure of human 7SK snRNA, together with associated proteins, is shown. (B) Structural comparison of the HIV TAR RNA and the P-TEFb binding motif of the three hairpins of human 7SK snRNA. The conserved nucleotides are circled. Nucleotides essential for Tat binding are shaded. The inverted Tat binding-like motif of 7SK snRNA is boxed. [EGLOFF2005]

5.2 P-TEFb - PolII interaction

Both CycT1 and CDK9 co-immunoperticipate RNA Pol II. Proteins containing the 551 N-terminal residues or only sequences from positions 231 to 611 and 350 to 611 bound RNA Pol II [TAUBE2001].
Thus the histidine-rich stretch, which is conserved between CycT1 and CycT2, is required for binding the C-terminal domain of RNA Pol II. Also, the binding of CycT1 to CTD requires more than five heptapeptide repeats in the CTD and the histiine rich stretch of CycT1 [TAUBE2001].
Kinetic analysis indicates that P-TEFb preferentially phosphorylates CTD that is already partially phosphorylated, but that otherwise extensive phosphorylation does not occur in a processive manner. Experiments were conducted with Pol II with and without CTD, which led to conclusions that CTD is the physiological target of P-TEFb. DRB-sensitive transcripts arose only when CTD was intact. [MARSHALL1996].
The interaction between C-terminal regions of RNA Pol II, CycT1 and distal sites enables P-TEFb to act as a transcriptional coactivator. Thereby P-TEFb can link activators at enhancers and PIC at promoters, which results in productive elongation [TAUBE2001].
It has been shown that CycT1 is tethered upstream or downstream of promoters and coding sequences. P-TEFb plays a general role in mediating effects of enhancers. P-TEFb activates transcription form proximal and distal sites upstream and downstream

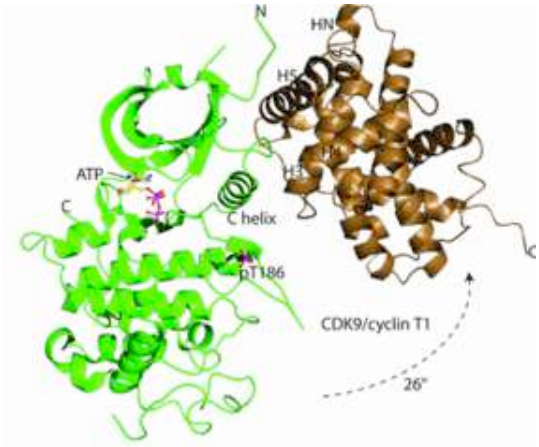

Figure 21: **Diagram showing molecular structure of CycT1 and CDK9** [www.biochemsoctrans.org]

of the promoter and coding sequence of a reporter gene, PPR (promoter proximal regions), CP (core elements) and CTD of RNA Pol II were required for these effects of P-TEFb.
In most cases, labelled CycT1, CDK9 and RNA Pol II are not superimposed but the Cdk9 or CycT1 proteins exist in overlapping regions with Pol II. This indicates that although there is a limited degree of co-association of CDK9 or CycT1 with RNA Pol II, the majority of CDK9 and CycT1 is not present at sites containing RNA Pol II [HERRMANN2001]. This observation is consistent with the theory of factor accumulation at active transcription sites. Furthermore, in cells treated with DRB, CycT1 co-colocalized with enlarged speckles whereas CDK9 was present at speckles it did not appear to become enriched in these regions. This suggests that the CycT1 component of TAK/P-TEFb is responsible for the association of the kinase complex with nuclear speckles. A different labeling type was observed for mutants which contained up to the first 433 amino acid residues of CycT1. These mutants gave a diffuse pattern of labeling without significant accumulation of high signal foci. These results claim that a recognition region between 433-533 is necessary for speckle compartmentalization.

6 The biochemistry of P-TEFb role in transcription elongation

RNA Pol II transcribes all mRNA-encoding genes as well as some genes that encode structural or regulatory RNAs. [SAUNDERS2006] RNA Pol II characteristic is it's C-terminal domain (CTD) which consists of 52 tandem hepta-peptide repeats of canonical sequence YSPTSP. To initiate transcription, activity of the TFIIF (CDK7:CycH) factor is required to begin promoter clearance and synthesis of short nascent RNA. These short

transcripts are normally subject to rapid degradation [BENTLEY1995, REINES1999]. After synthesizing 50 ribonucleotides, RNA Pol II is recognized by negative elongation factor (NELF) and DRB-sensitivity inducing factor (DSIF) causing promoter-proximal pausing. To overcome the inhibitory effect of NELF/DSIF and initiate productive elongation, P-TEFb is recruited to the paused/poised RNA Pol II. After phosphorylation of NELF and Spt5 (DSIF subunit), NELF leaves RNA Pol II, DSIF stays and becomes a positive elongation factor.[FUJINAGA2004, KIM2001, PING2001]. P-TEFb phosphorylates Ser2 of CTD, increasing its affinity towards components of splicing and polyadenylation machineries [SIMS2004, FABREGA2003, MARSHALL1992]. Thus, P-TEFb allows the transition into productive elongation, producing long transcripts from which mRNAs are derived. At the end of the transcription cycle, the phosphorylated Pol II is recycled by the action of CTD phosphatases (eg.FCP1) into the hypophosphorylated IIa form, allowing it to participate in a fresh round of transcription [CHO1999, MANDAL2002].
The elongation stage of eukaryotic transcription is highly regulated, critical not only for generating the full length mRNA transcripts but also for the coupling of transcription with other major gene expression events, such as pre-mRNA capping, splicing and polyadenylation [SIMS2004].
The following section shortly explain the steps of RNA Pol II transition from initiation to elongation.

6.1 Promoter-proximal Pausing of the RNA Pol II: the essence of gene regulation for most protein-transcribing genes

Historically, transcription initiation was considered the rate limiting step of the expression of many genes [HOCHHEIMER2003]. however, also early studies showed genes that surpass this concept (C-myc, junB and HSP70) [AIDA2006, BENTLEY1986, ROUGVIE1988] This number of genes nowadays rose to a significant number [MUSE2007, ZEITLINGER2007]. Among these genes are genes involved in development, cellular response to stimuli, cell communication, cell adhesion and differentiation which all demonstrated promoter-proximal RNA Pol II stalling.
This indicated shat P-TEFb might be a primary sensor to various developmental demands - theoretically, P-TEFb could work as a platform capable of accommodating diverse stimuli and respond to them by switching on and off appropriate sets of genes, along with cooperative function of developmental activators and repressors [KOHOUTEK2009].
All together, it seems that elongation block could represent a highly specific controlled step in transcription regulation.
In order for Pol II to enter productive elongation, it must undergo structural and functional maturation. Promoter escape (promoter clearance) describes earliest steps in this maturation process, during which the polymerase breaks its contacts with promoter-sequence elements and at least some promoter bound factors and silmutaneously tightens its grip on the nascent RNA.

Promoter Escape- elongation stage 1

Promoter escape has been shown to be rate-limiting for transcription elongation in vitro, at least for some promoters. The process of promoter escape begins with the onset of transcription initiation at which point the transcription complex is known as the initially transcribing complex (ITC). Promoter escape is considered complete when the nascent RNA associates stably with the transcription complex. The transcription complex is then called an early elongation complex (EEC) that, although stable continues to show characteristics that are distinct from a fully functional elongation complex. In eukaryotes, abortive initiation by PolII is markely reduced on the addition of the fourth nucleotide, but promoter escape is not yet complete. This transition to a metastable transcription complex is often referred to as escape commitment, and occurs quickly compared with subsequent events during promoter escape [KUGEL2000]. EECs are more prone to backtracking and arrest than mature elongation complexes.

Promoter-proximal pausing: elongation stage 2

Promoter proximal pausing or transcriptional stalling is a phenomenon whereby Pol II pauses in the 5′ region of the transcription unit and only progresses efficiently into productive elongation on stimulation by appropriate signals. It constitutes an important step in the regulation of PolII transcription elongation in vivo and functions as a checkpoint before committing to productive elongation. The polymerase can escape rapidly from the pause into the productive elongation phase, and this highly dynamic level of regulation enables the rapid alteration of transcriptional output.[LIS1998] Escape form the pause continues to be a rate limiting and regulatory step after gene induction [GIARDINA1992].
Candidates for pausing control: DRB inhibits transcription elongation but not transcription initiation. DRB sensitivity inducing factor DSIF and negative elongation factor NELF were both required for the inhibition of transcription by DRB in vitro. DSIF and NELF cooperate to repress transcription elongation, and their negative effects can be overcome by the action of a protein that is inhibited by DRB [PRICE2000].

Productive elongation: stage 3

Promoter escape and promoter proximal pausing are the main rate limiting stages of transcription elongation. P-TEFb is required for the production of long transcripts in vitro and for HIV-1 transcription, which is regulated at the level of transcription elongation[BARBORIC2005, PRICE2000]. The observation that tethering CDK9 or CycT1 to promoters activates gene expression also indicates that the recruitment of P-TEFb can be a rate-limiting step for escape to productive elongation in eukaryotes in vivo. P-TEFb localizes to active genes [LIS2000] and its depletion causes defects in gene expression [NI2004, SHIM2002] Furthermore, the inhibition of P-TEFb can globally decrease the

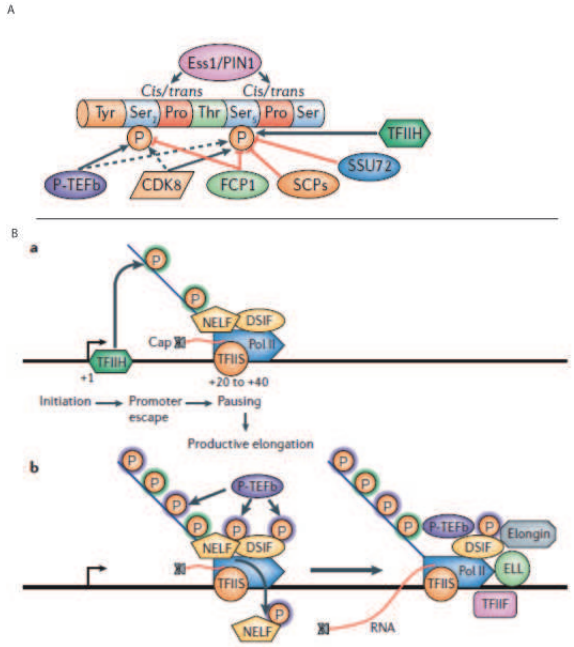

Figure 22: **Transcription factors mediating phosphorylation and the escape of promoter-proximal pausing to productive elongation** (A) Proteins known to regulate phosphorylation status of CTD (B) Promoter-proximal pausing and escape to productive elongation: (a) TFIIH-mediated phosphorylation of Ser5 of the carboxy-terminal domain (CTD) of RNA polymerase II (Pol II) occurs on pre-initiation complex formation or before promoter-proximal pausing. (b) P-TEFb-mediated phosphorylation of DSIF, NELF and Ser2 of the Pol II CTD stimulates productive elongation [SAUNDERS2006]

density of PolII on genes [CHAO2001]. A plausible reason for elongation control is to couple transcription with RNA processing [PRICE2000]. Evidence is mounting that phosphorylation of the CTD allows the recruitment of processing factors, including those involved in capping, polyadenylation, and possibly splicing (reviewed in [BENTLEY1995, MINIVIELLE-SEBASTIA1999]). The large subunit of DSIF stimulates mRNA capping [WEN1999] and phosphorylation of specific residues in the CTD have a differential effect on recruitment and activation of the capping enzyme [HO1999].

6.2 Role of P-TEFb in RNA Processing

P-TEFb has been proposed to mediate the coupling of transcriptional elongation with pre-mRNA splicing. F.ex. CycT1 is known to interact with Tat-SF1 [FONG2000], which is a nuclear protein implicated in stimulating general and HIV-1 transcriptional elongation [CHO1999, KIM1999, LI1998, PARADA1999, ZHOU1998,1996] but also Tat-SF1 is a homologue of the yeast splicing factor CUS2[107] can also interact with the spliceosomal U snRNPs to form a multisubunit complex, which strongly stimulates Pol II elongation when directed to an intron-free DNA template [FONG2001]. Notably, inclusion of splicing signals in the nascent transcript further stimulates transcription, supporting

the notion that the recruitment of U snRNP near the elongating polymerase is important for transcription. Tat-SF1-U snRNP complex stimulates both transcription and splicing, recruitment of this dual function factor to Pol II by P-TEFb is believed to mediate an efficient coupling of transcriptional elongation with splicing.
For the relatively short, intronless genes, such as the human U2 snRNA gene, P-TEFb is not an essential elongation factor [MEDLIN2005]. Rather, it functions exclusively as an RNA-processing factor for recognition of the 3′ box RNA 3′ end processing signal. The role of P-TEFb as an activator of transcriptional elongation can be separated from its role in RNA 3′ end processing.

7 Physiological modulations of P-TEFb activity

Multiple mechanisms have shown to regulate CDK9 kinase activity:

1. CDK9 kinase activity is dependent on association with the CycT subunit [PENG1998,I, II]
2. Phosphorylation on the T-loop by CDK9 itself or another kinase activates the kinase activity [NAPOLITANO2003]
3. LC sequestering [MICHELS2004, NGUYEN2001, YANG2002, YIK2003]
4. positive regulation by Brd4 [YANG2005, JANG2005]
5. acetylation and de-acetylation, acetylation promotes, while de-acytalation by N-CoR/HDAC3 inhibits the elongation function [FU2007]

This equilibrium (amount of large complex) is tightly regulated in the cell naturally/physiologically and serves as one of the key regulating mechanisms of transcription at the phase of elongation.
Recruitment of the SC does not guarantee elongative production per se. Current pattern of post-translational modifications (phosphorylation, acetylation, ubiquitination) of subunits of P-TEFb ultimately decides whether productive elongation will occur.
Besides the inhibition by the large complex, P-TEFb activation or inhibition depends primarily on post-translational modifications of CDK9 and its associated cyclin. These are of great interest with respect to their functions in the regulation of P-TEFb activity in diverse cellular responses (stress, cytokines, cell communication), disease and development.

Certain stress or pathological conditions induce liberation of SC:

1. - PI3K/Akt signaling pathway disrupts LC by phosphorylating Hexim1 on two serine and two threonines in the CycT1 binding domain, after HMBA treatement.[CONTRERAS2007]

2. - UV and HMBA disrupt P-TEFb by cooperative action of Ca2+ calmodulin-protein phosphatase 2B(PP2B) and protein phosphatase 1 (PP1alpha) [CHEN2008]

3. - Ubiquitination of Hexim is not involved in Hexim1 proteasome/mediated protein degradation but rather interferes with inhibition of P-TEFb [LAU2009] Also, Ubiquitination of CycT1 and CDK9 by Skp2 controls its protein turnover and interaction with Tat/TAR respectively. [BARBORIC2005, KIERNAN2001]

4. - Acetylation of CycT1 triggers dissociation from LC and activation [CHO2009] Acetylation of CDK9 on Lys44 located in ATP binding domain by p300/CBP increases its kinase activity to CTD[FU2007]

Phosphorylation, acetylation and ubiquitination participate in regulation of P-TEFb activity.

7.1 Phosphorylation

Phosphorylation of Cyclin and CDK9 is a key feature of P-TEFb regulation in vivo. Several serine and threonine residues at its C-terminus must be phoshoprylated for P-TEFb activity first [FONG2000, GARBER2000], but full activation is completed only after conserved Thr186 in the T-loop is phosphorylated, triggering major conformational changes in the heterodimer (CycT1:CDK9) leading to exposition of ATP binding pocket together with substrate site [LI2005, CHEN2004, BAUMLI2008] Phosphorylation of Thr186 is also a prerequisite for the assembly of the large complex [LI2005, CHEN2004]. Presumably the large complex bears principally active P-TEFb for acetyltransferase release of stored P-TEFb to support transcription of genes involved in given cellular responses.

7.2 Acetylation

Histone acetylation clearly plays a critical role in transcriptional regulation, growing evidence however indicates that acetylation of non-histone proteins also plays a role in histone regulation.
The cell presumably has many physiological ways of obtaining the ideal ratios between the two complexes, but one of them is shown to be by the regulation of acetyltransferase activity. It has been shown indeed that P-TEFb is a substrate of the p300 acetyltransferase, which acetylates CycT1 at four lysines in a predicted coiled-coil domain at the C-terminal domain close to histidines. The balance between inactive and

active P-TEFb is shifted to the inactive form in the absence of CycT1 acetylation. Reversible acetylation of cycT1 is a critical intracellular mechanism by which the association of P-TEFb with its physiological inhibitor hexim1 and 7SKRNA is regulated. Acetylation of cyclin T1 serves as a physiological switch that liberates P-TEFb from its endogenous inhibitors Hexim1 and 7SK snRNA [CHO2009].
N-Cor and its related SMRT protein were identified initially as corepressors for nuclear receptors such as thyroid hormone receptors (TR) and retinoic acid receptors (RAR) [CHEN1995, HORLEIN1995]. These proteins are implicated in in repression by many different transcription factors (see [GLASS2000] for review]. Repression mediated by SMRT and N-CoR is sensitive to trichostatin A (TSA), a histone deacetylase (HDAC) inhibitor. SMRT and N-CoR have been reported to associate with a number of HDACs [HEINZEL1997, HUANG2000, KAO2000, NAGY1997]. Among N-CoR associated proteins, HEXIM1 was identified. A subfraction of N-CoR is associated with HEXIM1/P-TEFb [FU2007]. They also found that CDK9 within the P-TEFb complex is acetylated in vivo. K44 seems to be the site. Kinase activity of K44R mutant was significantly crippled compared to that of WT CDK9. I.e. kinase activity of P-TEFb is regulated by acetylation of the CDK9 subunit. This also affects transcriptional elongation activity [FU2007]. Targeting components of the N-CoR complex to the HIV LTR reporter suppresses transcriptional elongation.

7.3 P-TEFb specificity

Only a specific subset of P-TEFb-dependent genes are transcribed in response to a given intra or extracellular stimuli. There is two important mechanisms which help P-TEFb to decide which genes should be turned on or off:

- A layer of control is provided by functional interaction with **specific cofactors** (chromatin remodeling complexes, mediators) bound at transcription sites. Once P-TEFb is recruited to the promoter, it is exposed to interactions with other multiprotein complexes and to their catalytic activities resulting in post-translational modifications triggering activation or inhibition of P-TEFb activity.

- The other one is the result of cooperative effect of **signaling pathways** regulating P-TEFb activity. Signaling pathways serve, most likely, two primary functions in P-TEFb biology: first to trigger release from the LC, second to target and modify components of P-TEFb complexes.

P-TEFb presumably achieves its broad binding capacity towards myriad transcription factors by the variety of complexes it has. There is 8 different complexes of active P-TEFb and 16 for inactive complexes.

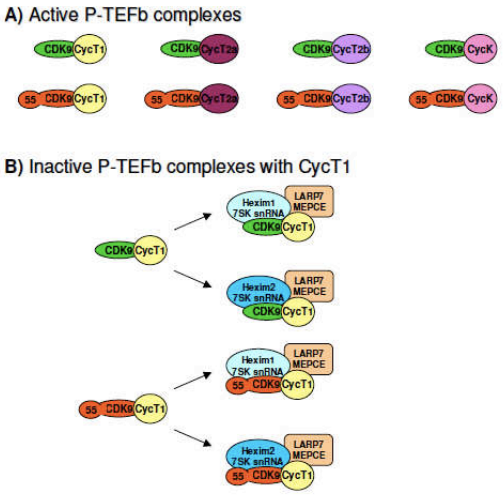

Figure 23: **Active and inactive P-TEFb complexes** (A) Active PTEFb complexes. CDK942 (green oval) and CDK955 (orange oval) can separately bind to individual CycT1 (yellow circle), CycT2a (violet oval), CycT2b (lavender oval) and CycK (pink oval). (B) Inactive P-TEFb complexes with CycT1. Only large complexes with CycT1 are presented for illustration, but the same would apply for CycT2a, CycT2b and CycK too. Complexes of 42- and CDK955 with CycT1 are presented at the left side. 'Large' complexes consisting of CDK9/CycT1 are at the right side. Hexim1/7SK snRNA (light blue oval), Hexim2/ 7SK snRNA (turquoise blue oval), MEPCE/LARP7 (light orange oval) [KOHOUTEK2009]

7.4 P-TEFb regulation in cell cycle

Each phase or intercalating transition of the cell cycle is controlled by spatio-temporal expression of CDKs and appropriate cyclins, but the case of CDK9 and C-type cyclins, levels and association of CDK9 kinase activity remains unchanged, and no dramatical fluctuations. [GRANA1994]
At this point, it is believed that Brd4 can provide information on the function of P-TEFb in cell cycle control, since it is implicated in transition of epigenetic memory through binding to acetylated histones [JANG2005, YANG2005, MOCHIZUKI2008]. Indeed, a dramatic increase in P-TEFb-Brd4 interaction was observed from late mitosis to early G1 phases of the cell cycle and active recruitment of P-TEFb to the chromosomes, followed by initiation of transcription of key genes for G1 progression. [YANG2008].
Also, silencing of CDK9 in cells by RNA interference led to enrichment of cells in G1 phase of cell cycle supporting function of P-TEFb in the G1/S transition. Since CDK9 has a strong kinase activity towards pRB, but not histone1, this finding suggests its involvement in the G1/S transition [LUCA1997, BETTENCOURT-DIAS2004].

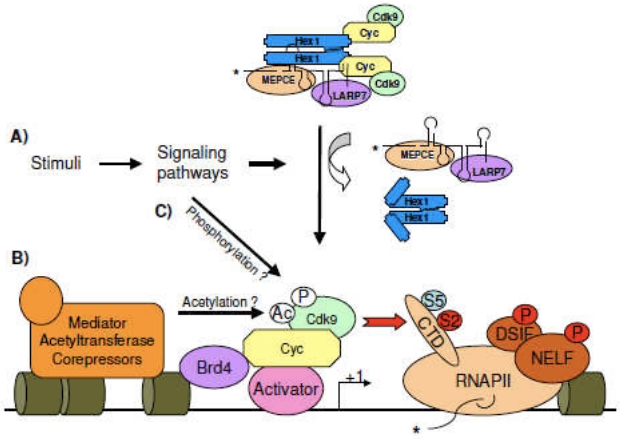

Figure 24: **Regulation of P-TEFb activity during transcription** (A) P-TEFb is inactivated in the large complex. After given stimuli (UV radiation, cytokines, hypertrophic signals), active P-TEFb is released from the large complex by activity of signaling pathways downstream of these stimuli. Then, P-TEFb is recruited to the responsive promoter/s either by a specific activator (pink oval) such as MyoD or a co-activator, such as Brd4 (violet oval). P-TEFb is engaged at the promoters with poised RNAPII phosphorylated on Ser5 (light blue oval with letter S5) in CTD mediated by TFIIH. P-TEFb initiates transcription elongation by phosphorylating Ser2 of CTD in RNAPII (red oval with letter S2), DSIF or NELF (red ovals with letter P). Still, activity of P-TEFb can be controlled by two additional mechanisms. (B) If there is a co-factor (acetyltransferase, mediator, corepressor) associating with P-TEFb at the promoter, then the activity of P-TEFb will depend on particular post-translational modifications mediated by these co-factors, for example acetylation of Lys44 and 48 in CDK9 (white oval with letters Ac). C) Also, signaling pathways activated by given stimuli can modify components of the small complex, for example phosphorylation of CDK9 on Thr28 and Thr186 (white oval with letter P), and additionally modulate final activity of P-TEFb. Khaki barrels represent nucleosomes, and +1 depicts transcription start site.) [KOHOUTEK2009]

8 Inhibition of P-TEFb activity: Concentration speculations

Inhibitors of P-TEFb such as DRB and flavopiridol inhibit transcription by RNA polymerase II and cause apoptosis in a variety of cell lines and tumors [KELLAND2000, PRICE2000, CHANG1997, DE FALCO1998]. A fundamental question for the use of CDK9 inhibitors as drugs is to what extent CDK9 inhibition, especially for chronic indications, will be compatible with normal cellular functions in a way that does not elicit toxicity.
Many studies have shown that CTD independent general transcription factor mediated initiation and RNA synthesis in vitro is possible. P-TEFb is the main processivity effector, but in fact it has not yet been shown rigorously if/to what extent CDK9 is redundant for transcription in general [WANG2008].

8.1 Flavopiridol

Flavopiridol has been shown to inhibit a number of CDKs [SENDEROWITZ2000]. Under appropriate conditions it can be used to selectively inhibit P-TEFb. Flavopiridol inhibition of P-TEFb is not competitive with ATP.[CHAO2000], since kinetic analysis best fit an uncompetitive model - flavopiridol binds to the ATP site of Cdk9 very tightly and consequently inactivates the enzyme [CHAO2000]. Flavopiridol docks in the ATP-binding site. Treatement results in blockage of cell cycle progression, promotes differentiation and induces apoptosis in various types of cancerous cells [SENDEROWICZ2000]. Nuclear run-on assays were performed to determine extend of inhibition of RNA PolII in vivo at flavopiridol concentrations that ranged from those likely to be effective against HIV to those used in chemotherapy. For each flavopiridol titration the IC50 value calculated was roughly half of the concentration of P-TEFb. As a control, using DRB as the kinase inhibitor, the tight correlation between the drug and the enzyme concentration was not observed. High salt concentrations break DRB- P-TEFb interaction, but not flavopiridol, indicating that this interaction is based on hydrophobic contacts.
The anti-profilerative effect of flavopiridol is mediated through P-TEFb inhibition. The best evidence for this comes from a screen for compounds that block HIV Tat transactivation, which uncovered a number of P-TEFb inhibitors [MANCEBO1997].

9 Brd4 recruits P-TEFb to cellular genes

Several gene specific regulators have been shown to interact with P-TEFb [GARRIGA2004], but activators do not ubiquitously recruit P-TEFb.[LIS2000]. In human cells, the bromodomain-containing protein BRD4 is presumed to be responsible for recruitment of P-TEFb to most genes through its interacting with acetylated histones [JANG2005] - this is why HDAC is not a good analog to DRB].

Brd4, a ubiquitously expressed nuclear protein of 200kDa, belongs to the conserved BET protein family [DEY2000] whose members contain two tandem bromodomains and a single extra terminal domain [JEANMOUGIN1997] The bromodomain has been recognized as a functional module to help decipher the histone code through interacting with acetylated histone tails [ZENG2002] Brd4 has been shown to bind actively transcribed chromatin regions through a direct interaction with acetylated histone H3 and H4 [DEY2003]. Brd4 also remains bound to chromatin during mitosis, suggesting a possible role for this protein in transmitting epigenetic memory across cell division [DEY2003,2000].

The Brd4 molecule interacts with P-TEFb through its double bromodomain, and this interaction enhances P-TEFb dependent phosphorylation of the Pol II CTD and transcriptional activation [SERIZAWA1993, KLEBL2006].

Functional analyses have demonstrated that the Brd4 bound P-TEFb represents the transcriptionally active form of P-TEFb that is capable of phosphorylating the CTD and stimulating elongation in vivo and in vitro [JANG2005, YANG2005]. Domain analysis indicates that the two bromodomains of Brd4, which are known to bind to acetylated histones, are also required for the Brd4-P-TEFb interaction in vivo. On the P-TEFb side, CycT1 but not CDK9 is able to interact with Brd4 in vitro as a glutathione S-transferase fusion protein [JANG2005].

It is not clear whether Brd4 is released from P-TEFb or whether it tracks along with P-TEFb and the elongating PolII once it has recruited P-TEFb to the template. So far, it seems it is the free P-TEFb that is probably involved in the actual elongation process. Recruitment role of Brd4 can be functionally fulfilled by Tat which directly recruits P-TEFb to the HIV-1 LTR through formation of the Tat-TAR-P-TEFb ternary complex [JANG2005, YANG2005].

Brd4 has been implicated in playing a growth-stimulatory role. Mice lacking both alleles of Brd4 gene are lethal to embryos, Brd4 heterozygotic mice display pre and postnatal growth defects associated with a reduced proliferation rate [HOUZELSTEIN2002]. In primary cell cultures, heterozygous cells also display reduced proliferation rates. Brd4 is also required for the proper progression of the cell cycle.

10 Clinical Implications of P-TEFb as a target molecule

Unlike other CDKs, CDK9 does not regulate cell cycle, but promotes RNA synthesis in genetic programs for cell growth, differentiation and viral pathogenesis. As a result of this, deregulation of P-TEFb activity naturally manifests itself in pathological phenotypes.

Portraying the crucial importance of P-TEFb in development, both C. elegans and Drosophila organisms prove lethality at the embryological stage by inactivation or knockdown of P-TEFb [SHIM2002, EISSENBERG2007]. Ectopic activation of P-TEFb exhibits dramatic consequences for normal development also. Cardiac hypertrophy (in mouse) [HUANG2004] and aberrant splicing (in zebra fish) (suggesting a fundamental role for

P-TEFb in coupling transcription elongation with alternative splicing) [BARBORIC2009], were both caused by depletion of P-TEFb large complex.
In an experiment, [KOHOUTEK2009 I] RNAi approach was used to downregulate CycT1 or CycT2 and check for changes in the expression of of genes influenced by the depletion by microarrays. Following results were found:

1. CycT2 reduction affected genes participating in the TGFbeta and Wnt signaling pathways, and autophagy. inner cell mass and trophoectoderm during embryogenesis expression. ubiquitin-proteasomal system, Likewise, it showed to be indispensable for rapid degradation of maternal protein during transition from oocytes to embryos.

2. CycT1 knock down decreased expression of genes involved in fatty acid and glucose metabolism, cell communication and cell cycle.

Glucose metabolism was affected in both cases, but targeted genes were different.

10.1 Oncology

Resistance to apoptosis is a general hall mark of cancer [HANAHAN2000]. As a rule, oncogenic transformation involves multiple successive genetic modifications that together promote cell survival, and the final transformed tumor genotype, therefore, frequently includes up-regulated anti-apoptoctic and pro-survival components that must be sustained by continuous RNA Pol II activity [KOUMENIS1997]. This opens a therapeutic window for the use of transcriptional inhibitors in cancer. Untransformed cells have a significant tolerance towards transient inhibition of RNA Pol II activity, whereas a transformed cell would be much more susceptible to this inhibition and would undergo caspase-induced apoptotic death [WANG2008].
A study [STONE2003] focused on identification of novel tumor antigens associated with serous ovarian cancer identified 9 immunogenic antigens, among them Hexim1, to be potential targets for immunotherapy (by SEREX immunoscreening). After, in studies of mixed-lineage leukemia (MLL) fusion proteins in leukemic transformation, another group found that the gene for the histone methyltransferase MLL often participates in chromosomal translocations that eventually create MLL fusion proteins associated with very aggressive forms of childhood acute leukemia[HESS2004, SLANY2005]. Two proteins(AF4 and ENL), common associating partners of MLL in childhood acute leukemia were found to bind and utilize P-TEFb for their transformation properties [BITOUN2007, MUELLER2007]. All this indicates that therapies involving inhibition of P-TEFb activity might be an option.
As an example of the P-TEFb deregulation, Hexim1 has been shown to bind estrogen receptor alpha through its basic region and block ERalpha mediated gene expression [WITTMANN2005]. Over expression of Hexim suppressed proliferation of breast cells. Indeed Hexim1 was down regulated in samples from invasive breast cancer patients in

comparison to Hexim1 level in normal breast tissue [WITTMANN2003].
In chronic lymphocytic leukemia (CLL), unlike in most other cancers, transformation does not involve an aberrant cell cycle. CLL cells are mostly accumulated mature B cells in G0/G1 phase [KITADA1998]. Clinical activity with a CDK inhibitor were reported here with flavopiridol: marked efficacy in refractory genetically high risk CLL was observed with the drug [CHRISTIAN2007]. In vitro studies of CLL patient samples reveal flavopiridol inhibits CTD phosphorylation, leading to reduced RNA synthesis and a decline of short-lived anti-apoptotic proteins, especially Mcl-1 and X-linked inhibitor of apoptosis (XIAP), which ultimately results in reinstatement of the ability of CLL cells to undergo apoptosis. Also, flavopiridol has been demonstrated to induce apoptosis by activating caspase-3, which cleaves poly(ADP-ribose) polymerase and commits CLL cells to p53-independent apoptosis [BYRD1998]. Indeed, Mcl-1 down-regulation alone is sufficient to promote mitochondrial membrane depolarization and apoptosis in acute lymphocytic leukemia (ALL) and CLL cells [HUSSAIN2007].

Larp7 C-terminus is often deleted in human tumors suggesting that activation of P-TEFb mediated by LARP7 destabilization of large complex is important for proliferation and tumorigenicity of cancer cells. [HE2008]. Genetic inactivation of MXC (drosophila homologue of LARP7) resulted in overgrowth of lymph glands and hematocyte over-proliferation [REMILLEUX-LESCHELLE2002].
Thus, generally it is likely that ectopic activation of P-TEFb in cancer cells serves to support transcription of key tumor-progressing genes, unchecked proliferation ultimately converging in tumorigenesis.[KOHOUTEK2009] In breast cancer, activation of SC seemed sufficient to promote malignant transformation [HE2008]. But in acute childhood leukemia, simple activation has no effect - rather misplaced recruitment of P-TEFb through oncogenic chimeric proteins (MLL-ENL) is the driving force. In heart, ectopic expression also didn't lead to tumor formation. This all implies the existence of a buffering mechanism in cells to deal with elevated P-TEFb activity.

10.2 Virology

The main motivation underlying the search for suitable host targets for antiviral chemotherapy is the expectation that this strategy might prevent the rapid emergence of resistance observed with many drugs that directly target genetically flexible viruses [WANG2008]
Active P-TEFb recruitment has also been reported for B-cell cancer-associated Epstein-Barr virus by nuclear antigen EBNA2 [BARK-JONES2006] and for T-lyphotropic virus type1 by the transriptional activator Tax [ZHOU2006].
Two questions are important: [WANG2008]
1. Is transcription of the viral genome selectively sensitive to CDK9 inhibition
2. Are cells of the immune system able to tolerate CDK9 inhibition since it appears to be important in the activation and differentiation of both Ba and T cells.
It was shown by [BIGLIONE2007] that DRB flavopiridol and roscovitine despite be-

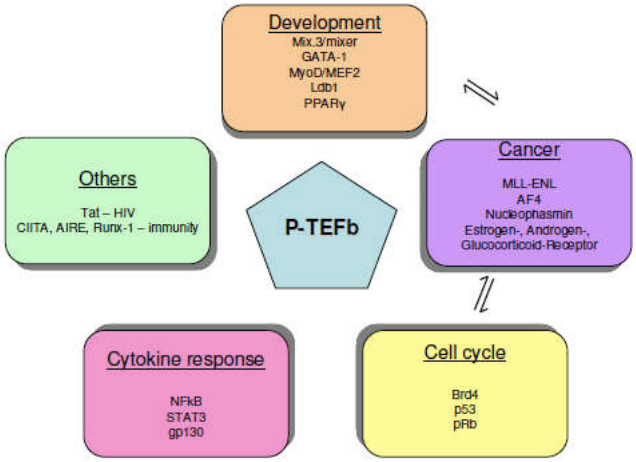

Figure 25: **Role of P-TEFb in a broad spectrum of biological processes** P-TEFb (blue pentagon) participates in many different biological processes, such as development (light orange oval), cancer (violet oval), cell cycle (yellow oval), cytokine response (pink oval) and others (green oval). Abbreviations in each oval represent particular transcription factors which have been found to employ P-TEFb in given biological phenomena (more information in the text). Importantly, misregulation of P-TEFb-dependent transcription factors involved in development or cell cycle could also significantly contribute to malignant transformation of normal cells, as depicted by arrows in this figure. [KOHOUTEK2009]

ing incompletely CDK9 selective, can block HIV-1 replication at concentrations that are not cytotoxic. [SALERNO2007] showed also that it's possible to inhibit CDK9 activity pharmacologically at a level that results in effective blocking of viral transcription and replication but that does not significantly affect T-cell activation.

10.3 Tat recruits P-TEFb to the TAR element in HIV transcription

Tat is a small protein encoded by HIV and other lentivirus genomes that is required to activate the promoter contained within the viral LTR. This strong trans-activator is targeted to the viral promoter through interaction with a region of the nascent RNA transcript called TAR. Tat associates with a three nucleotide bulge in the stem of a hairpin structure that forms spontaneously in TAR. The functional consequence of this association is the enhancement of processivity of RNA Pol II molecules initiating from the LTR such that long primary transcripts are produced [KAO1987, LASPIA1993, MARCINIAK1991, TOOHEY1989]. These transcripts in turn are differentially spliced to form all viral gene products. In the absence of Tat, short abortive transcripts that encode no proteins are predominately produced [KAO1987] The enhancement of processivity brought about by Tat requires at least one cellular cofactor: the P-TEFb. Only CycT1 can support Tat transactivation, T2a and T2b do not [NAPOLITANO1999, WIMMER1999] nor does CycK since it lacks the cysteine residue at position of 261 of cycline T1 that is required

for a zinc-dependent interaction between CycT1 and HIV-1 Tat. Evidence suggests that also another region on the amino-terminal side of the cyclin box (amino acid 29) is important for recognition of TAR [TAUBE2001]
Tat is able to accomplish this by recruiting P-TEFb to the 5'end of the nascent viral transcript (nucleotides +1 to +59), which forms a stem-loop RNA structure called the trans-acting response (TAR) RNA element. Tat specifically binds to the TAR RNA at the three nucleotide bulge and several flanking nucleotides in the double-stranded RNA stem just below the apical loop. CycT1 of P-TEFb recognizes specific residues in the apical loop of the TAR RNA while Tat also interacts directly with CycT1 near its cyclin box region. Tat, TAR, and P-TEFb allow the formation of a stable ternary complex that results in the recruitment of P-TEFb to the vicinity of the stalled PolII where it can phosphorylate the CTD and lead to elongation.

Transcription from the HIV promoter requires the recruitment of P-TEFb through its association with Tat-bound to the nascent TAR RNA [PETERLIN2006, BANNWARTH2005, BRADY2005] In contrast to LC, the P-TEFb/Tat/TAR complex is active [ZHOU2000] The basic Tat sequence involved in TAR binding is highly similar to the basic HEXIM1 sequence involved in 7SK binding [YIK2004].

Tat/P-TEFb transactivation is unique in that Tat induces P-TEFb to phosphorylate the CTD at both Ser2 and Ser5 positions and promotes pre-mRNA 5'-end capping [ZHOU2006, SAUNDERS2006]. Recently, phosphorylation of Thr29 in CDK9(42) within the HIV elongation complex was able to block transcription of viral RNAs. [ZHOU2009].
Given the importance of p300/CBP in the acetylation of Tat and activation of HIV transcription, it is not surprising that the HIV virus utilizes the same acetyl transferase complex to acetylate Tat in order to stabilize formation of Tat-P-TEFb-TAR complex to initiate viral transcription [OTT1999]. Therefore, it seems that the virus intentionally subverts natural cellular cofactors of P-TEFb to support its own replication cycle.
An interesting lentiviral vector has recently been engineered associating four different cassettes including U6, 7SK and two RNA PolII promoters driving four different shRNA sequences [BRAKE2008] This vector has been used to efficiently down-regulate HIV-1 that escapes single shRNA inhibition.
Recognition by the Tat viral protein of the TAR RNA is one of the first case of RNA/protein couple reported to control eukaryotic transcription [BERKHOUT1989].

10.4 Cardiology

Cancer is characterized by hyperplasia, but many forms of heart disease display hypertrophy (increase of size of terminally differentiated cardiomyocytes.) Cardiac hypertrophy occurs as a result of intrinsic haemodynamic stress, f.ex. as a result of diminished heart function in myocardial infarction, as well as in response to extrinsic biomechanical stress, typically as a result of hypertension. Although the hypertrophic response is initially beneficial adaptation to pathological stress from cardiovascular disease, in long term this response becomes decompensated and can lead to heart fail-

ure, at least in part though apoptotic and necrotic cell death. [CLERK2007]. There is evidence that hypertrophy increases the risk of cardiac morbidity and mortality [ESPOSITO2002, GARDIN2004], and inhibition of hypertrophy is beneficial in this respect [GARDIN2004]. Hypertrophy is characterized by global increases in mRNA and protein synthesis, and thus depression of CDK9 rather than CDK7 has shown to be limiting for cardiac hypertrophy [SANO2002]. On the basis of this, CDK9 has been proposed as a relevant drug target, either directly though its kinase function or in the pathway leading to CDK9 activation through dissociation of LC in the heart [KULKARNI2004, SANO2004].

Part IV

Nuclear Targeting of P-TEFb: Results and Discussion

Transcription factors that interact with macromolecular complexes on chromatin exhibit high mobilities within the nucleus, transiently and repetitively contacting their target sites. The research project described in this thesis sets out to investigate dynamics of general transcription factor P-TEFb.
P-TEFb is a heterodimer consisting of subunits CycT1 and Cdk9 [PENG1998, PETERLIN2006, PRICE2006] which in its active form phosphorylates the Ser5 residues on the CTD of Pol II and the negative transcription elongation factors NELF and DSIIF [MARSHALL1996, PENG1996], causing Pol II to switch from initiation to elongation phase [OTERO1999].
P-TEFb is considered a general transcription factor crucial to the transcription of most genes [CHAO2001, PRICE2001, SHIM2002]. It exists in two forms, the heterodimer alone and an catalytically inactive complex sequestered in 7SK snRNP. The catalytically inactive complex, 7SK snRNP, consists of the snRNA 7SK, Hexim1 [NGUYEN2001,YANG2001, MICHELS2003] and Larp7 (PIP7S) [HE2008]. The the two forms associate in a specific and reversible manner [NGUYEN2001]. Any inhibition of transcription, such as drugs or UV treatement triggers the breakdown of the 7SK complex and promotes accumulation of free P-TEFb [NGUYEN2001]. Likewise, it is possible to break down the large complex by 7SK RNA interference.
P-TEFb exists intracellularly in a dynamic equilibrium with its inactive form at $\sim$50% in HeLa cells [NGUYEN2001]. The ability to shift the equilibrium reversibly by intracellular signalling, stress or pathological conditions [CONTRERAS2007, CHEN2008, BARBORIC2005, KIERNAN2001, FU2007] indicates a highly regulated mechanisms of the equilibrium. This high regulation is not explainable enzymatically - by rendering $\sim$50% of the enzyme inactive, one does not limit it's activity with a significant degree.
Here with we pose the question of whether the mobility and changes therein could present a form of control of the activity of P-TEFb.
In order to study P-TEFb dynamics in the nucleus by in vivo imaging, a fusion protein of CycT1 was constructed with a GFP-tag at its N-terminus. The co-existence of the fusion protein with Cdk9 and its ability to phosphorylate the CTD of the RNA Pol II has been tested in vitro. The small active complex has a size of $\sim$ 70kDa, while the large has a size of $\sim$ 120kDa. GFP has a size of $\sim$ 30kDa; by which size-related effects of the GFP fusion protein on diffusion are not expected, since the relation of size scales as the cube root of mass.
A stable U2OS cell line expressing CycT1-GFP was constructed. The Western blot (Figure 27A) shows levels of endogenous CycT1 and the fusion protein expressed in our stable cell line being amplified by approximatively a factor of two. Immunoprecipita-

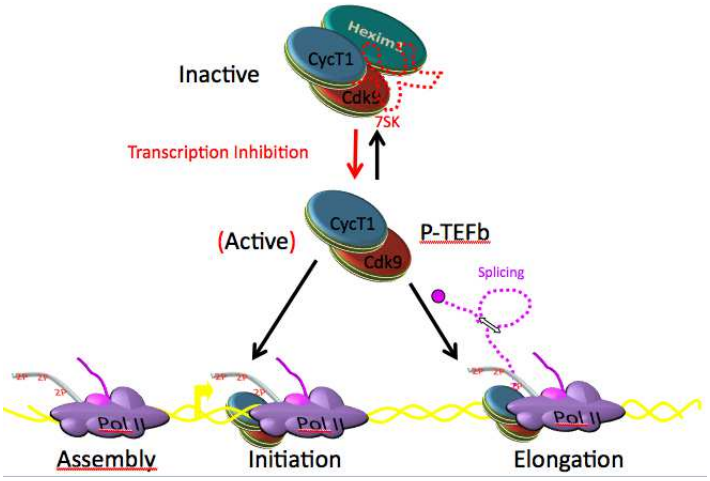

Figure 26: **Schematic drawing of the P-TEFb equilibrium** The small and large complexes co-exist in dynamic equilibrium. Upon transcription inhibition, the large complex is broken down in favor of the small complex, probably through a feedback mechanism from the paused RNA Pol II.

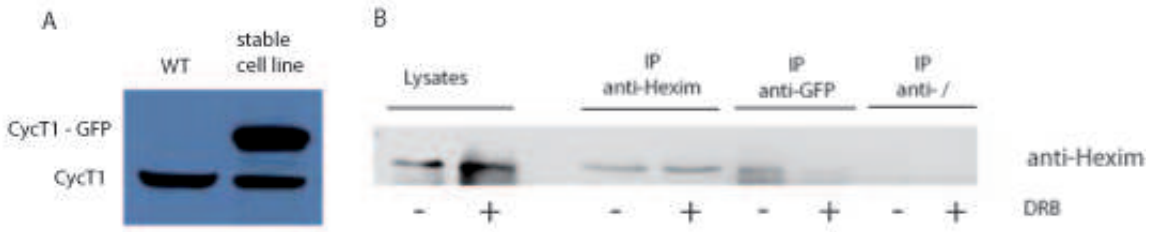

Figure 27: **Biochemistry of the CycT1-GFP construct** (A) Western blot showing exogenous expression of CycT1-GFP and the endogenous CycT1. (B) Immunoperciptation of CycT1-GFP with Hexim: by inhibiting transcription with DRB, the 7SK snRNP complex breaks down in favor of the small complex of P-TEFb, shown by the inability to co-immunoprecipitate Hexim with CycT1-GFP after DRB treatement.

tion of Hexim (Figure 27B) shows the breakdown of the large complex upon treatement with 5,6-dichlororibofuranosylbenzimidazole (DRB); a drug that inhibits the kinase Cdk9 specifically by competitive inhibition, and thereby stops transcriptional elongation. Thus, the fusion protein exhibits same trends of behaviour as endogenous CycT1 in response to treatement with DRB.

In order to understand the dynamics of the system, it is necessary to investigate it in both scenarios of the population ensemble behaviour and the single molecule level. The subsequent sections will provide an insight into the methods and results of the two approaches.

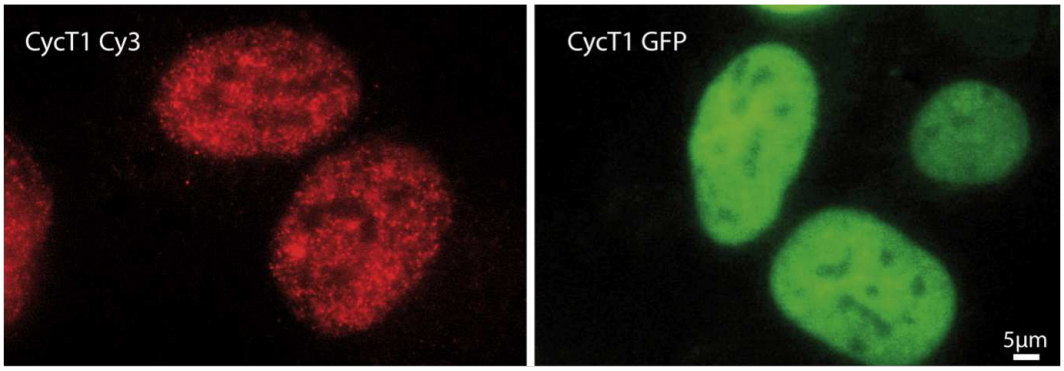

Figure 28: **Endogenous and exogenous CycT1 distribution** Immunofluorescence image of P-TEFb(left) and a CycT1-GFP stable cell line(right)

11 The mobility of P-TEFb ensemble molecules

Macroscopically, P-TEFb is distributed homogeneously throughout the nucleus, with the exception of nucleoli (Figure 28). We set out to investigate population dynamics and redistribution of P-TEFb in the nucleus by methods of FRAP and FLIP.

11.1 Fluorescence Recovery After Photobleaching

Investigating P-TEFb dynamics in the nucleus, fluorescence recovery by photobleaching (FRAP) measurements were conducted on the stable cell line expressing fluorescent CycT1-GFP. The FRAP curve shows full recovery and rapidly exchanging P-TEFb of a half-life $\sim 700ms$. By default, a bleach of $\sim 1\mu m$ diameter leads to a full recovery in $\sim 1s$ for a system with freely diffusing protein [STAVREVA2004].

By bleaching spots of different sizes and monitoring the fluorescence recovery in the smallest region common to all of these, one can determine the nature of the diffusion of the system.

In the case of P-TEFb, the recovery curves of different radii overlap fully (Figure 29B) - diagnosing a diffusion unlimited system, i.e. where diffusion is fast in comparison with binding and can thus be ignored. This is due to the ubiquitous exchange of fluorophores at their stationary binding sites all over the bleached area. In this case, the recovery will depend uniquely on the binding dynamics, and not on the distance from the bleach to the area of recovery observation.[2]

[2]See (Figure 9) for an explanatory diagram

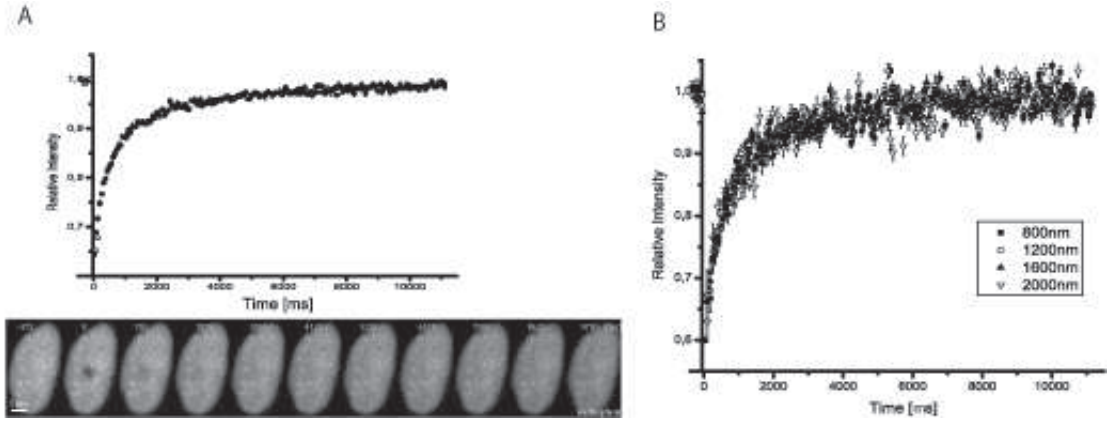

Figure 29: **Fluorescence Recovery After Photobleaching of CycT1-GFP in Nucleoplasm** (A)The FRAP experiment on CycT1-GFP. The curve shows full recovery with a half-life of $\sim 700ms$. (B) FRAP experiments conducted on bleach spots of different radii, showing recovery monitored at the minimal radius (800nm in this case). Overlapping curves signify a diffusion-unlimited system.

11.1.1 Quantifying the FRAP

The type of diffusion unlimited behaviour that our FRAP curve exhibits can be sorted into the reaction-dominant domain, since its recovery will depend only on binding. [BULINSKY2001] demonstrated analytically that rate constant for FRAP recovery is identical to the dissociation rate k_{off}.
In a simple reaction with a single binding step to the substrate:

$$F + S \underset{k_{off}}{\overset{k_{on}}{\rightleftharpoons}} C$$

where F, S and C denote the concentrations of the free protein, vacant binding sites and bound complex respectively. Then, in the reaction dominant case, the fluorescence recovery will depend on the dissociation rate of the protein from it's binding sites:

$$F(t) = 1 - C_{eq} exp(-k_{off})$$

such that the fit to the FRAP recovery yields k^*_{on} and k_{off}; since:

$$C_{eq} = \frac{k^*_{on}}{k^*_{on} + k_{off}}$$

. Here, it is assumed that the system is in equilibrium before photo-bleach and that binding substrates are immobile. Since the amount of binding sites is considered constant, the pseudo-association rate is directly proportional to the real association rate, since $k^*_{on} = k_{on} S_{eq}$.
Analyzing our FRAP curves, we are able to fit the results with two exponentials presenting two differently recovering populations of fluorophores. The dissociation rates of the slow and fast turnover populations were found to be have values of $k_{off-slow} =$

$0.03807ms^{-1}$ and $k_{off-fast} = 0.004653ms^{-1}$ with magnitudes of 60 and 40% respectively (Figure(31)). The residence times are herewith $26.2ms$ and $214.9ms$ respectively. These values stand for extremely high turnover rates when compared to RNA PolII ($2 - 280ms^{-1}$)[DARZACQ2007]. Also, the values are very comparable to the recoveries of other transcriptional activators [KARPOVA2008, MCNALLY2000, SHARP2006, RAYASAM2005, BOSISIO2006], thus CycT1 exhibits an comparable dissociation rates to f.ex. the one of NF-κB and other transcription factors[3].
Consistently, the $log(k_{off-slow}) = -3.6$ and $log(k_{off-fast}) = -5.7$ values lie in the reaction-dominant regime in the scheme of [SPRAGUE2004] in the field domain of the association and disocciation values where the model can be reduced to the simpler reaction-dominant case (see Figure(10)) and enables k^*_{on} values in the range of $0.1 - 100ms$ [SPRAGUE2006].
Furthermore, the two values obtained for the dissociation constant suggest two different natures of binding, where one could be specific binding to substrates, and the other unspecific binding which could be a prequisite to the specific.

11.2 Addressing Binding

Having established the reaction-dominant nature of P-TEFb, we proceed to address the specific binding and exchange of P-TEFb at active transcription sites. FRAP was conducted on a multiple gene array. The SJ cell line contains $\sim$ 200 copies of a gene cassette which enables visualizing of the gene array by marcation of LacI, monitoring of transcription by tagging of produced mRNA stem loops and visualization of produced protein by its accumulation peroxisomes. The system gives an amplification of the heterogeneously distributed active genes, such that one sees a clear accumulation of P-TEFb at the site (Figure 44). Upon bleaching, the recorded recovery curve shows rapidly exchanging P-TEFb with a half-life at $\sim 900ms$, confirming the high turnover rates predicted for transcription factors (Figure 30). A marked difference of $\sim$200ms in the half-recovery is found between heterogeneously distributed binding sites, and the homogeneous concentrated binding sites, where the recovery is delayed in the latter. this suggests that P-TEFb is immobilized onto high-affinity active transcription sites for longer than onto average genomic sites that contain unspecific as well as specific binding substrates.

Since an increase in binding sites does not change the dissociation rates, we can fit FRAP recoveries obtained on the active site with mass action equations. Herewith we obtain that the amount of slow turnover dissociation population has decreased by 10% at the expense of the faster turnover (Figure 31).[4] This suggests that binding plays an important role in the dynamics of P-TEFb. Furthermore, we may extend the argument that the slow dissociation constant represents the more stable specific binding of P-

[3] see review of [DARZACQ2009] for an exhaustive list

[4] By measuring parameters of the gene array such as density of binding sites and its dimensions, one can find approximations for the association constant also by using $k^*_{on} = Seqk_{on}$ and $C_{eq} = k^*_{on}/(k^*_{on} + k_{off})$.

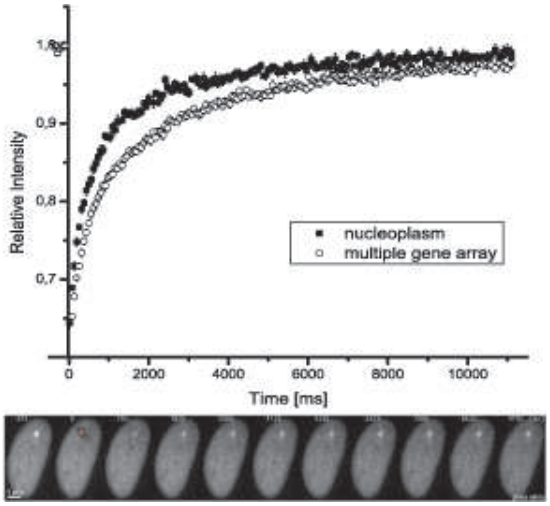

Figure 30: **FRAP of CycT1-GFP at the active gene array** The FRAP recovery after bleaching CycT1-GFP on the active gene array at the SJ cells. The curve is superimposed on the recovery obtained when bleaching nucleoplasm with homogeneously distributed binding sites. Binding clearly has the effect of attenuating the mobility of CycT1.

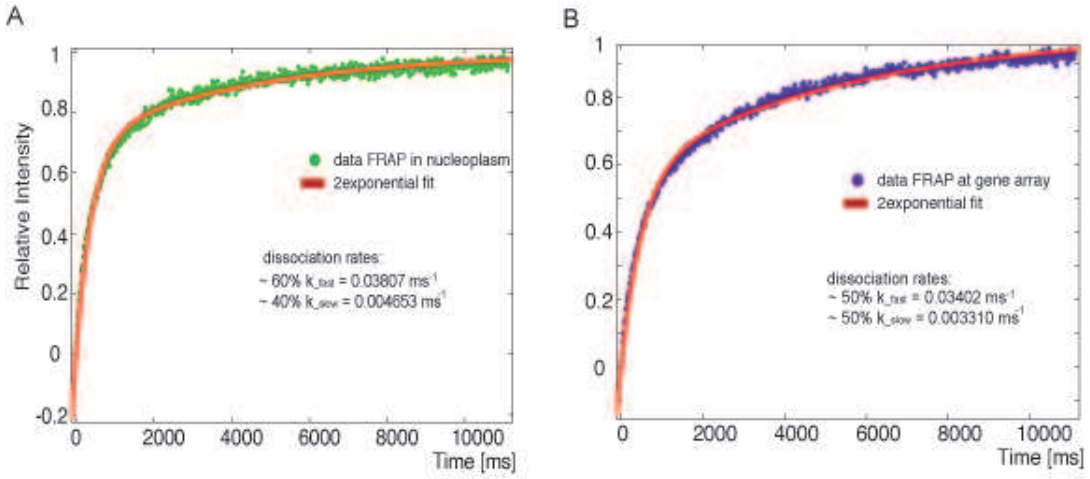

Figure 31: **Two exponential fits of FRAP recoveries in Nucleoplasm and the Active Gene Array** (A) bleach in the nucleoplasm and (B) bleaching at the active gene array. The population with the slow dissociation constant increases at higher concentrations of binding sites. The two speeds of recovery are comparable.

TEFb onto its substrate.

To confirm that dissociation constants obtained from the FRAP recoveries are identical, we refitted the two curves fixing them to their mutual average, and letting the population proportions vary. The result is shown in (Figure 32). Herewith, we observe that the population of molecules with slow dissociation constants rises by ≈15%.

The effect of DRB was tested for effects on FRAP curves for both cases in the nucleo-

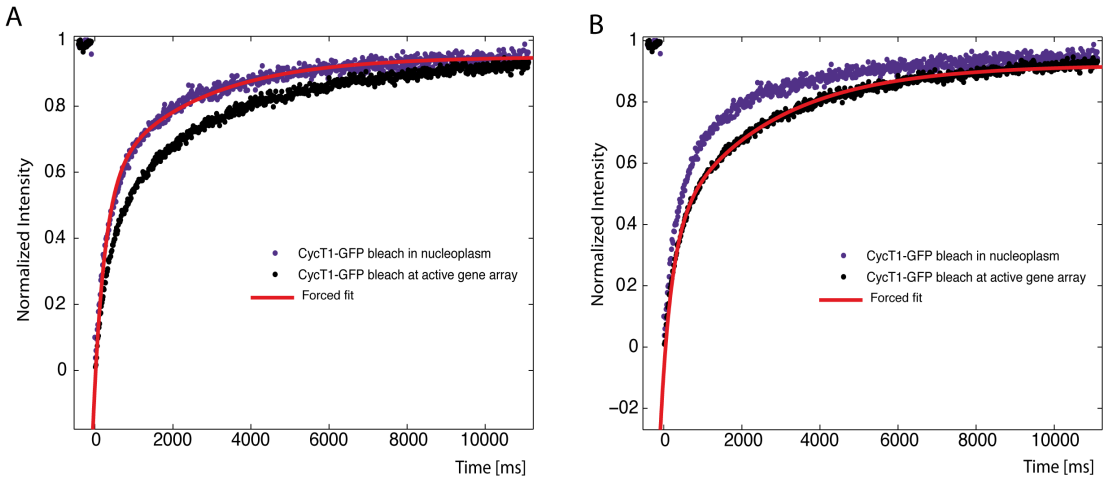

Figure 32: **Exponential fits of FRAP recoveries in Nucleoplasm and the Active Gene Array fixed at their average dissociation constants** (A) bleach in the nucleoplasm and (B) bleaching at the active gene array show good fits to the same dissociation constants of $k_{off-slow} = 0.03558ms^{-1}$ and $k_{off-fast} = 0.004026ms^{-1}$ with proportions of the fast dissociation constant at 38% in the nucleoplasm rising to 46% at the active gene array. Thus, proportion of slow dissociation constant rises when presented an increased concentration of binding sites..

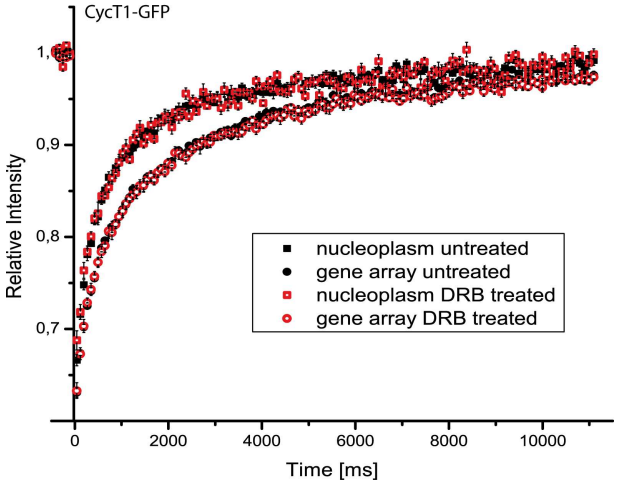

Figure 33: **DRB doesn't affect FRAP recovery of P-TEFb** Inhibition of Cdk9 does not prevent binding from occuring at the active gene array.

plasm and at the active gene array (Figure 33). The recovery remains unchanged, suggesting the same binding dynamics of P-TEFb in its inhibited state. Thus, 7SK snRNP does not affect the dissociation constant.

11.3 Fluorescence Loss in Photobleaching

Generally, the reaction dominant regime is entered by a combination of slower on-rates and low concentrations of binding sites [SPRAGUE2004], which describes the case of P-TEFb. Theory in the preceding analysis states that FRAP recoveries in the reaction dominant regime depend only on the residence time $\tau_{res} = 1/k_{off}$ of the molecule at it's binding site [BULINSKY2001, SPRAGUE2004]. Yet, the resolution of FRAP is limited since short distance translocations are sufficient to lead to full recovery, and short observation times allow the recording of a limited number of turnover events. The resolution of these turnover events is amplified in FLIP, which will enable us to observe spatial dynamics of P-TEFb over the entire nucleus with homogeneously distributed binding sites; and investigate the role of on-rates in the dynamics of transcription factors in the nucleus.
Fluorescence loss in photobleaching involves repetitive bleaching of a marked area and the monitoring of the decay of fluorescence thoughout the whole compartment. In this way, one can adress the mobility of tagged proteins at compartments and areas outside and at further distances from the bleach spot. Our FLIP experiments were calibrated to deplete all fluorescence of nuclei by using 1bleach/s for the duration of 500s. We use the first 100s imaged for normalization control.
The data is presented in the form of a radial analysis by recording the decay rate of each radius of the width of one pixel (160nm) with their center at the laser bleach.
In order to compare with a fluorophore that is expected to demonstrate pure diffusion without binding, FLIP was conducted on transiently transfected cells with YFP-nls (Figure 34A), A radial spread is still visible, indicating mild spatial dependance. To present a contrasting scenario, FLIP was also conducted on cross-linked nuclei fixed with 4%PFA. These decay curves provide a characterization of the bleach effects due to the laser uniquely (Figure 34B), on fully static populations of fluorophores. Note that the laser effect spans the entire nucleus.
Graphs were subsequently quantified by fitting each of the radii to a sum of exponentials in order to estimate the variation between all radial decays. For the immobilized cells, it was necessary to use a sum of three exponentials:

$$I = a\exp -bt + h\exp -dt + (1-a-h)\exp -gt + c$$

where I denotes the intensity, t the time, and c an eventual stationary fraction. a and h will denote the proportions of the fast, intermediate and slow decays.
In an absolutely stationary system such as the one of the fixed cells, we investigate the behaviour of the three decay parameters without constrainment. Taking the assumption that the fast decay stems directly from the immediate bleaching of molecules initially at the area of the laser beach; we fix the value of the fast decay speed at it's value of most significance (at low distances from the laser bleach) at the value of $k_{fast} = -1.5s^{-1}$. Then we reinsert this value into a sum of two exponentials used to fit the rest of the FLIP curves:

$$I = a\exp -bt + (1-a)\exp -k_{fast}t + c$$

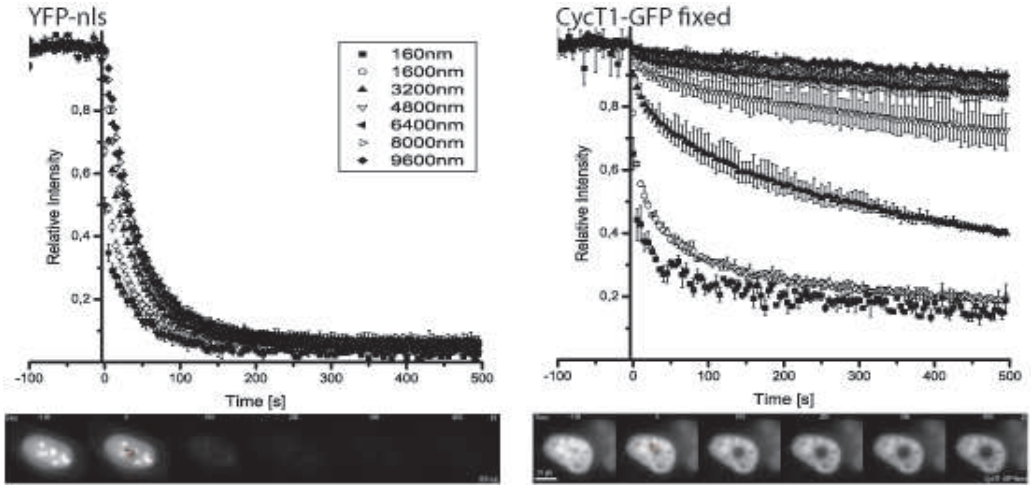

Figure 34: **FLIP decays of YFP-nls and fixed cells** The FLIP decay of YFP-nls (left) represents a freely diffusing molecule, whereas the fixed cells (right) represent a case where there is zero mobility.

We assume that the slower fraction, whose proportion rises at the expense of the fast towards the increasing distances from laser beam is due to mobility and slight bleachings caused by the Gaussian tails and scattering of the laser.
The values obtained from the slow decay and the manner in which they vary with increasing distance from the bleach will thus give us a parameter directly depicting the radial spread of the FLIP curves. Thus we plot these values in a graph depicting the slow decay rates agains the distance from the laser. Because of artifacts caused by the laser and the low amount of pixels at low radii, we fit these lines to first order polynomials to obtain slopes starting from a $6\mu m$ distance from the laser bleach. Considering the rising population of slow decay proportions, we weigh the significance of the fit proportional to the fractional population of the slow decay (Figure 35).

Addressing the system of study, FLIP experiments were conducted on the stable cell line containing fluorescent CycT1. In the endogenous case, the cell maintains its dynamic equilibrium between the small and the large P-TEFb complex [NGUYEN2001]. (Figure 27) shows that treatement with $100\mu M$ DRB over the duration of 1hour works to efficiently break down the large complex in favor of the small, creating a scenario in which cells treated contain only the small complex. The results from these FLIPs is shown in (Figure 36).
FLIP results show clearly faster dynamics in the untreated case with both complexes in comparison with the FLIP with only the small complex. This might seem paradoxical with respect to the sizes of the diffusing molecules, however, the small complex being catalytically active or inhibited maintains its binding via the CycT1 sub-domain and maintains its binding abilities that attenuate its diffusion. The data suggests that the large complex facilitates diffusion by making it impossible for the CycT1 to bind to its substrate and acts as a transport mechanism for the small molecule. This seems to be

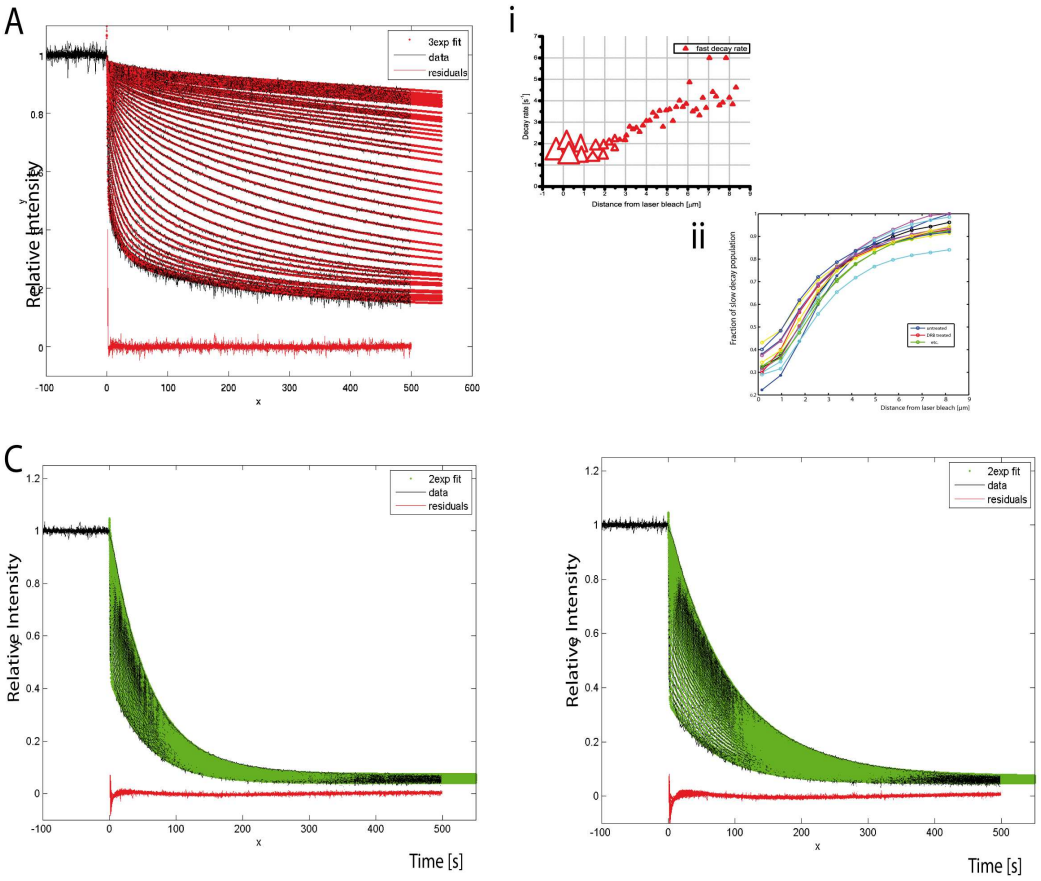

Figure 35: **FLIP Analysis to obtain parameter for radial dispersion** (A)The immobilized fluorophore FLIP is fitted to three exponentials to obtain the fast decay rate (i). Two exponential fits are used to fit the rest of the data (B) shows these fits in the cases of untreated and DRB treated CycT1GFP. The slow decay proportion rises with increasing distance from the laser bleach (ii) which is used as a weighing for the first order polynomial of the obtained slow decay rates.

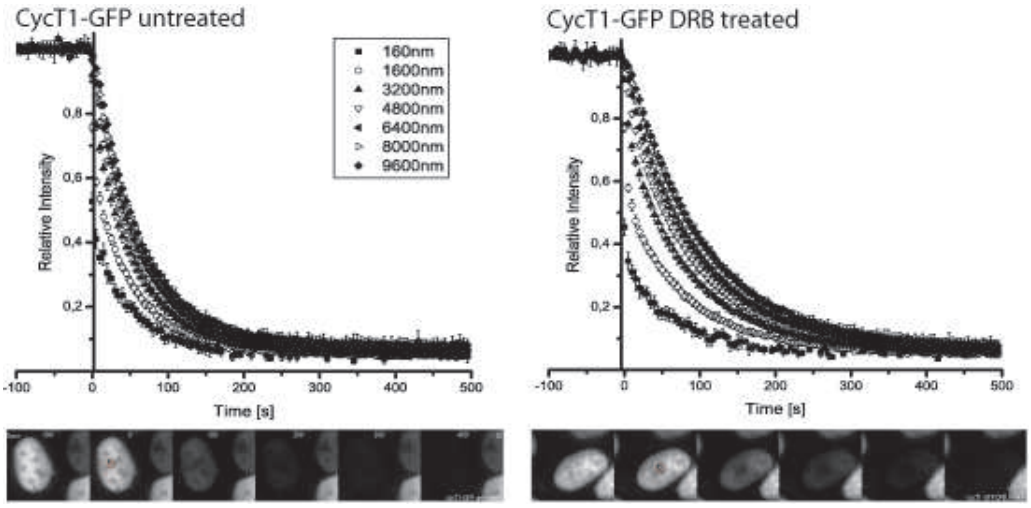

Figure 36: **FLIP decays of untreated CycT1-GFP stables and the DRB treated case** Radial dispersion is clearly increased in the case of DRB treatement, signifying a decrease in mobility.

a controlled diffusion mechanism by which the nucleus is able to efficiently transport P-TEFb around fields of unspecific binding sites by covering its binding affinity areas and by causing break down in order to liberate the active complex that can phosphorylate protein-coding polymerases to go into elongation phase.
Inhibition of transcription by cycline-dependent kinase 9 inhibitor DRB may have artifacts on the structure of the cell nucleus and other side-effects on transcriptional machinery. As a control, YFP-nls transiently transfected cells were tested for differences in the diffusion profiles upon treatement with DRB. This experiment yielded a diffusion profile identical to the one without DRB treatment.

The quantification of these experiments was made as described above. The result is shown in (Figure 37), which depicts clearly a steeper decrease of the absolute value of the slow decay rates in the case of higher radial dispersion with DRB. For a comparison, YFP-nls and immobilized fluorophore FLIP results are plotted.

Testing that the inhibition of transcription did not produce artifacts in the machinery to produce slower diffusions due to effects other than the breakdown of the large complex, the system was tested by conducting 7SK RNA interference on cells. The technique breaks down the large complex but keeping the small complex catalytically active and not inhibiting transcription, liberating the system from artifacts that could arise due to the inhibition. The result is similar: attenuation of diffusion is observed in the scenario where the large complex has been broken down, while the control with RNA interference against luciferase exhibits usual mobility identical to the natural case of both complexes being present in the cell. The FLIP curves are shown in (Figure 38). Magnitudes of the ν show similar trends as in the untreated and DRB case.
These observations change our conclusions derived from the FRAP-recovery. The FRAP results exhibit high turnover rates and a fast recovery. It assumes that the recovery rate

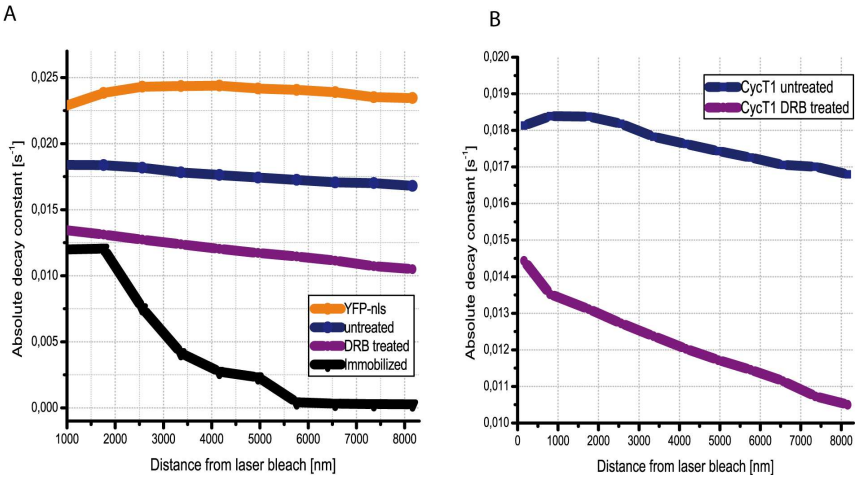

Figure 37: **Slow decay variance with distance from bleach for different FLIP experiments** Plot of slow decay rate variance with distance from bleach for YFP-nls, CycT1 untreated, DRB treated and immobilized fluorophores. The slope denotes the radial dispersion and is a measure of the spatial mobility of the fluorophore.

depends only on the dissociation rate of the molecule from it's stationary substrate. In the case of increased spatial and temporal resolution of FLIP experiments, we observe a clear radial dispersion presenting an attenuation of diffusion; after which it seems rather that it is the amount of LC and the k_{on} association rate that globally governs the mobility throughout the nucleus, rather than the k_{off} rate as explained by the FRAP; which might be relevant only for short distances and temporal scales.
The P-TEFb molecule, has short residence times but high binding frequency, and finds its substrates with a rate of k_{on} of target search. Since specific targets in forms of active genes exist throughout the entire nucleus, this k_{on} rate governs the molecule's diffusive properties.

11.3.1 Saturation of System

The dynamics of P-TEFb in the nucleus is controlled by a regulated diffusion using 7SK snRNP as a mask to transport the active complex. Endogenously, it is highly probable that P-TEFb is present in the nucleus in limiting concentrations. Upon exogenous expression of CycT1 - GFP, the endogenous amount of P-TEFb is not down-regulated (Figure 41A).
With our assumption of a constant number of binding sites[5], we pose the question of how the system might behave in an excess of P-TEFb. By over-expressing the fusion protein we are bound to increase the total amount of CycT1 in the nucleus.
Three stable cell lines with different levels of expression of CycT1-GFP were constructed

[5]In all FLIP experiments, an area of $\sim 300\mu m^2$ nuclei were used for experiment

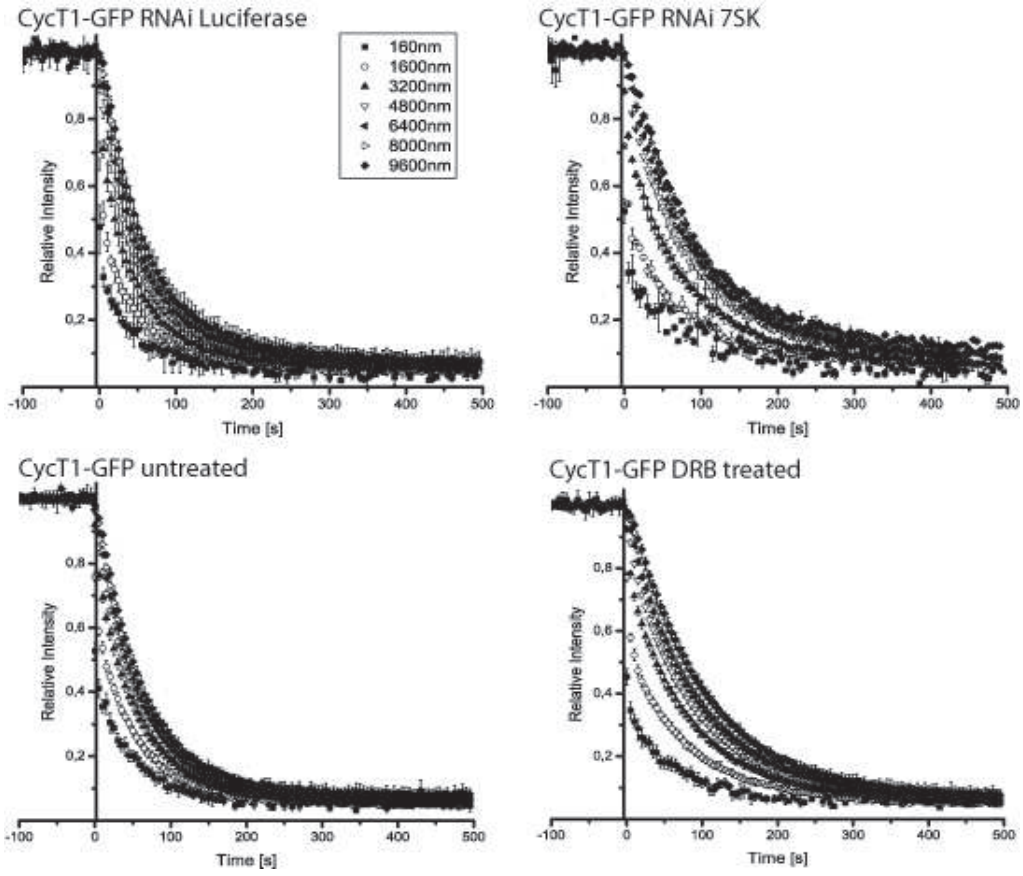

Figure 38: **FLIP decays of 7SK RNAi and control** Luciferase and 7SK; along with the untreated and DRB-treated cells below. Both treatement with DRB and 7SKRNAi produce FLIP curves of higher radial dispersion than their controls, indicating attenuated diffusion in the absence of the 7SK snRNP complex.

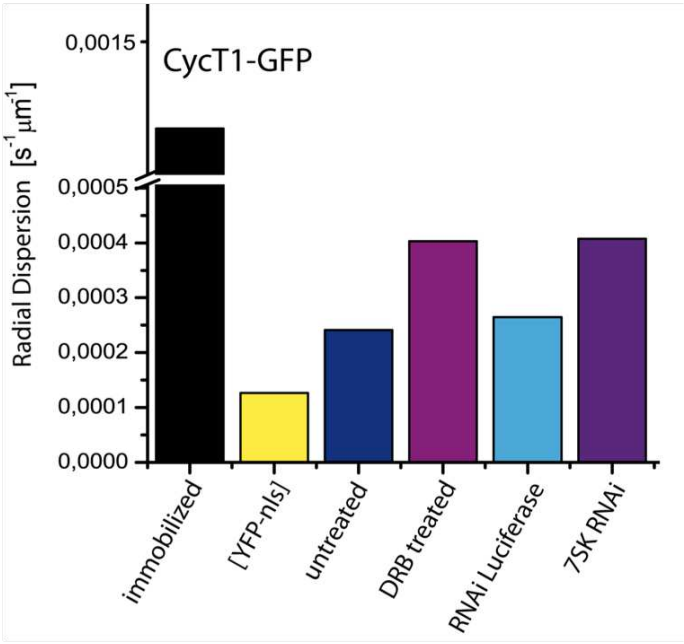

Figure 39: **Histogram showing the radial dispersion parameter** Rate of decay per distance from laser bleach portrayed for the four FLIP experiments. The values obtained for the untreated case and the RNAi Luciferase treatement are similar as expected. DRB treatement and 7SK RNA interference, both breaking down the large complex, show increased radial dispersion, meaning lower spatial mobility of CycT1.

and their motion profiles tested by FLIP. As expected, in a field of specific and unspecific binding sites, the results show that saturating the system with over-expressed exogenous CycT1-GFP gives rise to a free population once all binding sites have been saturated, and thus yields the effect of higher mobility of the fluorophore. This once more indicates that it is not the dissociation rate of the molecule that governs its mobility; since a decrease in vacant binding sites is directly related to the association rate.
In the experiments of this thesis, the stable cell line expressing the middle ammount of CycT1-GFP was utilized due to the low expression noise artifacts produced by the low-expressing cell line.

12 Probing Interaction Partner RNA Pol II

P-TEFb has its substrates on Ser5 residues which cycline-dependent kinase 9 phosphorylates in order to activate transcriptional elongation. Observing actively transcribing gene arrays, one sees both an accumulation of both RNAPolII and P-TEFb (Figure 44). Taube et al. [TAUBE2001] found interaction between the CTD tail of the RNA PolII and the histidine-rich domain of the CycT1. All this leads us to investigate the mobility of CycT1 in relation to RNA Pol II as its substrate.

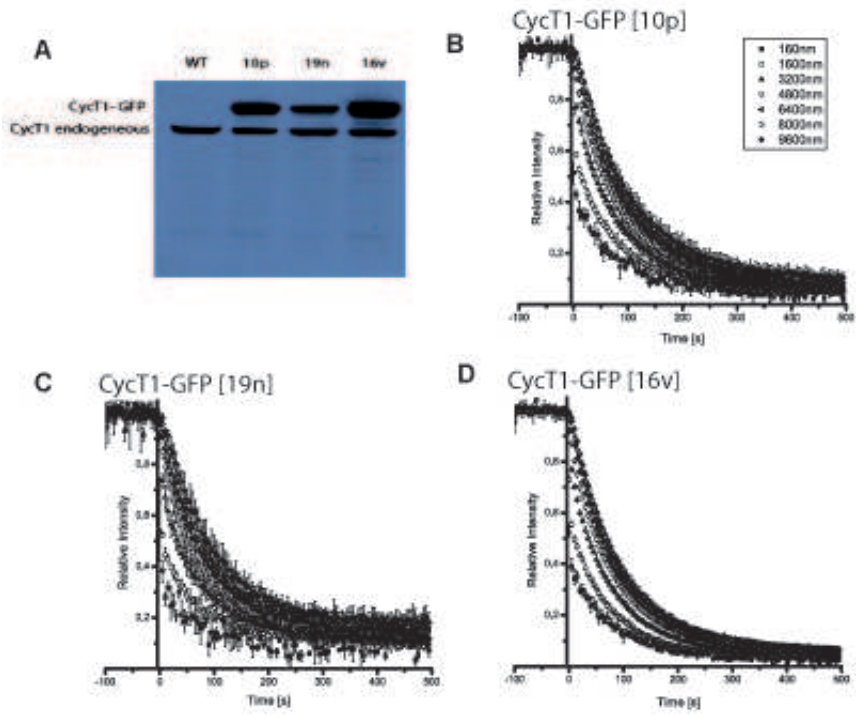

Figure 40: **Saturation of Binding Sites causes higher mobility of CycT1** (A) Western blot showing overexpression of CycT1-GFP in three differently expressing stable cell lines. (B-D) FLIP curves obtained by conducting experiments on these three cell lines.[7]

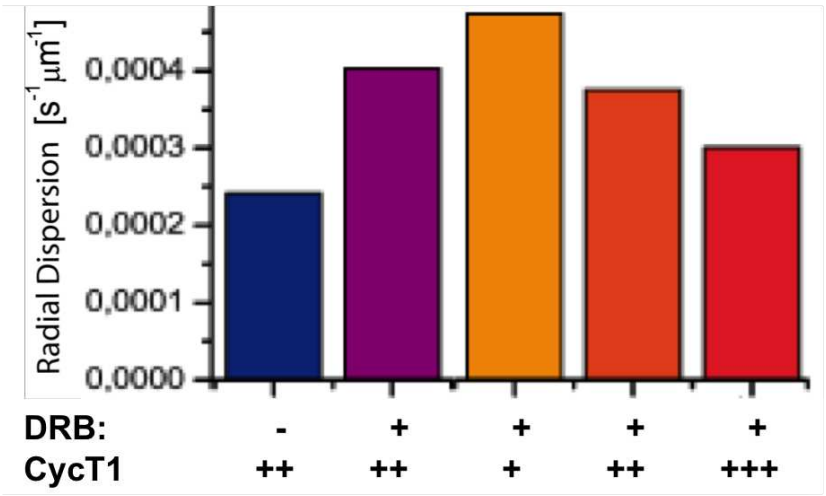

Figure 41: **Overexpression Effect on Radial Dispersion** With increased expression of CycT1, binding sites are saturated, giving rise to a freely diffusing population. The case with lowly expressing CycT1 shows attenuated mobility presented by a high value for the radial dispersion.

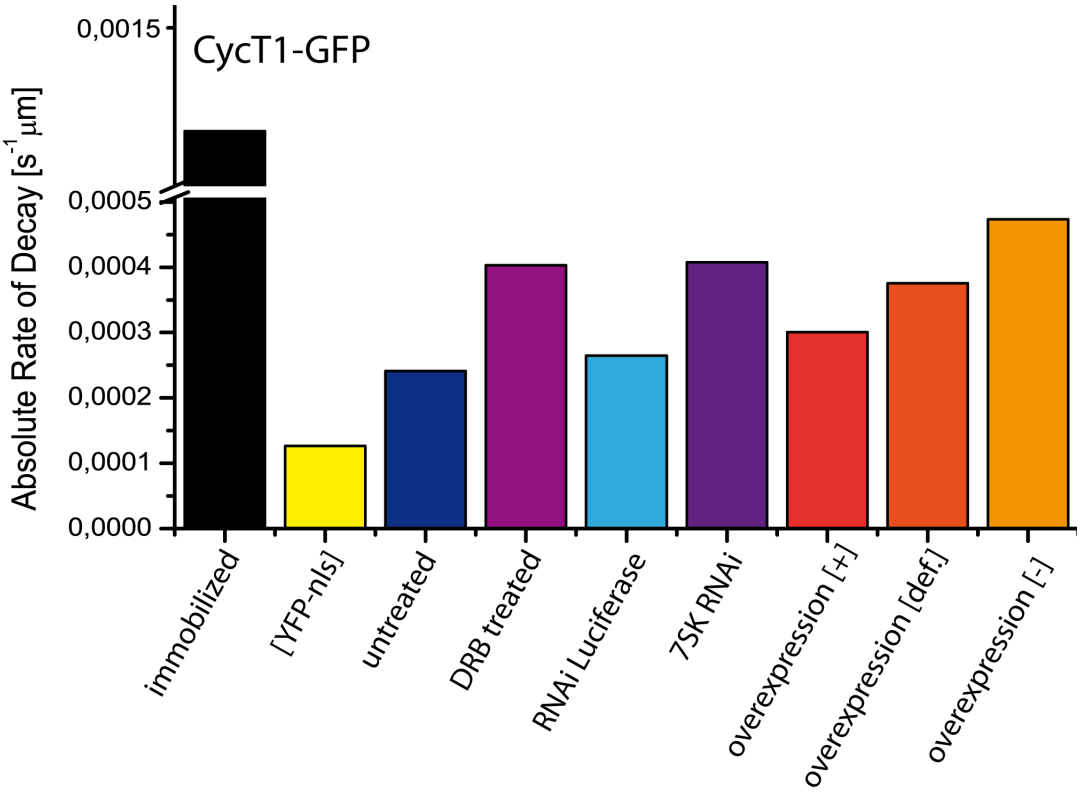

Figure 42: **Radial dispersion values summing the results of CycT1-GFP FLIP Experiments** All experiments, with the exception of YFP-nls, were carefully controlled in their nuclear area and expression levels.

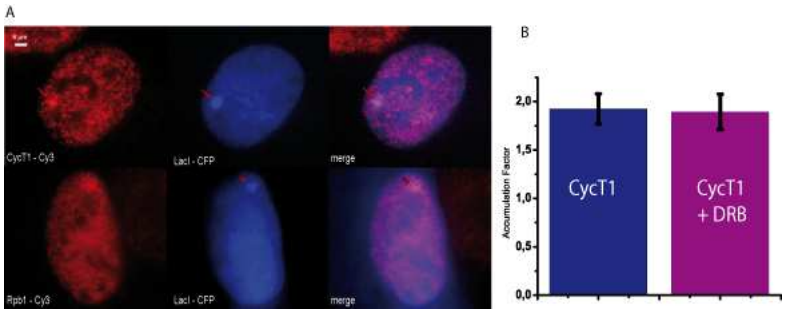

Figure 43: **Accumulation of P-TEFb and RNA PolII on Active Transcription Site** Immunofluorescence images of P-TEFb and RNAP II showing accumulation of the molecules on the active transcription site (marked with LacI-CFP). Histogram showing the accumulation factor of CycT1 compared to background. [9]

Since P-TEFb has binding sites ubiquitously present in the nucleus. By this co-localization and the hypothesis of P-TEFb substrates at the transcriptional machinery, the following experiments set out to investigate the dynamics of interaction between RNA PolII and CycT1.

Transcription inhibition causes a reduction in the engaged fraction of RNA Pol II, as shown by FLIP experiments conducted by [KIMURA2002]. Confirming these results, our FLIP experiments conducted on the stable α-amanitine resistant cell line containing fluorescent RNA Pol II as Rpb1-YFP, show gravely attenuated diffusion of the molecule. Upon inhibition of transcription by treatement with DRB, the FLIP experiments yield decays that exhibit slightly higher mobility. It has been shown that CycT1 only acts after the action of Cdk7 on Ser2 residues - and it is highly probable that elongating engaged polymerases stop on pauses on the DNA template upon transcriptional inhibition, serving as binding sites for P-TEFb.
Inhibition of transcription causes the inverse effect of decreased mobility of the transcription factor P-TEFb. However, upon comparison of the mobility profiles with CycT1-GFP which contain the opposite trend of diminishing mobility with treatement of DRB, one can not exclude RNA Pol II as the binding candidate of CycT1: the engaged fraction is still large enough to account for the immobility of CycT1.

12.1 Probing the interaction by FLIM

To investigate the interactions between the two molecules by FRET, acquisitions of lifetime measurement of complexes were performed on living cells stably expressing Rpb1-YFP and transiently transfected with CycT1-CFP. These two fluorophores, upon coming into each others proximity of $\sim$5nm or closer, will produce a FRET signal which in the case of live cell imaging can be used to measure the lifetime of the complex. (Figure 46) shows the control picture containing only CycT1-CFP, and subsequently images of cells containing both fluorophores. The complete lifetime imaging system and the charac-

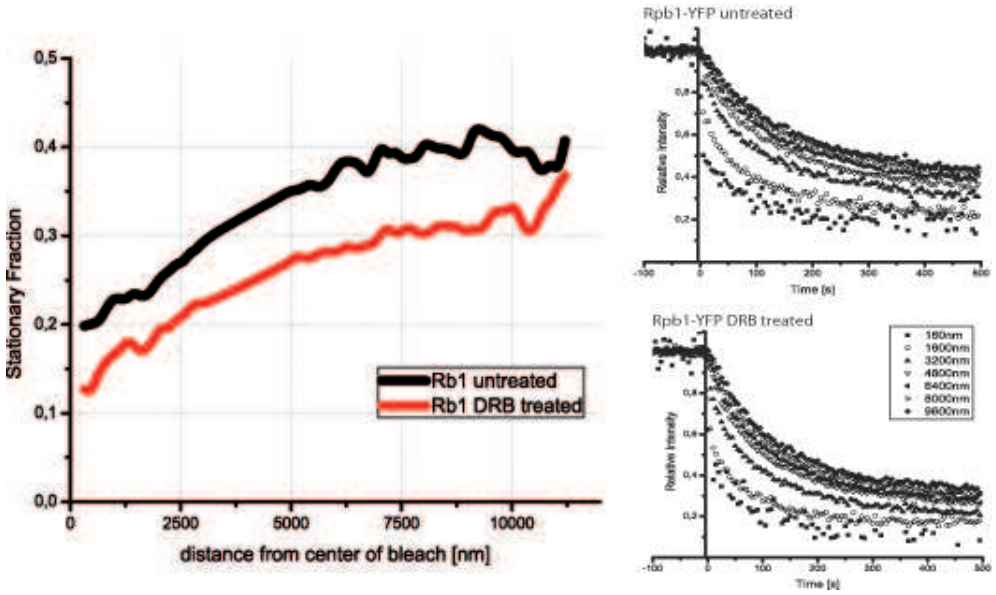

Figure 44: **FLIP decays of RNA Pol II with and without DRB treatement** FLIP decays of α-amanitine resistant RNA PolII. This stable cell line does not contain endogenous polymerase due to selection by the drug, and represents a non-overexpressed scenario. A slight decrease of the stationary fraction of the polymerase, obtained by fits to two exponentials of the FLIP curves, is observed.

terization process applied is described in [WAHARTE2006].
A slight lifetime decrease can be measured when comparing fluorescence lifetime images of cells expressing CycT1-CFP (2,87+/- 0,01 ns) and co-expressing CycT1-CFP/Rpb1-YFP (2,83+/-0,02 ns). While looking more carefully at the lifetime distribution per pixel, it is noted that for the double-transfected samples, a shift in lifetime distribution is observed as well as systematically low lifetime values down to 2,5ns indicating restricted areas where stronger interactions occurs. Upon addition of DRB to the previously mentioned samples, no lifetime decrease is observed in the case of cells expressing CycT1-CFP alone; while DRB induces an increased lifetime shift to the lower values (2,81+/-0,01ns) indicating higher affinity between CycT1 and RNA Pol II.
Furthermore, upon addition of DRB red spots are obvious throughout the nuclei, showing areas of increased interaction. These spots were observed previously in FLIPs upon depletion of the fluorescent protein as spots with slightly longer residence times. Since the mobile population of the large complex is eliminated in this case, the active and highly sticky small complex tends to stay in places of active places which could represent active genes. One useful experiment to conduct here would be the FLIM imaging of an active gene array which would remove any doubt of the spots localizing spots of increased interaction between the two molecules at transcriptionally active genes.

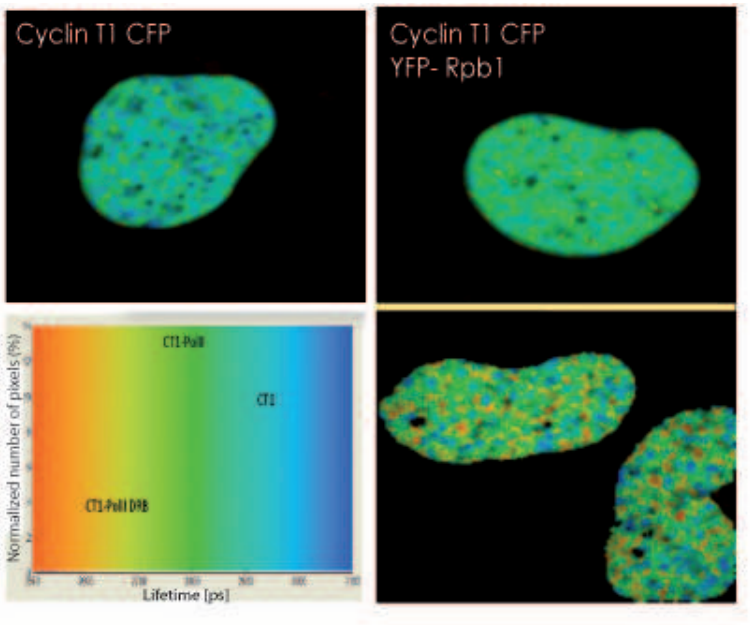

Figure 45: **Fluorescent lifetime measurement of interactions on CycT1 and Rpb1** FLIM images of CycT1-CFP, CycT1-CFP and Rbp1-YFP, and finally the latter treated with DRB. Courtesy of Corentin Spriet.

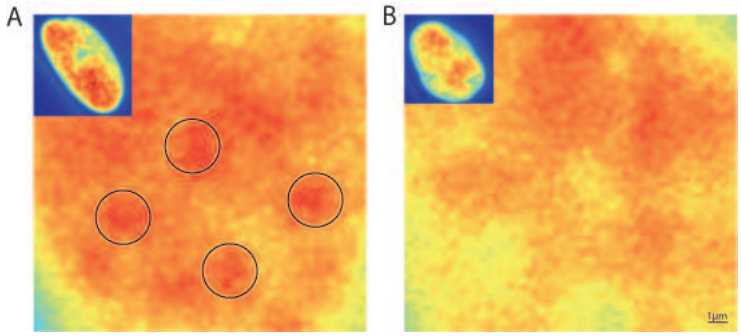

Figure 46: **Nuclear environment with and without DRB treatment** FLIP images 10 frames after bleach (insert: entire cells) (A) zoom into the nuclear environment after treatement with DRB: already after 10 bleaches, most of the freely diffusing population is depleted and hotspots, or speckles of P-TEFb accumulation are visible. Note the absence of nucleoli after inhibition of transcription. (B) zoom into the nucleoplasm in an untreated cell. The freely diffusing population is dynamically replenished, covering possible hotspots.

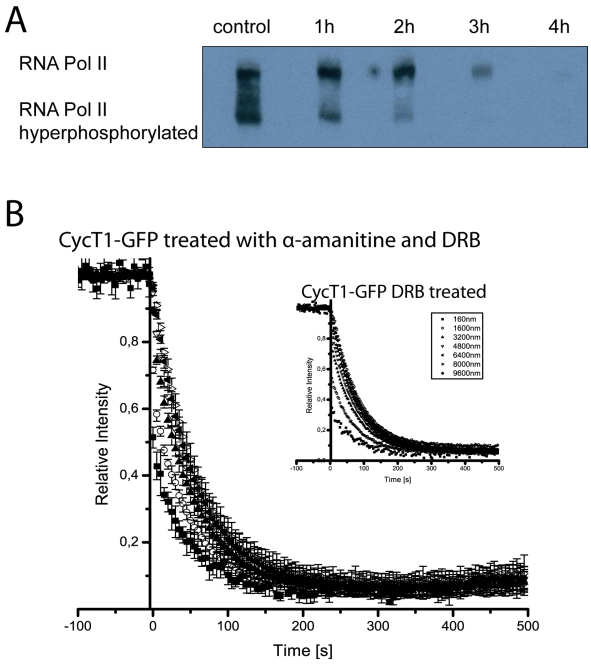

Figure 47: **Rpb1 subunit of RNA Pol II attenuates mobility of CycT1** (A) Western blot showing the absolute decay of the RNAP II Rpb1 subunit after 4hours of treatement. (B) FLIP decay of CycT1-GFP on cells treated with α-amanitine and DRB; recovery of P-TEFb mobility is observed, signifying a loss of binding sites. The drug triggers breakdown of the Rpb1 subunit contaning the CTD of the RNA Pol II, which is a substrate of CycT1 [TAUBE2002] Upon this breakdown, CycT1 regains mobility as seen by the low radial dispersion of the graph.

12.2 Eliminating the Substrate

Having established the interaction between the two molecules, we set out to investigate the dynamics of P-TEFb once its substrate is eliminated. α-amanitine is a drug that triggers the breakdown the Rpb1 subunit of the RNA PolII in the course of 4h [NGUYEN1996]. In theory, α-amanitine triggers breakdown of the large complex since it inhibits transcription. To be consistent with the control, we added DRB to the stables expressing CycT1GFP cell line after treatement of α-amanitine. The FLIP results of α-amanitine and DRB treated and the untreated case did not differ: they both show diminuated radial dispersion (as compared to its control with DRB (Figure 48insert)). Thus, P-TEFb regains all of it's mobility caused by the breakdown of the large complex. Untreated cells however, also exhibit some binding to substrates as is visible by the difference of their FLIP decays when compared to YFP-nls or binding deficient mutants. Although RNA PolII is now considered one of the binding partners attenuating the diffusion of P-TEFb, it might not be the only one.
Possible artifacts of α-amanitine treatement were tested on YFP-nls, with no change in this molecule's mobility profile.

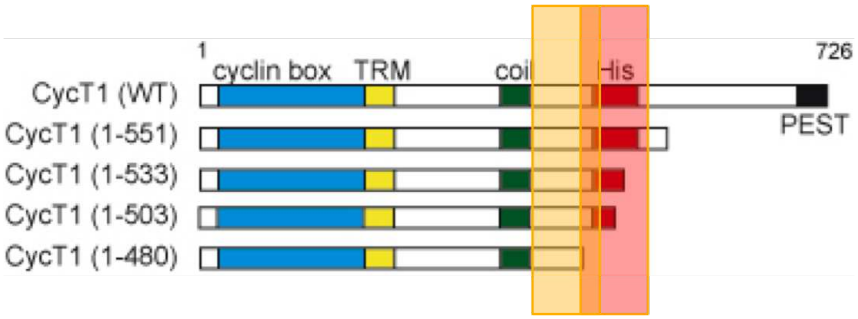

Figure 48: **Scheme mapping truncation constructs of CycT1-YFPnls** Red shading: the histidine region known to bind to CTD [TAUBE2001] and the yellow shading central region known to bind to Brd4 [JANG2005]. Construction by Nina Verstraete.

12.3 Testing of binding-defective mutants

P-TEFb activates transcription from proximal and distal sites upstream and downstream of the promoter and coding sequence of a reporter gene; and interaction between C-terminal regions of RNA Pol II, CycT1, and distal sites enables P-TEFb to act as a transcriptional co-activator. The interaction between CycT1 and the CTD was established in nuclear extracts in vitro by Taube et al. [TAUBE2001]. They found that indeed the region responsible for this interaction is the histidine-rich section of CycT1 at the nucleotides 480 - 551 towards the N-terminal domain of CycT1.
Mapping the interaction on specific regions of the CycT1 subunit, we constructed truncations in collaboration with the lab of Olivier Bensaude, to exclude the complete, and specific subparts of the histidine region described by [TAUBE2001] and investigate the central region described by Jang et al. [JANG2005] that was shown to bind Brd4.
Our constructs included:

- CycT1(1-490) includes the coiled-coil region. Does not interact with Brd4 or Rbp1 [JANG2005, TAUBE2001]
- CycT1(1-503)
- CycT1(1-533) includes the both coiled coil and histidine-rich region. Interacts with Brd4 [JANG2005], and pulls down GST Rpb1 (prel.data, O.Bensaude lab)
- CycT1(1-551) as above, this truncation is shown to interact with both Brd4 [JANG2005] but also with Rbp1 [TAUBE2001].

To test the involvement of these truncated versions in the transcriptional machinery, their accumulation on active gene arrays on SJ cells was probed with transient transfections of each of the constructs. The resulting images showed little accumulation of the CycT1(1-551) including the entire histidine region and the WT protein only. Thus, the region involved responsible for binding Brd4 does not seem sufficient to recruit P-TEFb to a higher concentration on the active gene array. Normalizing the signal to the

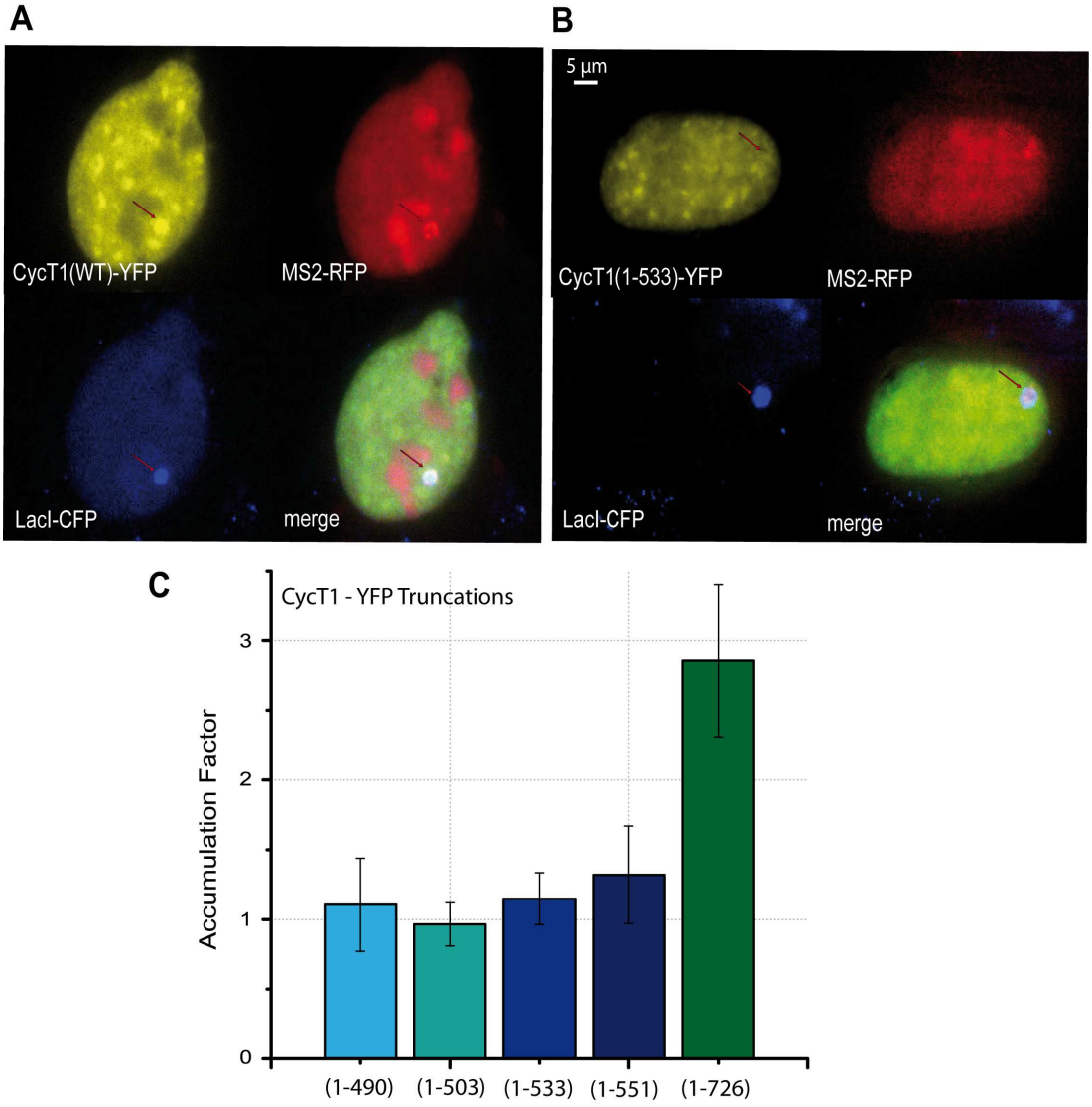

Figure 49: **Accumulation of P-TEFb truncations on active gene array** (A)Transient transfection images of accumulation of CycT1-YFP truncations and (B) CycT1(WT) on the active transcription site. Histogram depicting relative accumulations.

background, the accumulation levels are shown in (Figure 50)[10] . The accumulation of the CycT1(1-551) is much lower compared to the CycT1 WT.

Followingly, we set out to test the mobility of each of these mutants, FLIP experiments were conducted to show their interaction profiles on the homogeneous distribution of binding sites in the nucleus. In accordance with accumulation experiments, the CycT1(1-533)-YFP treated with DRB FLIP decay showed a radial distribution smaller

[10]See appendix (Figure 62) for method

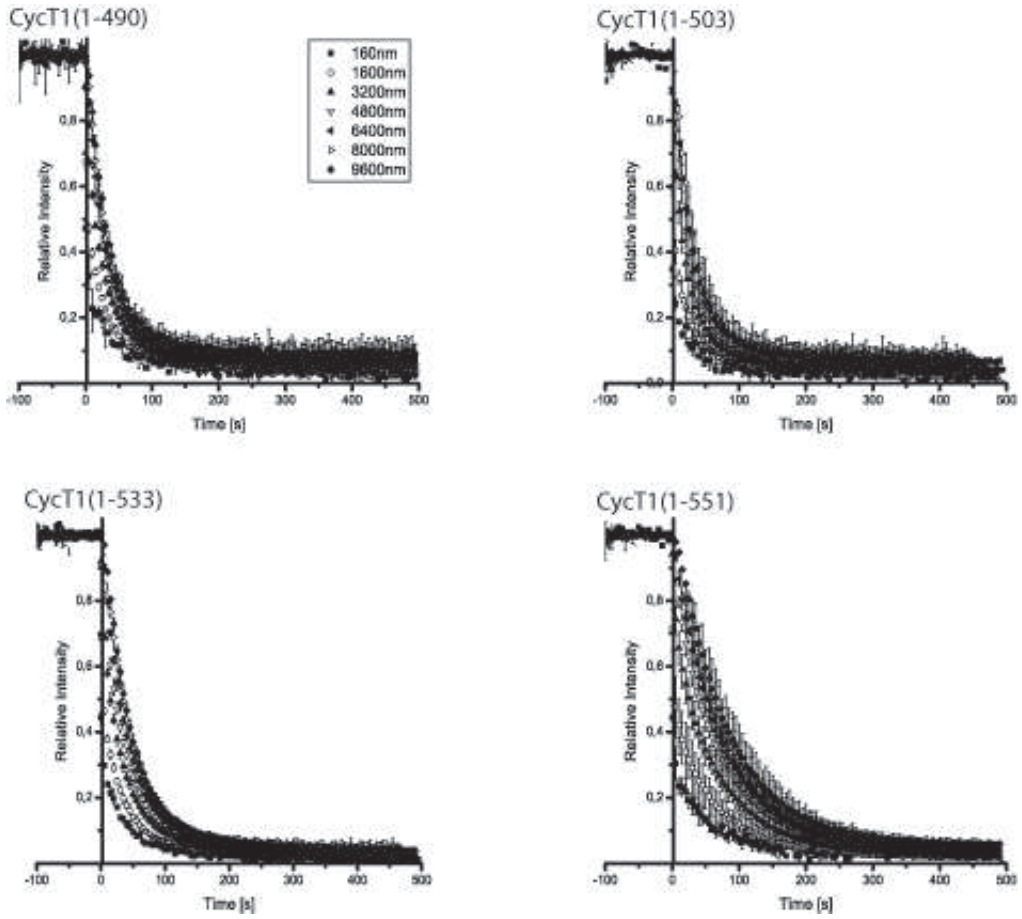

Figure 50: **FLIP decays of transiently transfected cells with truncated CycT1-YFP treated with DRB** The attenuation of mobility due to DRB is seen to a considerable extent only in the mutant containing all of the histidine-rich region CycT1(1-551).[12]

than the WT protein without DRB treatment. Truncations excluding all of the histidine region CycT1(1-490, 1-503) exhibited a lower radial distribution comparable to the one of free diffusion as YFP-nls. The truncation including all of the histidine region (CycT1(1-551)) regained most, but not all of the value as observed in the WT transcription factor treated with DRB.

13 P-TEFb Single Molecule Dynamics

Observation of ensembles of molecules provides information about the distribution and mean field behaviours of molecules. At the expense of this information, single molecule dynamics can provide information about the system such as signatures of

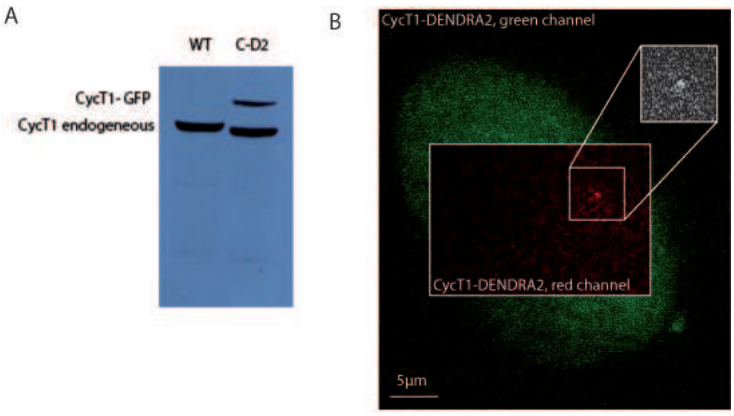

Figure 51: **Imaging CycT1-DENDRA2** (A) Western blot showing stable cell line with low expression levels of CycT1-DENDRA2, (B) The live cell expressing CycT1-DENDRA2 in the green channel (left) and in red channel with low activation power (right)

single molecules portraying their movements by measurement of translocations, and observation of traces to find even change of modes of movement by binding or complex formation.
A real-time PALM setup conducting imaging on live cells was used to investigate single molecule dynamics of P-TEFb. Using a DENDRA2 tag on CycT1, it is possible to visualize single molecules of P-TEFb by severely reducing the density molecules imaged in a single frame. The setup uses an excitation laser at 561nm at maximal power to image the red channel. A low power laser of 405nm was pulsed at intervals of 2seconds and pulse duration of 10ms enables scarce stochastic activation of single DENDRA2 molecules. The area imaged was truncated to include the maximum rectangular area possible inside of the nucleus, enabling faster imaging of 12.5ms exposure time due to data transfer, and thus making it possible to track the single transcription factor.

13.1 Single Molecule Analysis

Recognition of single molecule depends heavily on the signal to noise ratios. Several factors contribute to this, the most important being autofluorescence and out-of-focus activated molecules that contribute to the background. The movies obtained from single molecules recordings are analyzed in the following steps:

- Recognition of single particles by subtraction of background and smoothing
- Graph aggregation [13] to eliminate signal too small to be a single molecule
- Least squares Gaussian fit to localize the molecule with sub-diffraction precision

[13] by MATLAB 7.0 toolbox

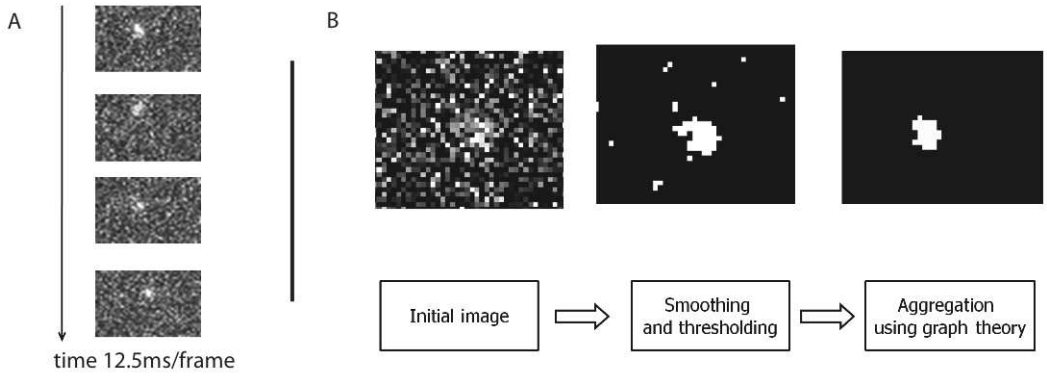

Figure 52: **Single particle detection** (A) A typical trace showing single molecule tracking; (B) Single molecule detection. Courtesy of Vincent Recamier

- The above is done for each frame, enabling translocation measurements over time.

The prevalent reason that long tracks are improbable in our experiments is due to the escape of the particles out of focus.

From tracks of single molecules it is possible to extract information such as the mean square distance (MSD) of the particle, which is the distance covered by a single fluorophore in a given amount of time. MSD can then be used to extract the diffusion coefficient of the diffusing speices.

$$MSD =< |r(t) - r(0)|^2 >$$

where <> denotes the average over all traces recorded. In case of diffusive processes, the graph of MSD vs. time is linear and the diffusion coefficient can be estimated as the slope.

Traces obtained from the recorded data can be presented in a cumulative histogram portraying the frequency distribution counting the number of displacements within the interval $[r, r + dr]$ for each value of t_{exp} from all observed trajectories. This denotes the probability distribution of absolute molecular displacement as a function of the exposure time. The cumulative histogram will indicate whether there are different modes of motion within the population of fluorophores, identifying the sub-populations by fitting. Assuming random diffusion in two dimensions:

$$p(r,t)dr = \frac{1}{4\pi Dt} exp(-r^2/4Dt)2\pi r dr$$

where $p(r,t)dr$ is defined as the probability that a particle starting at the origin will be found at time t within a shell of radius r and a width dr. The diffusion coefficients should not change with increasing exposure time, but are bound to get more inexact. The upper limit of diffusion constants detected is defined by the MSD that the molecule

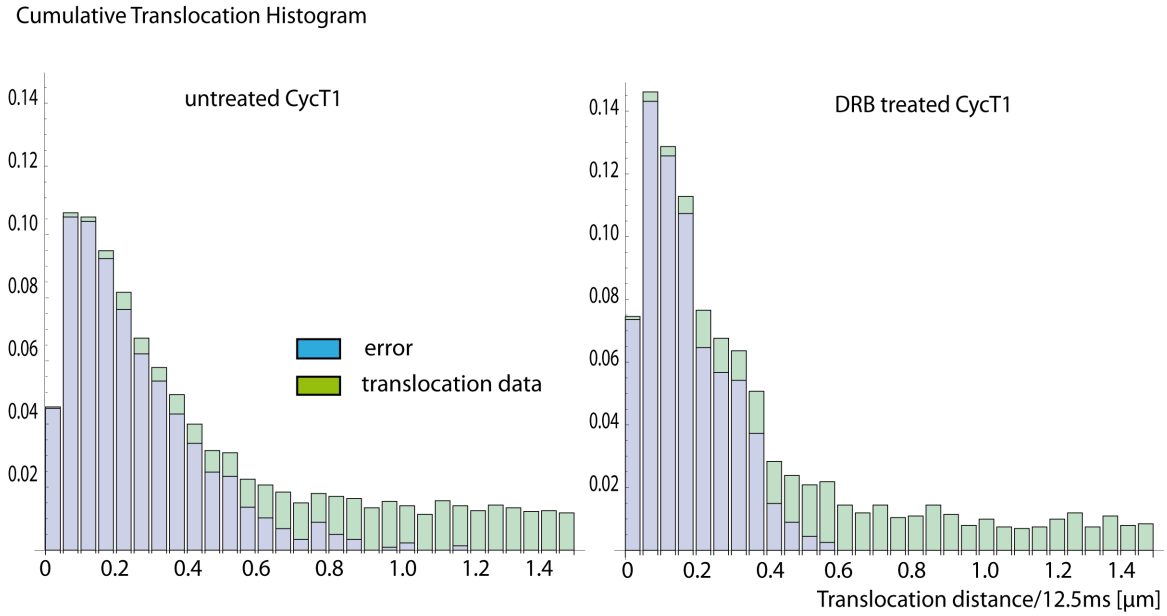

Figure 53: **Single Molecule Translocations of P-TEFb** (A) Translocation histograms of CycT1-DENDRA2 untreated (left) and DRB treated (right). The green shading represents erroneous detection, which is amplified in the case of DRB.

moves over the exposure time δt. This value must be smaller than the are of the Airy disk characteristic of the objective lens used; in order to avoid blurring of the image and reducing SNR and thus localization precision. The upper limit for the measurable diffusion coefficient is estimated by

$$D_{max} <= \frac{\lambda^2}{NA^2\delta t}$$

where the limiting factors are the exposure time and the size of the observation slice.

The single molecule tracking image sequences were recorded for both untreated and DRB treated cells. Comparing the cumulative histograms of the two cases, it is evident that the relative fraction of the fast-moving population diminishes in size at the advantage of the slower moving population in the case where the large complex of P-TEFb is broken down (see histogram of Figure(54)). In our case the fits excluding the error yielded two populations in the untreated case and only one in the DRB treated case; loosing the fast moving population that represents ≈10% in the case of the current fit in the untreated case.

This is in accordance with the FLIP experiments, since this result indicates that the small complex by itself cannot travel over longer distances. Due to the error arising of frequent delocalization of fast populations, one cannot take conclusions on the relative magnitude of the three populations. However, the relative comparison in the case with and without the large complex is valid, and concludes, as previously, that the large complex would be responsible for traveling longer distances, while the small complex

is capable of constrained target search spanning short translocations.
The mean square distances obtained from the single molecule tracks can be fitted against the time course, the slope yielding the diffusion coefficient. This process however assumes pure diffusion, ignoring sub-diffusion and binding, which are the characteristics of our system.

13.2 Error Calculations

The signal versus noise ratio is of immense importance when tracking single molecules. In the analysis of image sequences, an acceptance parameter thresholding the signal was set below which there was no detection of single molecules. Setting this parameter at an estimatedly decent level reduced false detection of background signals, but setting the threshold too high will eliminate the detection of blurs or slightly out of the focal plane signals produced by single particles that are scanning the area and produce a motion blur during the exposure time. This could lead to shorter tracks and loss of data.
Proof that single molecules are being imaged is the one-step bleach that occurs giving the characteristic signature of single molecules. DENDRA2 molecules have a bleaching half-life of 600ms (Figure 55), which enables theoretical tracking of the particles over 6s at 12ms/frame. Naturally, such long tracks are impossible, majorly due to the escape of the particles outside the focal volume, which is estimated to be $\sim 1\mu m$, and depends on the objective's numerical aperture and magnification.
The limited size of the focal plane when imaging in 2D gives another source of error-namely the overestimation in fractional size of the slow population in comparison with the fast, since molecules are much more probable to escape from focus if moving longer distances in the same time of acquisition.
Another source of error arises in the case of high concentrations of particles activated in frames. To estimate this error and the certainty that a single and same particle is being tracked in the image sequence, the decay rate was taken into account, which gives the probability of the same particle being imaged after 7seconds in the movie to be 1%. To estimate the longest translocation distance possible, the image sequences recorded were shuffled so as to have the first and the image recorded after 7seconds always in the consecutive orders. Then, the probability of tracking the same particle was estimated. The graph in (Figure 54) shows the resulting error calculation, which has to be recalculated on all movies individually since it is highly dependent on particle density.

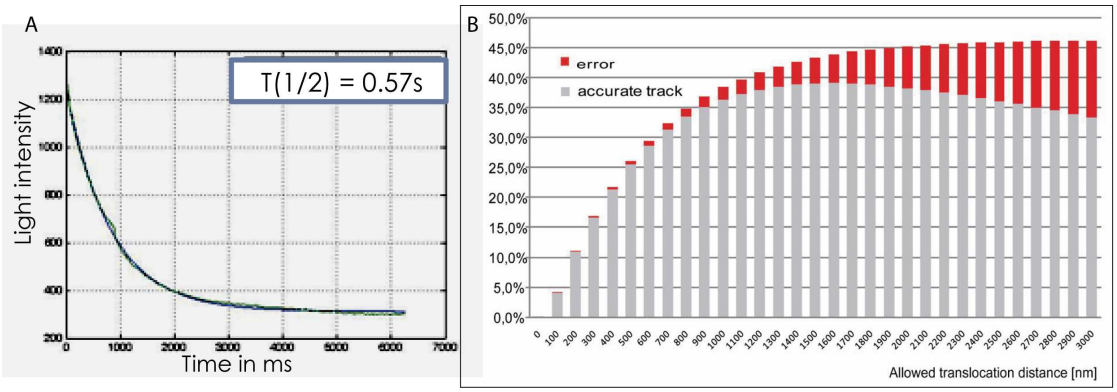

Figure 54: **Single Molecule Error Analysis** (A) Decay curve portraying fluorescence survival lifetime of CycT1-DENDRA2; with a half-life of $\sim$ 600ms. (B) On the basis of this lifetime, image sequences were re-shuffled to fit have each consequent 7s frames after each other and the error estimated. The maximal translocation distance allowed in this case is $1.5\mu m$.

Part V

Modelling of the Biological System

14 Differential Equations

The FLIP system is simulated using diffusion and binding. The two processes are described using differential equations: by the heat equation for diffusion and Michaelis-Menten binding kinetics for interactions, it is possible to simulate the data presented.
The heat equation describes the traveling of heat through a conductor, and can be readily applied to diffusion:

$$\frac{\delta T}{\delta t} = D_1 \times \frac{\delta^2 T}{\delta x^2}$$

where T is the rate of diffusion over space x, and D_1 the diffusion constant of the system. In this simplified case, only two dimensions are considered and there is two boundary conditions:
$T(0,t) = 0$ for the absorbing boundary condition at the bleach spot; and
$\frac{\delta T}{\delta x}(L,t) = 0$ for the reflecting boundary condition at the borders of the nucleus, there L is the distance from the center of the bleach to one point on the boundary.
Assuming an excess of binding sites compared to the transcription factor, consider the reaction:

$$TF + P \rightleftharpoons TF - P$$

where TF is the transcription factor, P the substrate. Assuming first order chemical kinetics, this reaction is governed by:

$$\frac{dT}{dt} = k_1[TF - P] - k_{-1}[TF][P]$$

Combined, the system is governed by:

$$\frac{dT}{dt} = D_1 \times \frac{\delta^2 T}{\delta x^2} + k_1[TF - P] - k_{-1}[TF][P]$$

which predicts an exponential decay of the fluorescence, along with a linear dependance on the distance from the bleach spot in the case of only the small complex (non-equilibrium) and no dependance on the distance whatsoever in the case of the presence of both complexes.
Simulations of the experiment that make it possible to model the system become however much more complicated. Here one needs to add extra dimension to the system, consider with great accuracy the depletion of fluorophores at each time step and its duration, approximate the geometry and volume of the nucleus, and considering two complexes and several binding constants, the fit is left with six free not easily constrainable parameters. The diffusion coefficients measured in vitro are not usable and crowded environments such as the nucleus pose addition problematics with respect of the nature of diffusion that occurs within them.
In collaboration with Dr.Holcman's group at ENS Paris, an attempt was made at modelling of the FLIP experiments by coupled partial differential equations and taking into account exact experimental parameters:

- 800nm radius of bleach, 75% of population within this radius bleached each time
- $12\mu m$ radius of nucleus
- $\sim (1 - \frac{0.8^2}{12^2})^n$, where n is the number of bleaches. r = 0.0044, but when the decays of all rings were averaged together and fitted to one exponential to obtain the ratio that is removed with each bleach, r = 0.0137, which is a factor of ~ 3 larger than calculated.

The diffusion constants of the small complex and the large are approximated by Stokes law. In the simulations, only the binding and unbinding rates of the active TF to the mask and to the bound state were changed. The equilibrium state depending on these rates and has to be calculated for each simulation. Another assumption is that binding to the mask and bound state is not saturated. The spectrum (DRB effect) was been able to be reproduced by strengthening the binding and increasing the lifetime of the bound complex; taking the conclusion that with very fast diffusion constants, one obtains a significant radial dependency of the decay curves only with binding.

Unfortunately this method gave rise to an excessive amount of free parameters and was computationally very expensive and thus was not continued.

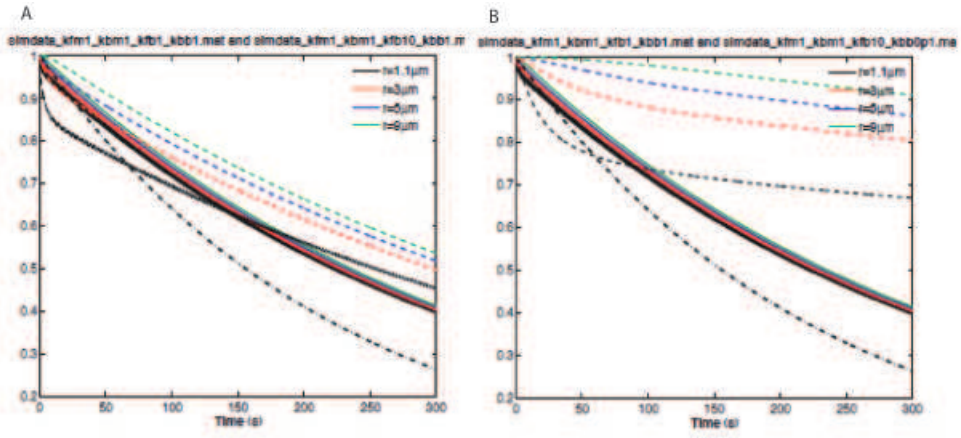

Figure 55: **Simulations of the P-TEFb FLIP dynamics using simple diffusion and binding** (A) Simulation where active, bound and masked states are comparable: (continuous line, at equilibrium 33% of TF are in active, masked and bound states respectively); versus the case where binding is 10-fold stronger(dashed line: in this case, the equilibrium is shifted versus the bound state and most TFs are in the bound state). (B) The lifetime of the bound complex is ten times larger compared to (A), concluding that with such fast diffusion constants, one obtains a significant radial dependency of the decay curves only with binding. Courtesy of Jurgen Reingruber

15 Compact vs. Non-Compact Modes of Movement

Another attractive possibility to describe the system under study was one that included into its calculations the nuclear environment. In the collaboration with Dr.Voiturier and Dr.Benichou, the TF's movement was attempted explained by compact and non-compact modes of movement.
Attempting to interpret FLIP by the temporal decrease of concentration of fluorophores: Theoretically, one can show that the concentration in proteins at a time t and a distance r of the irradiated zone, $c(r,t)$ is identical in a FLIP experiment to the probability of survival (i.e.staying fluorescent) $S(r,t)$. In the case of modelling FLIP data of YFP-nls, which has a minimal space dependance, the mode of transport is characterized by a weak dispersion of the typical reaction time (which is defined as above through the median S(typ)...) which leads to the deduction of a non-compact type of transport. Theoretical results give S the form:

$$S(r,t) = \Pi(r) exp(\frac{-t}{< \bar{T} >})$$

where $< \bar{T} >$ is the mean global time of first passage (GMFPT) in the irradiated zone, where the scaling for the prefactor Π is the following:

$$1 - \Pi(r) \propto \frac{1}{r^{d_f - d_w}}$$

Figure (57A) shows the realized adjustment for one of the curves of YFP-nls: The form chosen corresponds to formula of $S(r,t)$ where the parameters of adjustment are $< \bar{T} >$

and Π, on which one adds noise given by a time constant which is the third parameter of adjustement. The results give values of $\Pi = 1$, $noise = 0.05$ and $GMFPT \sim= 1min$. The dispersion of the $< \bar{T} >$ time is inferior to 5%, indicating that GMFPT theoretically does not depend on r. Figure (57b) shows the $1 - \Pi$ after these adjustments, in function of r. which can give an estimation of the difference

$$r^{d_f - d_w} \approx 0.68$$

which, in the case of simple 3D diffusion this value is 1.
Contrary to the motion profile of YFP-nls, FLIP experiments conducted on RNA Pol II show significant dispersion of the typical reaction time, and hence could be considered of a compact nature, In this compact case,

$$S(r,t) = \Pi(r)\Sigma_{k=0}^{\inf}\alpha_k^{1-2v}\frac{J_v(\alpha_k)}{J_{-v+k}(\alpha_k)}exp(-\frac{\alpha_k^2 d_w d_f}{2(d_w^2 - d_f^2)}\frac{t}{< \bar{T} >})$$

where $v = d_f/d_w$, $\alpha_0 < \alpha_1 < ...$ which are the real zeros of the Bessel function J_{-v} which assumes cylindrical symmetry.
In the compact case,

$$\Pi(r) \propto r^{d_w - d_f}$$

Thus by dividing every curve of different radii by $r^{d_w - d_f}$, one obtains a collapse of curves, and obtains a value

$$r^{d_w - d_f} \approx 0.35(\pm 0.05)$$

Generally, the values of $r^{d_w - d_f}$ of compact exploration systems were situated between 0.6 and 1. This adjustement was taken for the radii between 10 and 30 due to the high noise levels on other. Figure(57D) shows the collapsed curve by the compact equation of S(r,t), where the d_w and d_f were arbitrarily chosen from the triangle of Sierpinski, knowing that the formula is at variations in this dimensions in the compact case. Not using any noise, $GMFPT \sim= 4h$. Since one does not control silmutaneously both d_w and d_f, it is the value of GMFPT that is pertinent, and herewith expectable.

15.1 Finding the diffusion constant of P-TEFb

Applying these theories above on the case of P-TEFb, one takes the assumption that P-TEFb exists intracellularly in three forms:

- the big complex B, diffusive ($D_B \propto R_B$)
- the small complex S, diffusive ($D_S \propto R_S$)
- the bound L, where mobility is supposed negligible ($D_L = 0$)
- $B \rightleftharpoons S$ with equilibrium constant K = [B]/[S] in the untreated case, but [B] = 0 in the case with DRB treatement.

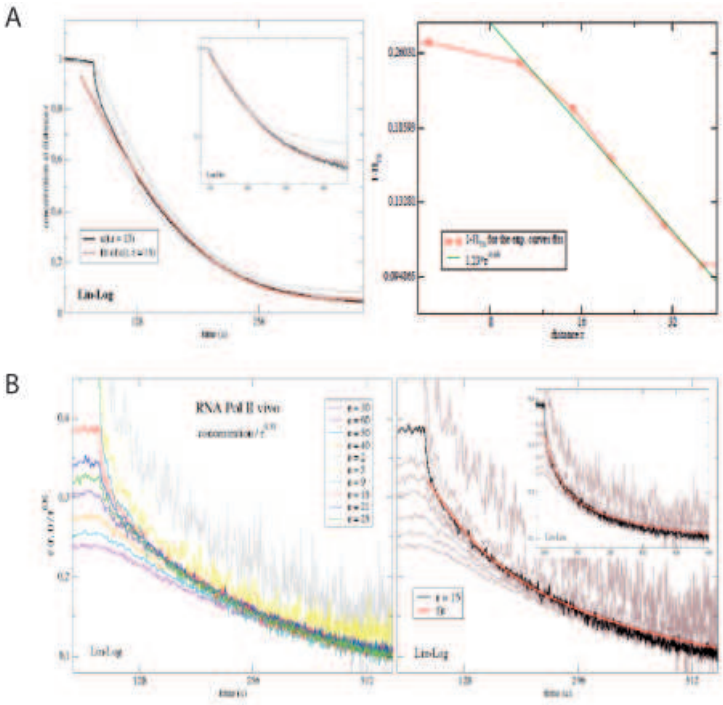

Figure 56: **Collapse of FLIP Curves using Compact/non-Compact movement assumption for RNA PolII and YFP-nls** (A) Adjustment of one of the radial FLIP decays (r = 15) for YFP-nls for the theoretical form of $S(r,t)$ plus noise, plotted on lin-log graphs (left), Adjustement of the curve of the obtained parameters for Π in function of r (right). (B)FLIP decay curves of RNA PolII, divided by r^{α} with $\alpha = 0.35$ for collapse (left), Adjustment of one of the curves (r=15) with the formula S(r,t) for the compact case. Courtesy of Olivier Benichou and Raphael Voituriez.

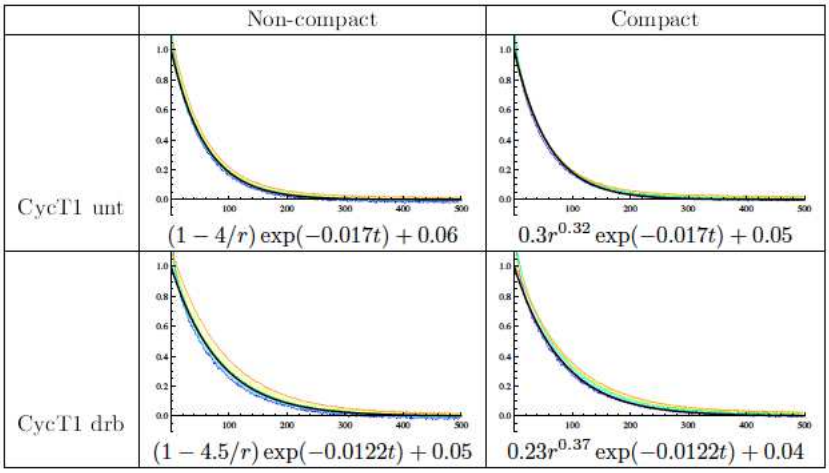

Figure 57: **Collapse of FLIP data on P-TEFb** with a fixed noise level(c). The radii blue-cyan-green-yellow-orangered range from 10 - 60 respectively. Courtesy of Claude Loverdo

- $S \rightharpoonup^{k_{on}} L$
- $k_{on} = k^*_{on}[free_sites]$, with k^*_{on} a constant, and $[free_sites]$ the concentration of free sites for S on RNA PolII. Like this, if free sites are in excess, k_{on} is constant. In case free sites are limited, as in the case of their occupation after treatement with DRB, then $k^{DRB}_{on} <= k^{UNT}_{on}$.
- an assumption is that the probability of detachment of L (passage of L to S), k_{off} is fixed. $K' = \frac{k_{on}}{k_{off}}$.

Assuming that exchanges between L, S and B are very rapid:

$$D_{eff} = \frac{S}{B+S+L}D_S + \frac{B}{B+S+L}D_B$$

denoting the concentrations.
Fitting the collapsed curves of FLIP with an exponential, the characteristic exponential decay is $\tau_{DRB} \simeq 81s$ and $\tau_{UNT} \simeq 58s$ (Figure 58). It is supposed that $\tau \propto 1/D_{eff}$.
Thus, one obtains:

$$r_t = \frac{\tau_{DRB}}{\tau_{UNT}} = \frac{D^{UNT}_{eff}}{D^{DRB}_{eff}} = \frac{(1+r_hK)(1+K'_{DRB})}{1+K+K'_{UNT}}$$

where r_h is the ratio of the small vs. big complex, and r_t is known as the ratio of the decay times.
Assuming steady state kinetics (constant K' (k_{on})), one makes K vary with proportions of B, S and L:

$$r_t = \frac{(1+r_hK)(1+K')}{(1+K+K')}$$

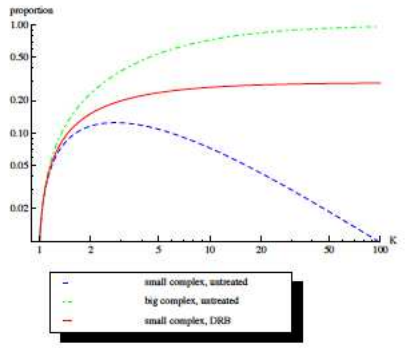

Proportion des différentes espèces en fonction de K

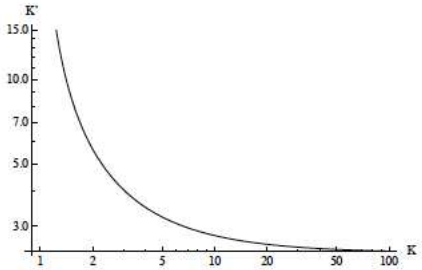

K' en fonction de K

Figure 58: **Variance of K** under the assumption that $K'_{DRB} = K'_{UNT}$. Courtesy of Claude Loverdo

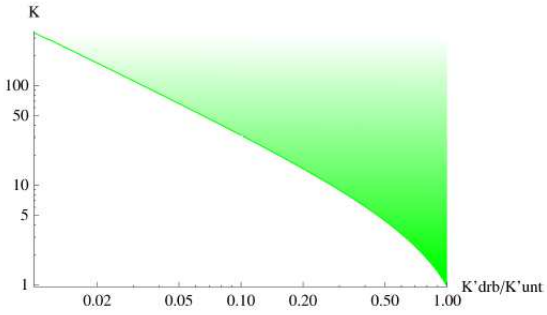

Figure 59: **Pertinent domain for K and** K'_{DRB}/K'_{UNT}. Courtesy of Claude Loverdo

The curve behaviour shows that K cannot take any value: if $K' \rightarrow \inf$, $r_t \rightarrow 1 + r_h K$, thus $K_{min} = (r_t - 1)/r_h \simeq 0.97$. This means that there is case of K, as much small complex as large complex, which is incoherent with what is known from glycerol gradients: there is around 30 - 50% of large complex in a mixture of them. It is noted that if K is close to K_{min}, the proportion of mobile CycT1 becomes very small, such that the effective diffusion will diminish.
In the case of variable k_{on}, one has $K'_{DRB} <= K'_{UNT}$. The more K' varies between the untreated and DRB case, the more this domain is restrained (Figure 60).
Since RNA Pol II has a lot of free sites, we should prevalently find ourselves in the case where K' is fixed.
The FLIP curves collapsed in the non-compact case are fitted with:

$$S(r,t) = (1 - \alpha/r)exp(-t/\tau)$$

where

$$< t(r_0) >= \tau(1 - \alpha/r_0)$$

with r_0 as the distance of departure. IF the geometry is approximated with a sphere (cell) of radius r_+ and with a bleach centered inside the sphere, of radius r_-, the mean first passage time is given by:

$$< t(r_0) >= \frac{-r_0^3 r_- + r_0 r_-^3 + 2r_0 r_+^3 - 2r_- r_+^3}{6Dr_0 r_-} \simeq \frac{r_+^3}{6Dr_-}(1 - r_-/r_0)$$

r_0 was expressed in pixels on the fit, the fit corresponding to $r_- = 4 - 4.5 pixels$ which was close to the expected 5pixels. Thus there is the case

$$\tau = \frac{r_-^3}{6Dr_-}$$

and the diffusion can be estimated as $D \simeq \frac{r_-^3}{6\tau r_-}$. Taking $r_- = 0.8\mu m$, $r_+ = 10\mu m$, one gets a diffusion constant of $D \sim 3\mu m^2/s$. One has to note that this expression is very dependent on r_+ and yields a significant error on the diffusion constant if not correctly estimated.
By the diffusion formula

$$D_S \simeq \frac{k_B T}{6\pi\eta R_S}$$

By taking the density of the nucleoplasm as $\eta \simeq 2.10^{-2} Pas$, one obtains $D_S = 5\mu m^2/s$. Thus, one needs $\sim 60\%$ of small complex in the case of DRB treatement to obtain this diffusion coefficient. This is not possible (the maximum limit of the proportion of S in DRB being at 30%).
However, everything calculated is in the order of magnitude, if one has overestimated r_+, D_{eff} could have been underestimated; η could have been taken as a lower value.
In conclusion, it is possible to explain the results of FLIP with the large and small complexes diffusing normally and the DRB case having the effect of deplacing the equilibrium versus the bound state. However, the equilibrium constant obtained is at the limit of what was expected. The results do not exclude processes that are completely different such as sub-diffusion, etc.

Part VI

Summary and Discussion

This thesis sets out to investigate the dynamics of transcription factors in the nucleus. Nuclear proteins move through the nucleus by the process of diffusion, and the vast majority of molecular interactions that have been measured in live cell nuclei are sufficiently transient to allow their principal components to move with characteristics of effective diffusion [MISTELI2001, PHAIR]. Considering the geometry of paths, as well as the high density and crowded environment of the nucleus; numerous calculations have shown that diffusion is not only the least energy-consuming method of transport, but also the most efficient one in such an environment[14]. In the midst of such conditions, and the simple (stochastic) transport mechanism utilized, arises the query of how a nuclear protein reaches its target site and so performs its action on substrates at the times required by the cell to yield a fully functional correctly balanced system of gene expression. Target searches have been previously defined with the first passage time, which is the time taken for a randomly diffusing particle to reach its target. In the complex nuclear environment filled with substrates of unspecific interactions, and with a homogeneous and limited distributions of the nuclear proteins, the time taken to reach a specific target seems to be inconsistent with the efficiency by which biological systems operate.
This leads us to the general condundrum that this thesis aspires to answer: if at each point in time the general transcription factor needs to be efficiently distributed throughout the nucleus, working in crowded environments and low concentrations (presumingly), how does it efficiently reach its target site, and at the same time maintain its availability? Will its target search depend on its initial position, and if yes, what biological implications will this have with respect to gene regulation?

16 Controlled Diffusion Mechanisms

The positive transcription elongation factor (P-TEFb) consists of a CycT1 and a Cdk9 subunit which can phosphorylate Ser5 residues on the CTD tail of the RNA Polymerase, thus initiating the elongation phase and production of messenger RNAs. Since no nearly no protein-coding genes are set into activation without the action of Cdk9, this process is considered as one of the central reactions controlling gene regulation. Naturally, the importance postulates the demand for a highly controlled mechanism of regulation of P-TEFb levels and action in the nucleus.
There is several different methods to control the activity of a transcription factor: by its abundance, herewith also spatial abundance, and by modifications of its activity. [NGUYEN2001] found that the catalytically active P-TEFb in cells exists in two forms

[14]For molecules below the size of 100nm in diameter, as stated by [LOVERDO2008]

in equilibrium: the active P-TEFb complex (small), and sequestered in a larger complex with 7SK snRNP and Hexim1; the larger complex being catalytically inactive. Furthermore, it was possible for them to show that inhibition of transcription causes breakdown of the large complex; which presumably occurs as a result of a feedback mechanism from RNA Pol II that is blocked in the initiation state. This provides us with a useful manipulation tool for understanding the functional mechanisms of the P-TEFb system: upon treatement with a transcription-inhibiting drug DRB that acts specifically on Cdk9, we produce a scenario where most of the large complex is broken down at the expense of the small. Establishing that the inactive small complex still maintains its binding abilities (FRAP), we are able to investigate the dynamic behaviour of the P-TEFb in situations of equilibrium between the two complexes and in the situation where only the small complex is present.
Probing the dynamics of fluorescently tagged P-TEFb in live cells, fluorescence recovery after photobleaching (FRAP) experiments show fast recoveries consistent with diffusion processes. Furthermore, FRAP conducted on actively transcribing artificial gene arrays show that binding attenuates the molecule's mobility. Both of these FRAP curves do not change upon treatement of DRB, showing the same binding profiles and FRAP mobility despite the inhibition of the Cdk9 kinase - it is CycT1 that is indeed responsible for the binding. However, the resolution of FRAP with respect to spatial information is limited: for the recovery, it is sufficient to have a fast turnover rate and high exchange dynamics to produce rapid recovery curves, whereas the distance-to-target issue remains unaddressed. Keeping in mind that an average cell has around 6000 active genes at a given time, and that binding sites are heterogeneously but but to an approximation evenly distributed throughout the volume of the nucleus, we address the spatial dynamics of P-TEFb by conducting fluorescence loss in photobleaching (FLIP), which amplifies the observation of binding effects by increasing measurement space as well as time of the experiment.
The results obtained from FLIP experiments clearly demonstrate an attenuation in the mobility of P-TEFb in the case where only the small complex is present. Considering the sizes of the small and large complexes and the high density of the nucleus, this result might look paradoxical at first. However, we have to remember that the small complex is the catalytically active one that is shown to bind to the RNA PolII, while the large is unable to bind as Taube et al. [TAUBE2002] implies. Thus, herewith we have the case where both complexes in equilibrium maintain high mobility (FLIP) and homogeneous distribution (FLIM) of the nuclear factor; whereas the small complex shows clear attenuation of its mobility, and even some accumulations at specific hot spots with high Pol II concentrations throughout the nucleus (FLIM), which could represent transcription factories.
Consistent results were obtained in single molecule measurements: upon recording traces of single P-TEFb molecules and plotting the translocations into a histogram, one obtains a clear decrease in the long-range traveling population in the case where the large complex has been broken down. The population of the short-range traveling molecules rises at its expense.

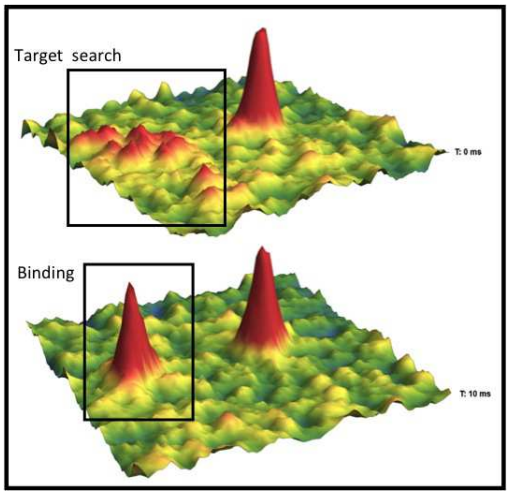

Figure 60: **Single molecule target search by motion blur and binding by a stable PSF signal** Intensity field graphs of two subsequent frames depicting the recorded target search (by the large complex) and subsequent binding (by the small complex)

We conclude that the 7SK snRNP acts as a nuclear transporter of the small catalytically active complex, and uses 3D diffusion to transport it throughout the nuclear environment. This indicates indeed that diffusion within the nucleus is a process that can tightly be regulated by the cell with means of sequestering the active into inert complexes that freely diffuse around the nucleus. The small complex sequestered within the big does not change its conformation, enabling fast release and recruitment to genes. The distribution of free P-TEFb in the form of the large complex thus presents the population efficient in recruiting factors to newly activated sites at longer distances from it's initial positions, while the small complex is efficient in maintaining its pool of active complexes and (re-)activating genes at shorter distances to its initial starting position.
Mathematically, one can imagine the large complex performing 3D diffusion throughout the volume of the nucleus, whereas in the vicinity of the substrate, the small complex conducts 1D diffusion in order to find the target. This method would optimize the target search process and is consistent with the geometry controlled kinetics [BENICHOU2010]: it is highly plausible that activated genes form structures that increase the concentrations of TFs in their vicinity ([BENICHOU2010 found 3xfold higher reaction rates in a 100nm geometrically constrained case than in a homogeneous distribution]) One aspect of the images obtained by FLIM after treatement of DRB may indicate such hotspots of transcription which trap the weakly diffusing small complex in such geometrical structures.
As most transcription factors, P-TEFb is limited in the nucleus and requires a processes of distribution and activity. An experiment conducted on cell lines stably expressing different levels of tagged P-TEFb shows an interesting artifact of overexpression of the nuclear protein: it seems that at high expression levels, the substrate gets saturated, resulting in an apparent regain of mobility due to the increased free population. Artifi-

cially, the DRB situation can be considered as an amplifier of the limiting of the situation.
The equilibrium between the P-TEFb large and small complex is tightly regulated and affected by cellular signaling on several levels such as growth, differentiation status, acetylation and ubiquitination. Thereby, it is implicative that the nucleus possesses a controlled system of gene regulation in the cell that is greatly helped with the dynamic profiles of the two molecules. As an example, it has been implicated that differentiated cells tend to shift their equilibrium towards the small complex. This is indeed profitable, since it is in a differentiated cell's interest to maintain certain genes active while decreasing the probability of transcription of others.
Inhibition of transcription by kinase inhibitors could affect processes in the nucleus and produce artifacts. This is why the control was conducted by conducting RNA interference on 7SK. 7SK RNAi efficiently breaks down the large complex, producing a small complex that is catalytically active. Our result was confirmed by this method, as well as a binding-defective truncation mutant of CycT1 that exhibited the same mobility profile upon treatement with DRB as with the untreated case.
In addition to sequestering into the large complex, [KOHOUTEK2009] presents in his review 8 different active complexes of P-TEFb and 16 variants of inactive complexes, possibly portraying a palette of different binding affinities and equilibrium constants for each of those; that all contribute to gene regulation.; along with possibilities of physiological modulations of activity such as phosphorylation acetylation, etc.

17 P-TEFb's interaction with PolII

The histidine-rich region of CycT1 has been shown to interact with the CTD of RNA Pol II by [TAUBE2001]. In this thesis, we investigate whether the binding to RNA Pol II indeed is responsible for the attenuation of diffusivity of P-TEFb inside the nucleus.
FLIM images conducted on cells transiently transfected with fluorophore tags capable of FRET on P-TEFb and RNA Pol II show clearly interaction between these two proteins. An interesting result is obtained when these interactions are measured and mapped after the treatement of DRB: the interaction areas shrink to several spots and there is apparently higher accumulation of P-TEFb alone, as well as P-TEFb in direct interaction with RNA Pol II. In the case where these hot-spots show active genes [15] this is consistent with DRB treatement producing a limiting situation of the system by locking the small complex to active gene arrays.
To probe the mobility, FLIP experiments were conducted on cells treated with $\alpha - amanitine$ (a poison known to trigger the degradation of the subunit Rpb1 of RNA PolII within 4h). After treating these cells with DRB, a scenario that would theoretically give attenuated diffusion of the nuclear protein, the FLIP curves clearly show a regain

[15] The experiment is on the way for an induced gene array

of mobility - it is thus concluded that RNA PolII is indeed one of the main binding partners of P-TEFb.
Truncation mutants of CycT1 were constructed to exclude all and parts of the histidine region shown to interact with CTD. These were tested both by FLIP and their extent of accumulation on active gene arrays. Consistently, it was shown that truncations not including the entire histidine region show facilitated mobility upon treatement with DRB. Similarly, truncation trends show a great increase in accumulation on gene arrays when the histidine region is included in the truncations. Here however, a loss of accumulation occurs when the entire length of the molecule is not included. We can speculate that the tail after the histidine region possibly stabilizes the interaction.

18 Parameterization of Dynamics

In terms of determination of physical parameters of diffusion and binding coefficients of the P-TEFb system, the present thesis is a clear example of a 'low input, high throughput, no output' approach [BRENNER2010].
As presented in the results sections, FRAP recoveries of CycT1-GFP tested positive for diffusion-uncoupled behaviour in the experiment of multiple sized bleach radii. This signifies that diffusion of P-TEFb occurs on a much faster time scale than binding, and thus that these two processes may be separable and the FRAP curves fitable by exponentials to yield dissociation constants. The fits yielded resicence times of $28.1ms$ and $248.38ms$ which are consistent with the literature[16]. Here, it is assumed that having the binding concentrations constant, the recovery curve will depend only on the dissociation constant. However. FLIP experiments that increase the spatial resolution showed that mobility of the transcription factor is not dissociation - but association limiting. The binding itself is of very short time scales when compared to the target search conducted by both the large and the small complexes. Furthermore, the association constant, directly associated with the mean first passage time, depends heavily on concentration of binding sites and volume of the nucleus.
The modelling of FLIP results by interdependent partial differential equations modelling diffusion and binding in consideration of the system's experimental parameters yielded likely simulations of the scenario; predicting that an increase in the binding activity is able to produce a higher radial dispersion as observed experimentally. The fitting of these to the experimental data was not feasible due to the inability to constrain the system's parameters sufficiently to yield deterministic fits.
The use of models predicting geometrically dependent dynamics attempted to describe the P-TEFb system with both the small and the large complex as a diffusion-facilitated, non-compact case while the case with only the small complex present with attenuated diffusion presented the compact case of movement. The survival time for fluorescent P-TEFb was modelled, yielding values of diffusion coefficients as $D_S \sim 5\mu m^2$, signifying

[16] see review of [DARZACQ2007] for a list of relevant values

that $\sim 60\%$ of the freely diffusing large complex was necessary to yield this diffusion coefficient - a case which is on the border of consistence with experimental data, where the proportion of large complex in the case of treatement with DRB is maximally 30%. However, assumptions on the equilibrium constants were made, as well as on the density of the nucleus, the radii of the diffusing molecules and the experimental bleaching parameters, especially a high dependence of cell volume was observed, consistent with the extent of variation of the radial dispersion when conducting FLIP experiments on cells of different volumes treated with DRB. Consistent with the compact mode of movement, but quantitatively not very feasible, these results implicate a possibly much higher complexity of the system including more parameters to model.

19 Conclusions, Considerations and Perspectives

The research project of this thesis presents data supporting a model of controlled diffusion by which the nucleus transports it's proteins and enables efficient delivery to target sites. Moreover, it links the biochemistry of a crucial and general transcription factor, the P-TEFb, to it's dynamic behaviours, implicating that gene expression also has a role in the spatial distribution and target search efficiency.
The experiments in the present thesis were conducted on cells over-expressing CycT1 with the exogenous CycT1-GFP. Western blots showing different expression levels of exogenous CycT1 do not seem to downregulate the endogenous amount of the molecule produced. Since there exist indications that the system is limiting, over-expressing a molecule intrinsically present at relatively locally low concentrations inevitably produces a saturation of the system, buffering the extent of the effects that could be expected. Furthermore, FLIP experiments are highly dependent on the volume of the cell under experiment. The resolution of FLIP falls drastically with decreasing volume.
Single molecule dynamics, due to low transfection levels, efficiently overcomes this problem to give credible observations of dynamics of the transcription factors and mean square distances covered. Its limitations however lie in the speed and length of tracking of the single molecules. According to Nynquist sampling theorem, images must be acquired at least at twice the highest frequency of the movements for the data to be suitable for analysis by iterative detection. However, a limitation of the sampling rate is the sensitivity of the camera: an image must be registered to detect movement in subsequent frames, and in some cases biological processes are too fast. In the future, high speed imaging will be able to separate transient and rapid events from diffusional processes, and brighter fluorophores with longer lifetimes, as well as 3D imaging, will enable longer tracks with less error in estimation of the rapid populations.
The controlled diffusion mechanism utilized by the P-TEFb equilibrium in U2OS cells is furthermore to be tested in other types of cells. An interesting hypothesis is the one of the dynamic behaviour of P-TEFb in cells after differentiation. Drugs that induce differentiation have been shown to cause breakdown of the large complex, which dy-

namically would be feasible for the cell - as observed in the FLIM images, hot-spots of high interaction between CycT1 and RNA PolII appear after breakdown of the large complex, indicative of higher efficiency of guarding transcribing cells active, while lowering the probability of activation of new genes.
Bulkiness of fluorescent tags could likewise present an issue in the potential modified dynamics inside a crowded environment like the nucleus. As a protein such as GFP of $\sim 30kDa$, it is likely to have some effects on the diffusion of a protein such as the small complex, whose size makes up only ~ 2 times the size of GFP. A way to avoid these artifacts is the use of small molecule labels such as the FlAsH (fluorescein arsenic helix binder) and ReAsH (resorufin arsenic helix binder) which are fluorescent biarsenicals that specifically recognize genetically inserted binding motifs, which contain four cysteine amino acids (tetra-cysteine motifs).

Part VII

Materials and Methods

20 Cell Culture

All cell culture was conducted in type II hoods. Cells were kept in incubators with saturating humidity, 37 degrees Celsius and 5% CO_2, and with Dulbeccos Modified Eagles Medium from Sigma-Aldrich (St. Louis, MO), supplemented with 10% fetal bovine serum from Invitrogen (Burlington, ON) and 1% peniciline/streptomycin; herewith denotes as DMEM.

20.1 Splitting cells

The cell lines used in the research were U2OS human osteosacroma WT and SJ and NDH human fibroblasts. Both of them shared the same splitting technique.
Materials:

- trypsine
- PBS
- DMEM

10cm diameter plate of cells is washed with 5ml of PBS 1x. 2ml of trypsine 10x was added and left for 30s-1min, then removed. The plate was knocked to release the cells, then resuspended in 10ml of DMEM, and split into 3plates of different concentrations, 1ml - 3ml of cells into a total volume of 10ml DMEM in the new plate. The 1ml concentration has to be split again the next 3-4days.

20.1.1 Splitting cells on coverslips

For live cell imaging, cells were split into 35mm diameter dishes containing a total of 2ml medium and a coverslip of 25mm diameter. Coverslips were kept sterile but taken directly from the commercial package. Prior to imaging, cells were washed with PBS to avoid autofluorescence by phenol red from DMEM.

20.2 Transfections

20.2.1 Transient

Materials:

- DMEM without antibiotics
- FuGene HD from Roche Diagnostics Canada (Laval, QC)
- plasmid 1γ

$100\mu l$/35mm dish of DMEM without antibiotics was used for transient transfections. $3\mu l$ FuGene was added and let for 10min to form bubbles. Then $1\mu l$ of 1γ concentration plasmid is added to the mixture and left for 30 - 45minutes. After, the mix was added dropwise into the 35mm dish with cells. All transfections were left overnight prior to imaging.

SJ Induction

For experiments involving the active gene array, the cells were transfected with the above protocol; using plasmids at a concentration of $1\mu M/\mu l$: TetON, MS2-RFP, CycT1 - YFP or Rpb1-YFP and LacI-CFP at a concentration of $0.2\mu M/\mu l$. The following day, cells were induced with a final concentration of $5\mu M$ of doxycycline heclate. [sigma]. Usually activated and transcribing gene arrays were seen after 6hours of incubation with Dox.

20.2.2 Stable Cell lines

Stable cell lines were constructed by following the FuGene protocol for transfection in 10cm diameter plates. The following day, the medium was changed containing selection antibiotic geneticin/G418 150microliters per 10ml. The selection period lasted up to $\sim$2weeks, after which colonies of single cells that incorporated the plasmid in the genome were selected using cylinders and split into 96-well plates. These were amplified under G418 selection and tested by fixing on coverslips.

20.2.3 RNA Interference

For double stranded RNA 40μM concentration is needed for plates of 35mm diameter.

1. 6μl dsRNA + 170μl OPTIMEM
2. 4μl Oligofectamine + 16μl OPTIMEM

Both are left at 5-10minutes at room temperature. During this time, all cell medium in dishes is changed to serum- and antibiotic-free DMEM and put back into the incubator. Then, solution 1 is added to solution 2, and left at room temperature fro 15 - 20minutes. In the meantime, cells are washed with OPTIMEM, and 800μl OPTIMEM is added per well. To each dish, 200mul of the prepared solution is added and mixed by whirling. The dishes are left for the next 4h in the incubator. After 4hours, 500μl of DMEM with 30% serum is added to the 1000μl solution per dish, so as to have a final concentration of 10% serum. These plates are left overnight in the incubator, and the same protocol is repeated the next day.

20.2.4 Freezing Cells

The protocol of splitting cells is followed, but the cells are resuspende in 3ml instead of 10ml. Then, they are pooled into a 15ml tube and spun in a centrifuge at 0.8rpm for 5min. The tube is emptied, then knocked on to resuspend the cells in the leftover. 1ml of FCS pure was added and mixed to resuspend homogeneously. Then 1ml of FCS with 20% DMSO was added and mixed by pipetting. The suspension was alliquoted into 2cryogenic tubes of 1ml volume. This gave 2vials per dish. The vials were wrapped in paper towels and left at -20 degrees C overnight, then transfered to -85degrees C freezer. They can be left there for a maximum of two weeks, then transfer to liquid nitrogen is necessary.

20.2.5 Defreezing Cells

Contrary to the slow freezing, cells need to be defrozen fastly to avoid formation of crystals. The vials when taken out of the liquid nitrogen are transported on dry ice, then put into a water bath at 37degrees C. When liquid, They are suspended in 15ml tubes with 2ml DMEM, and span at 0.8rpm for 3min to wash for DMSO. The tubes are emptied to leave the percipitated cells, and the cells are resuspended into 1ml of DMEM, then transfered to a 10cm dish with 9ml DMEM pre-heated at 37degrees C. The medium is changed the following day after all cells are attached.

21 Bench works

21.1 Fixing Cells

In order to visualize accumulation profiles on active gene arrays, U2OS cells were transiently transfected and induced, then fixed on coverslips 6h after induction. To fix cells, the 35mm diameter plates were washed with 1ml PBS, then 500μl PFA 4% was added for 15minutes and kept in the dark. The next three washes with PBS last 5minutes each, after which the coverslips were taken out and with a drop of mounting medium, put face down on microscope slides and kept at -20degrees C.

21.2 Immunofluorescence

Materials:

- PFA 4%
- 20% Triton 100x
- 1M glycine PBS

- 3% BSA PBS
- Tween 20%
- Solution for Anti-body: 1μl tween 20%, 20μl BSA 3%, 179μl PBS.

Coverslips in 35mm diameter dishes are washed in PBS and fixed according to the above protocol. Then, the following incubations are conducted:

1. 0.2% Triton 100x in PBS for 15min
2. 100mM glycine in PBS for 10min
3. 3% BSA in PBS for 30min
4. 1st anti-body in 0.1% tween, 0.3% BSA in PBS for 1hour
5. 0.1% tween 20 in PBS for 10minutes
6. 2x PBS washing for 10minutes each
7. 2nd anti-body FITC at the dilution of 1/50 - 1/250 in 0.1% tween, 0.3% BSA in PBS for 1hour in dark
8. 0.1% tween 20 in PBS for 10min

The coverslips can then be mounted on microscope slides as above.

21.3 Western Blot

Materials:

- 100μl of LDS + DTT (500μl LDS(4x), 1400μl H2O, 100μl DTT 1M)
- PBS
- MES buffer
- transfer buffer 10x (425ml H2O, 50ml 100% EtOH and 25ml 20x transfer buffer)
- TBST (TBS 1x, 0.1% tween 20)
- TBST 5% milk (2.5gmilk powder, then add 50ml TBST)

Cells on 10cm dishes are washed with PBS, then lysed with 100μl of LDS + DTT. These are then collected with a cell scraper into eppendorf tubes on ice. The eppendorf tubes are set to boil at 95degrees C for 10minutes. Then they are put on ice for 5minutes. These samples can then be frozen and kept. The lysed cells need to be sonicated in order to liquidize. Then they are loaded on a 10% gel and ran at 90V with a protein ruler in MES buffer for about 2h (for a protein sized 70kDa). Normally a volume of 10 - 15μl is

sufficient per well.
During the gel running, prepare 4xpaper, 2xnitrocellulose, 4xsponges (see drawing) for the transfer sandwitch. All components are wetted in transfer buffer with ethanol. Set up sandwitch as in figure, and run at 30V for 1h at room temperature or overnight at $\sim$100mA at 4 degrees C.
The nitrocellulose is then tested for protein transfer by observing stripes with ponceau rouge. The ponceau is recycled and the nitrocellulose is washed with TBST. Then, TBST 5% milk is used to saturate the membrane with protein at a horizontal whirling turner for 1hour at room temperature.
Prepare the 1st anti-body solution: 1/50th dilution of the antibody into 7ml TBST 5% milk. This solution is used to immerse and mix the nitrocellulose membrane for 1hour at RT or overnight at 4degrees C on the turner. After this, the membrane is washed three times with TBST, for 5minutes each wash.
Second antibody cocnentration is used at 1/200 dilution, into 7ml of TBST 5% milk. Again, this is left for 1h room temperature or overnight in the cold room on the turner, and subsequently washed with TBST three times, for 10minutes per wash.
The ECL solution is prepared, and the nitrocellulose blots are placed on a glass surface and immersed with this solution homogeneously. The papers are then put into the exposure box with the film (in the dark room). One exposure is conducted over 15s, the other one over 15min; and the resulting film is developed.

21.4 Midi-preps

Competent bacteria E.Coli DH5α are taken out of the -80degrees C into ice flakes. Working in the vicinity of a bunsen burner, add 0.2μl of DNA plasmid (at 1mg/ml) into $\sim 20\mu l$ of bacteria. Leave on ice for 30min.
Heat schock the bacteria by putting it in a heat bath for 30s at 42degrees C. Then put them back on ice for 2minutes. Add 950μl LB (growth-medium) without antibiotic to each mixture in a 10ml tube which allows air flow. Put the tube into a stirrer for 1hour at 37 degrees C. According to the resistance plasmid, take agarose plates with Ampicillin or Kanamicine. Working in the vicinity of a bunsen burner, take a glass 'distributer' or sterile glass beads to spread the bacteria on plates. On each plate, place, $\sim 100\mu l$ of bacterial medium and distribute. If using glass 'distributer', burn in between each distribution. Turn the agarose plates upside down and place them into a bacterial incubator to form colonies overnight.
Prepare 1000x dilutions of Ampicilin or Kanamycine antibiotics at 50mg/ml starting concentration. Work under flame. For each plasmid, take 3ml of 2YT medium + 1000x diluted corresponding antibiotic. Take a pipette tip and pick up a colony from the agarose matrix. Then throw in the pipette into the medium in falcon tubes which allow air flow. Put into stirrer for the next 6hours at 37 degrees C. After 6hours, put this solution into a big flask and stir overnight at 37degrees C in a 100ml LB volume, with 1000x antibiotic.
Allocate the liquid into 50ml falcon tubes on ice. Centrifuge these at 4000rpm for 20min-

utes at 5degrees C and remove supernatant. If more bacteria-juice is left, do this again. Next, take the 'NucleoBond' Midi/Maxi kit for preparations and follow steps.

22 Technical setup

22.1 FRAP setup

Components:

- filter wheel
- QUANTEM CCD Camera
- Nikon Microscope
- 60x objective
- Software: Metamorph
- DG4 box Xenon light
- stage with pilot control
- Nikon PFS (perfect focus system)
- custom-made laser box with 405nm and 488nm lasers of 25mW

Fast FRAP imaging was needed to record the recovery of fluorescence of CycT1. For this, the imaging window was cropped to dimensions enabling the transfer time of 15ms per frame. Here, it is necessary to pay attention to the time of bleaching in large bleach areas, since exchange occurs during the bleaching: a 1/10 of recovery duration of bleach comes within an acceptable error. The bleaches of the experiments in this thesis lasted a maximum of 4frames, i.e.60ms.
FLIP data was likewise conducted on this setup. The parameters for bleaching the nuclei of the stably expressing CycT1-GFP cell line were of ten minute durations per experiment, and 1bleach per second. Wide-field mode was used, with an exposure of 50ms and gain at 400. First hundred seconds there was no bleach, and that threshold is used afterwards as a qualitative template for bleach correction due to imaging.

22.2 PALM setup

Images were taken in wide-field configuration and, unless otherwise stated, the experiments were acquired under continuous illumination of both, activation and excitation laser light.

Activation laser power was finely tuned during acquisition, in order to maintain the density of activated fluorophores constant; typical values of activation and imaging laser power densities on the sample were 7x10-3 to 3x10-2 kW/cm2 (405 nm), 4 kW/cm2 (561 nm), 1 kW/cm2 (532 nm), and 2.7 kW/cm2 (641 nm). Single-molecule tdEosFP signals were separated with a 561 nm dichroic (Di01-R561-25x36) and a single band 617 nm emission filter (FF01-617/73), expanded through a 1.5x lens in the tube-lens of the microscope and acquired with an Andor iXon EMCCD camera (512 x 512 pixels, pixel size 16 m) at frame rates of 25 or 50 ms for up to 30 minutes. The low-resolution, conventional fluorescence images of the pre-converted form of tdEosFP were taken using a mercury lamp for illumination (excitation: Semrock FF01-485/20, emission: FF01-525/30).

Components:

- filter wheel
- Andor CCD Camera
- Nikon Ti Eclipse Microscope
- 100x objective (N.A. 1.49)
- Software: Micromanager by ImageJ
- Nikon fluorescence lamp
- Activation (405 nm / 532 nm) and excitation (561 nm / 641nm) lasers
- stage with pilot control by Nikon
- Nikon PFS (perfect focus system)

Wide-field configuration was used for all imaging. An image in the green channel was taken for every single molecule movie, to control the transfection levels. Subsequently, an area inside the nucleus was cropped to minimize transfer time (12.5ms) and the 561nm laser for imaging was turned on for 10s to bleach automatically pre-converted DENDRA2. Then the 405nm was started with pulses of 10ms duration, at intervals of 2s, and the images recorded.

22.3 FLIM Imaging

All FLIM imaging presented in this thesis was conducted by our collaborators Corentin Spriet and Laurent Helliot in Lille.
For live cell microscopy, cells were grown on glass coverslips and mounted in phenol-red free medium in a closed, heated chamber (Helmut Saur POC). Images are acquired using a 63x, Na 1.2, Water immersion objective. A two-photon pulsed excitation is given by the Coherent Mira 900-F laser at a wavelength of 810nm and a pulse frequency of 76MHz. . In order to minimize photo-toxicity, lifetime images were acquired at 3 mW

laser power (measurement at the objectives back pupil), during 10 mn.
Acquisitions were performed on U2OS cells wild type and ones stably expressing Rpb1-YFP and transiently transfected with CT1-Cerulean. Cells were observed with or without 1h DRB (5,6-Dichlorobenzimidazole 1-D-ribofuranoside , Sigma Aldrich) 100M treatment.
Fluorescence decay curves fits, allowing lifetime determination, are obtained using the SPCImage software. The choice between mono-exponential decay and bi-exponential decay fitting is done based on the reduced parameter and the shape of fitting curve residual. The weighted mean lifetime is used to compare lifetime images. Lifetime values are extracted from all pixels of a minimum of 11 cells per experiments.

23 Data Analysis

All image, data and statistical analysis was made using MATLAB 7.0 (Mathworks Inc.).

Part VIII

Bibliography

Aida M, Chen Y, Nakajima K, Yamaguchi Y, Wada T, Handa H: Transcriptional pausing caused by NELF plays a dual role in regulating immediate-early expression of the junB gene. Mol Cell Biol 2006, 26:6094-6104.

Anderson, C. M., G. N. Georgiou, I. E. G. Morrison, G. V. W. Stevenson, and R. J. Cherry. 1992. Tracking of cell surface receptors by fluorescence digital imaging microscopy using a charge-coupled device camera. J. Cell Sci. 101:415-425.

Ando, R., H. Mizuno, A. Miyawaki, Science 306, 1370 (2004).

Axelrod, D., D. E. Koppel, J. Schlessinger, E. Elson, and W. W. Webb. 1976. Mobility measurement by analysis of fluorescence photobleaching recovery kinetics. Biophys. J. 16:10551069.

Barboric M, Lenasi T, Chen H, Johansen EB, Guo S, Peterlin BM: 7SK snRNP/P-TEFb couples transcription elongation with alternative splicing and is essential for vertebrate development. Proc Natl Acad Sci USA 2009, 106:7798-7803.

Barboric M, Zhang F, Besenicar M, Plemenitas A, Peterlin BM: Ubiquitylation of Cdk9 by Skp2 facilitates optimal Tat transactivation. J Virol 2005, 79:11135-11141.

BartonG(1989) Elements of Greens Functions and Propagation(OxfordUniv Press, London).

Baumli S, Lolli G, Lowe ED, Troiani S, Rusconi L, Bullock AN, Debreczeni JE, Knapp S, Johnson LN: The structure of P-TEFb (CDK9/ cyclin T1), its complex with flavopiridol and regulation by phosphorylation. EMBO J 2008, 27:1907-1918.

Becker, W., Klaus Benndorf, Axel Bergmann, Christoph Biskup, Karsten Knig, Uday Tirplapur, Thomas Zimmer, FRET Measurements by TCSPC Laser Scanning Microscopy, Proc. SPIE 4431(2001) 94-98,

Becker, W., Axel Bergmann, Christoph Biskup, Thomas Zimmer, Nikolaj Klcker, Klaus Benndorf, Multiwavelength TCSPC lifetime imaging. Proc. SPIE 4620 (2002) 79-84

Becker, W., Axel Bergmann, Christoph Biskup, Laimonas Kelbauskas, Thomas Zimmer, Nikolaj Klcker, Klaus Benndorf, High resolution TCSPC lifetime imaging. Proc. SPIE 4963-30 (2003)

Benichou, O. C. Chevalier, J. Klafter, B. Meyer and R. Voituriez, Geometry-controlled kinetics 2010, Nature Chemistry.

Berg, O. G., Winter, R. B. von Hippel, P. H. Biochemistry 20, 69296948 (1981).

Bentley, D.L. Rules of engagement: co-transcriptional recruitment of pre-mRNA processing factors. Curr. Opin. Cell Biol. 17, 251256 (2005).

Bentley DL, Groudine M: A block to elongation is largely responsible for decreased transcription of c-myc in differentiated HL60 cells. Nature 1986, 321:702-706.

Berkhout, B., R. H. Silverman, and K. T. Jeang. 1989. Tat trans-activates the human immunodeficiency virus through a nascent RNA target. Cell 59:273282.

Bettencourt-Dias M, Giet R, Sinka R, Mazumdar A, Lock WG, Balloux F, Zafiropoulos PJ, Yamaguchi S, Winter S, Carthew RW, Cooper M, Jones D, Frenz L, Glover DM: Genome-wide survey of protein kinases required for cell cycle progression. Nature 2004, 432:980-987.

Betzig, E., Trautmann, J.K., Near-field optics: Microscopy, spectroscopy and surface modification beyond the diffraction limit. Science 257, 189-195

Bitoun E, Oliver PL, Davies KE: The mixed-lineage leukemia fusion partner AF4 stimulates RNA polymerase II transcriptional elongation and mediates coordinated chromatin remodeling. Hum Mol Genet 2007, 16:92-106.

Blazek D, Barboric M, Kohoutek J, Oven I, Peterlin BM: Oligomerization of HEXIM1 via 7SK snRNA and coiled-coil region directs the inhibition of P-TEFb. Nucleic Acids Res 2005, 33:7000-7010.

Bobroff, N. 1986. Position measurement with a resolution and noiselimited instrument. Rev. Sci. Instrum. 57:11521157.

Bosisio, D., Marazzi, I., Agresti, A., Shimizu, N., Bianchi, M. E. and Natoli, G. (2006). A hyper-dynamic equilibrium between promoter-bound and nucleoplasmic dimers controls NF-kappaB-dependent gene activity. EMBO J. 25, 798-810.

Braga, J., Desterro, J. M., and Carmo-Fonseca, M. (2004). Intracellular macromolecular mobility measured by fluorescence recovery after photobleaching with confocal laser scanning microscopes. Mol. Biol. Cell 15, 47494760.

Brenner, S. Sequences and consequences. Phil. Trans. R. Soc. B (2010) 365, 207212

Bres V, Yoh SM, Jones KA. 2008. The multi-tasking P-TEFb complex. Curr. Opin. Cell Biol. 20:33440

Brock, R., Vamosi, G., Vereb, G. Jovin, T. M. Rapid characterization of green fluorescent protein fusion proteins on the molecular and cellular level by fluorescence correlation microscopy. Proc. Natl Acad. Sci. USA 96, 1012310128 (1999).

Bulinski, J. C., D. J. Odde, B. J. Howell, T. D. Salmon, and C. M. Waterman-Storer. 2001. Rapid dynamics of the microtubule binding of ensconsin in vivo. J. Cell Sci. 114:38853897.

Byers, S.A., Price, J.P., Cooper, J.J., Li, Q., and Price, D.H. (2005). HEXIM2, a HEXIM1-related protein, regulates positive transcription elongation factor b through association with 7SK. J. Biol. Chem. 280, 1636016367.

Byrd JC, Lin TS, Dalton JT, Wu D, Phelps MA, Fischer B, Moran M, Blum KA, Rovin B, Brooker-McEldowney M, Broering S, Schaaf LJ, Johnson AJ, Lucas DM, Heerema NA, Lozanski G, Young DC, Suarez JR, Colevas AD, Grever MR (2007) Flavopiridol administered using a pharmacologically derived schedule is associated with marked clinical efficacy in refractory, genetically high-risk chronic lymphocytic leukemia. Blood 109: 399404

Chao, S. H. Price, D. H. Flavopiridol inactivates P-TEFb and blocks most RNA polymerase II transcription in vivo. J. Biol. Chem. 276, 3179331799 (2001).

Chen, R., Yang, Z., and Zhou, Q. (2004). Phosphorylated positive transcription elongation factor b (P-TEFb) is tagged for inhibition through association with 7SK snRNA. J. Biol. Chem. 279, 41534160.

Chen R, Liu M, Li H, Xue Y, Ramey WN, He N, Ai N, Luo H, Zhu Y, Zhou N, Zhou Q: PP2B and PP1alpha cooperatively disrupt 7SK snRNP to release P-TEFb for transcription in response to Ca2+ signaling. Genes Dev 2008, 22:1356-1368.

Cho, E.J., Kobor, M.S., Kim, M., Greenblatt, J., and Buratowski, S. (2001). Opposing effects of Ctk1 kinase and Fcp1 phosphatase at Ser 2 of the RNA polymerase II C-terminal domain. Genes Dev. 15, 33193329.

Cho S, Schroeder S, Kaehlcke K, Kwon HS, Pedal A, Herker E, Schnoelzer M, Ott M: Acetylation of cyclin T1 regulates the equilibrium between active and inactive P-TEFb in cells. EMBO J 2009, 28:1407-1417.

Churchman, L.S., Z. Okten, R. S. Rock, J. F. Dawson, J. A. Spudich, Proc. Natl. Acad. Sci. U.S.A. 102, 1419 (2005).

Condamin, S., Benichou, O. Moreau, M. First-passage times for random walks in bounded domains. Phys. Rev. Lett. 95, 260601 (2005).

Condamin, S., Benichou, O., Tejedor, V., Voituriez, R. Klafter, J. First-passage times in complex scale-invariant media. Nature 450, 7780 (2007).

Condamin, S., Benichou, O. Moreau, M. Random walks and brownian motion: a method of computation for first-passage times and related quantities in confined geometries. Phys. Rev. E 75, 021111 (2007).

Contreras X, Barboric M, Lenasi T, Peterlin BM: HMBA releases PTEFb from HEXIM1 and 7SK snRNA via PI3K/Akt and activates HIV transcription. PLoS Pathog 2007, 3:1459-1469.

Coppey, M. et al. Biophys. J. 87, 16401649 (2004).

Crank, J. 1975. Diffusion and chemical reaction. In The Mathematics of Diffusion. Oxford University Press, New York. 326351.

Darzacq X et al. In vivo dynamics of RNA polymerase II transcription. Nat Struct Mol Biol. 2007 Sep;14(9):796-806. Epub 2007 Aug 5.

Darzacq X et al. Dynamics of transcription and mRNA export. Curr Opin Cell Biol. 2005 Jun;17(3):332-9.

Darzacq X, Shav-Tal Y, de Turris V, Brody Y, Shenoy SM, et al. 2007. In vivo dynamics of RNA polymerase II transcription. Nat. Struct. Mol. Biol. 14:796806

De Falco, G., and Giordano, A. (1998) J. Cell. Physiol. 177, 501506

De Luca A, Esposito V, Baldi A, Claudio PP, Fu Y, Caputi M, Pisano MM, Baldi F, Giordano A: CDC2-related kinase PITALRE phosphorylates pRb exclusively on serine and is widely expressed in human tissues. J Cell Physiol 1997, 172:265-273.

Dekel, E. and Alon, U. Optimality and evolutionary tuning of the expression level of a protein. Nature Letters, Vol. 436/28 July 2005.

Deich, J., E. M. Judd, H. H. McAdams W. E. Moerner, (2004) Visualization of the movement of single histidine kinase molecules in live Caulobacter cells. In: Proc Natl Acad Sci USA. pp. 15921 15926.

Dey A, Chao SH, Lane DP: HEXIM1 and the control of transcription elongation: from cancer and inflammation to AIDS and cardiac hypertrophy. Cell Cycle 2007, 6:1856-1863.

Diribarne G, Bensaude O: 7SK RNA, a non-coding RNA regulating P-TEFb, a general transcription factor. RNA Biol 2009, 6:122-128.

Dundr, M., U. Hoffmann-Rohrer, Q. Hu, I. Grummt, L. I. Rothblum, R. D. Phair, and T. Misteli. 2002. A kinetic framework for a mammalian RNA polymerase in vivo. Science. 298:16231626.

Eissenberg JC, Shilatifard A, Dorokhov N, Michener DE: Cdk9 is an essential kinase in Drosophila that is required for heat shock gene expression, histone methylation and elongation factor recruitment. Mol Genet Genomics 2007, 277:101-114.

Egloff, S., Van Herreweghe, E., and Kiss, T. (2006). Regulation of polymerase II transcription by 7SK snRNA: two distinct RNA elements direct P-TEFb and HEXIM1 binding. Mol. Cell. Biol. 26, 630642.

Elf, J., Li, G. W. Xie, X. S. Science 316, 11911194 (2007).

Fabrega C, Shen V, Shuman S, Lima CD: Structure of an mRNA capping enzyme bound to

the phosphorylated carboxy-terminal domain of RNA polymerase II. Mol Cell 2003, 11:1549-1561.

Fong YW, Zhou Q: Relief of two built-In autoinhibitory mechanisms in P-TEFb is required for assembly of a multicomponent transcription elongation complex at the human immunodeficiency virus type 1 promoter. Mol Cell Biol 2000, 20:5897-5907.

Fromaget M, Cook PR. Photobleaching reveals complex effects of inhibitors on transcribing RNA polymerase II in living cells. Exp Cell Res. 2007 Aug 15;313(14):3026-33. Epub 2007 May 18.

Fu, T. J., J. Peng, G. Lee, D. H. Price, and O. Flores. 1999. Cyclin K functions as a CDK9 regulatory subunit and participates in RNA polymerase II transcription. J. Biol. Chem. 274:3452734530.

Fu J, Yoon HG, Qin J, Wong J: Regulation of P-TEFb elongation complex activity by CDK9 acetylation. Mol Cell Biol 2007, 27:4641-4651.

Fujinaga K, Irwin D, Huang Y, Taube R, Kurosu T, Peterlin BM: Dynamics of human immunodeficiency virus transcription: P-TEFb phosphorylates RD and dissociates negative effectors from the transactivation response element. Mol Cell Biol 2004, 24:787-795.

Garber ME, Mayall TP, Suess EM, Meisenhelder J, Thompson NE, Jones KA: CDK9 autophosphorylation regulates high-affinity binding of the human immunodeficiency virus type 1 tat-PTEFb complex to TAR RNA. Mol Cell Biol 2000, 20:6958-6969.

Garriga, J., and Grana, X. (2004). Cellular control of gene expression by T-type cyclin/CDK9 complexes. Gene 337, 1523.

Giardina, C., Perez-Riba, M. Lis, J. T. Promoter melting and TFIID complexes on Drosophila genes in vivo. Genes Dev. 6, 21902200 (1992).

Gordon, MP., T. Ha, P. R. Selvin, Proc. Natl. Acad. Sci. U.S.A. 101, 6462 (2004)

Gorski SA, Snyder SK, John S, Grummt I, Misteli T. 2008. Modulation of RNA polymerase assembly dynamics in transcriptional regulation. Mol. Cell 30:48697

Grana X, De Luca A, Sang N, Fu Y, Claudio PP, Rosenblatt J, Morgan DO, Giordano A: PITALRE, a nuclear CDC2-related protein kinase that phosphorylates the retinoblastoma protein in vitro. Proc Natl Acad Sci USA 1994, 91:3834-3838.

Grosveld F, Rodriguez P, Meier N, Krpic S, Pourfarzad F, Papadopoulos P, Kolodziej K, Patrinos GP, Hostert A, Strouboulis J: Isolation and characterization of hematopoietic transcription factor complexes by in vivo biotinylation tagging and mass spectrometry. Ann N Y Acad Sci 2005, 1054:55-67.

Gustafsson, M.G.L., J. Microsc. 198, 82 (2000).

Gustafsson, M.G.L., Proc. Natl. Acad. Sci. U.S.A. 102, 13081 (2005).

Halford, S. E. Marko, J. F. Nucleic Acids Res. 32, 30403052 (2004).

He, N., N. S. Jahchan, et al. (2008). "A La-related protein modulates 7SK snRNP integrity to suppress P-TEFb-dependent transcriptional elongation and tumorigenesis." Mol Cell 29(5): 588-99.

He N, Jahchan NS, Hong E, Li Q, Bayfield MA, Maraia RJ, Luo K, Zhou Q: A La-related protein modulates 7SK snRNP integrity to suppress P-TEFb-dependent transcriptional elongation and tumorigenesis. Mol Cell 2008, 29:588-599.

Hess, S.T., and W.W. Webb. 2002. Focal volume optics and experimental artifacts in confocal fluorescence correlation spectroscopy. Biophys. J. 83:23002317.

Hess JL: MLL: a histone methyltransferase disrupted in leukemia.Trends Mol Med 2004, 10:500-507.

Hochheimer A, Tjian R: Diversified transcription initiation complexes expand promoter selectivity and tissue-specific gene expression. Genes Dev 2003, 17:1309-1320.

Hofmann, M., C. Eggeling, S. Jakobs, S. W. Hell, Proc. Natl. Acad. Sci. U.S.A. 102, 17565 (2005).

Hollenbeck, K. J. 1998. INVLAP.M: A MATLAB function for numerical inversion of Laplace transforms by the de Hoog algorithm. http://www.isva.dtu.dk/staff/karl/invlap.htm.

Houtsmuller AB, Vermeulen W. Macromolecular dynamics in living cell nuclei revealed by fluorescence redistribution after photobleaching. Histochem Cell Biol. 2001 Jan;115(1):13-21.

Hu, T., Grosberg, A. Y. Shklovskii, B. I. Biophys. J. 90, 27312744 (2006).

Huang F, Wagner M, Siddiqui MA: Ablation of the CLP-1 gene leads to down-regulation of the HAND1 gene and abnormality of the left ventricle of the heart and fetal death. Mech Dev 2004, 121:559-572.

Jang MK, Mochizuki K, Zhou M, Jeong HS, Brady JN, Ozato K. Mol cell. 2005 aug19, 19(14) 523 - 34, the bromodomain protein Brd4 is a positive regulatory component of P-TEFb and stibumlates RNA plymerase II dependent transcription.

Janicki SM et al. From silencing to gene expression: real-time analysis in single cells. Cell. 2004 Mar 5;116(5):683-98.

Jeang KT, Xiao H, Rich EA. 1999. Multifaceted activities of the HIV-1 transactivator of transcription, Tat. J. Biol. Chem. 274:2883740

Jeronimo C, Forget D, Bouchard A, Li Q, Chua G, Poitras C, Therien C, Bergeron D, Bourassa S, Greenblatt J, Chabot B, Poirier GG, Hughes TR, Blanchette M, Price DH, Coulombe B: System-

atic analysis of the protein interaction network for the human transcription machinery reveals the identity of the 7SK capping enzyme. Mol Cell 2007, 27:262-274.

Lakowicz, J.R., Principles of Fluorescence Spectroscopy, 2nd. Ed., Plenum Press, New York 1999, [8] M. Elangovan, R.N. Day, A. Periasami, Nanosecond fluorescence resonance energy transfer-fluorescence lifetime imaging microscopy to localize the protein interactions in a single cell. J. Microsc. 205 (2002) 3-14

Lamond AI, Swedlow JR. RNA polymerase II transcription in living color. Nat Struct Mol Biol. 2007 Sep;14(9):788-90.

Laspia, M. F., P. Wendel, and M. B. Mathews. 1993. HIV-1 Tat overcomes inefficient transcriptional elongation in vitro. J. Mol. Biol. 232:732746.

Lau J, Lew QJ, Diribarne G, Michels AA, Dey A, Bensaude O, Lane DP, Chao SH: Ubiquitination of HEXIM1 by HDM2. Cell Cycle 2009, 8:2247-2254.

Li Q et al. Analysis of the large inactive P-TEFb complex indicates that it contains one 7SK molecule, a dimer of HEXIM1 or HEXIM2, and two P-TEFb molecules containing Cdk9 phosphorylated at threonine 186. J Biol Chem. 2005 Aug 5;280(31):28819-26. Epub 2005 Jun 17.

Li Q, Price JP, Byers SA, Cheng D, Peng J, Price DH: Analysis of the large inactive P-TEFb complex indicates that it contains one 7SK molecule, a dimer of HEXIM1 or HEXIM2, and two PTEFb molecules containing Cdk9 phosphorylated at threonine 186. J Biol Chem 2005, 280:28819-28826.

K. A. Lidke, B. Rieger, T. M. Jovin, R. Heintzmann, Opt. Express 13, 7052 (2005).

Liou LY, Haaland RE, Herrmann CH, Rice AP: Cyclin T1 but not cyclin T2a is induced by a post-transcriptional mechanism in PAMP-activated monocyte-derived macrophages. J Leukoc Biol 2006, 79:388-396.

Lippincott-Schwartz J et al. Studying protein dynamics in living cells. Nat Rev Mol Cell Biol. 2001 Jun;2(6):444-56.

Loverdo, C., Benichou, O., Moreau, M. Voituriez, R. Enhanced reaction kinetics in biological cells. Nature Phys. 4, 134137 (2008).

Karpova, T. S., Kim, M. J., Spriet, C., Nalley, K., Stasevich, T. J., Kherrouche, Z., Heliot, L. and McNally, J. G. (2008). Concurrent fast and slow cycling of a transcriptional activator at an endogenous promoter. Science 319, 466-469.

Kao, C. F. et al. Rad6 plays a role in transcriptional activation through ubiquitylation of histone H2B. Genes Dev. 18, 184195 (2004)

Kelland, L. R. (2000) Expert Opin. Investig. Drugs 9, 29032911

Kiernan RE, Emiliani S, Nakayama K, Castro A, Labbe JC, Lorca T, Nakayama Ki K, Benkirane M: Interaction between cyclin T1 and SCF(SKP2) targets CDK9 for ubiquitination and degradation by the proteasome. Mol Cell Biol 2001, 21:7956-7970.

Kim, J.B., and Sharp, P.A. (2001). Positive transcription elongation factor B phosphorylates hSPT5 and RNA polymerase II carboxyl-terminal domain independently of cyclin-dependent kinase-activating kinase. J. Biol. Chem. 276, 1231712323.

Kimura H, Sugaya K, Cook PR. 2002. The transcription cycle of RNA polymerase II in living cells. J. Cell Biol. 159:77782

Kohoutek J, Li Q, Blazek D, Luo Z, Jiang H, Peterlin BM: Cyclin T2 is essential for mouse embryogenesis. Mol Cell Biol 2009, 29:3280-3285.

Koumenis, C., Giaccia, A., 1997. Transformed cells require continuous activity of RNA polymerase II to resist oncogene-induced apoptosis. Mol. Cell. Biol. 17, 7306 7316.

Krueger BJ, Jeronimo C, Roy BB, Bouchard A, Barrandon C, Byers SA, Searcey CE, Cooper JJ, Bensaude O, Cohen EA, Coulombe B, Price DH: LARP7 is a stable component of the 7SK snRNP while PTEFb, HEXIM1 and hnRNP A1 are reversibly associated. Nucleic Acids Res 2008, 36:2219-2229.

Kubitscheck, U., O. Kuckmann, T. Kues, and R. Peters. 2000. Imaging and tracking of single GFP molecules in solution. Biophys. J. 78:2170 2179.

Kubitscheck, U., T. Kues, and R. Peters. 1999. Visualization of the nuclear pore complex and its distribution by confocal laser scanning microscopy. Methods Enzymol. 307:207230.

Kues T, Peters R, Kubitscheck U (2001) Biophys J 80:29542967

Kulkarni PA, Sano M, Schneider MD: Phosphorylation of RNA polymerase II in cardiac hypertrophy: cell enlargement signals converge on cyclin T/Cdk9. Recent Prog Horm Res 2004, 59:125-139.

Mancebo, H. S., Lee, G., Flygare, J., Tomassini, J., Luu, P., Zhu, Y., Peng, J., Blau, C., Hazuda, D., Price, D. H., and Flores, O. (1997) Genes Dev. 11, 26332644

Margaritis T, Holstege FC: Poised RNA polymerase II gives pause for thought. Cell 2008, 133:581-584.

Markert A, Grimm M, Martinez J, Wiesner J, Meyerhans A, Meyuhas O, Sickmann A, Fischer U: The La-related protein LARP7 is a component of the 7SK ribonucleoprotein and affects transcription of cellular and viral polymerase II genes. EMBO Rep 2008, 9:569-575.

Marshall, N.F., and Price, D.H. (1992). Control of formation of two distinct classes of RNA polymerase II elongation complexes. Mol. Cell. Biol. 12, 20782090.

Marshall, N.F., and Price, D.H. (1995). Purification of P-TEFb, a transcription factor required for the transition into productive elongation. J. Biol. Chem. 270, 1233512338.

Marshall, N.F., Peng, J., Xie, Z., and Price, D.H. (1996). Control of RNA polymerase II elongation potential by a novel carboxyl-terminal domain kinase. J. Biol. Chem. 271, 2717627183.

Marshall RM, Salerno D, Garriga J, Grana X: Cyclin T1 expression is regulated by multiple signaling pathways and mechanisms during activation of human peripheral blood lymphocytes. J Immunol 2005, 175:6402-6411.

Michels, A.A., Fraldi, A., Li, Q., Adamson, T.E., Bonnet, F., Nguyen, V.T., Sedore, S.C., Price, J.P., Price, D.H., Lania, L., and Bensaude, O. (2004). Binding of the 7SK snRNA turns the HEXIM1 protein into a P-TEFb (CDK9/cyclin T) inhibitor. EMBO J. 23, 26082619

Michels, A. A., V. T. Nguyen, et al. (2003). "MAQ1 and 7SK RNA interact with CDK9/cyclin T complexes in a transcription-dependent manner." Mol Cell Biol 23(14): 4859-69.

Misteli, T. (2001). "Protein dynamics: implications for nuclear architecture and gene expression." Science 291(5505): 843-7.

Montroll, E. W. Random walks on lattices. iii. calculation of first-passage times with application to exciton trapping on photosynthetic units. J. Math. Phys. 10, 753765 (1969).

Mueller, F., Wach, P. and McNally, J. G. (2008). Evidence for a common mode of transcription factor interaction with chromatin as revealed by improved quantitative fluorescence recovery after photobleaching. Biophys. J. 94, 3323-3339.

Mueller D, Bach C, Zeisig D, Garcia-Cuellar MP, Monroe S, Sreekumar A, Zhou R, Nesvizhskii A, Chinnaiyan A, Hess JL, Slany RK: A role for the MLL fusion partner ENL in transcriptional elongation and chromatin modification. Blood 2007, 110:4445-4454.

Muse GW, Gilchrist DA, Nechaev S, Shah R, Parker JS, Grissom SF, Zeitlinger J, Adelman K: RNA polymerase is poised for activation across the genome. Nat Genet 2007, 39:1507-1511.

Napolitano, G., P. Licciardo, P. Gallo, B. Majello, A. Giordano, L. Lania. 1999. The CDK9-associated cyclins T1 and T2 exert opposite effects on HIV-1 Tat activity. AIDS 13:14531459

Napolitano, G., B. Majello, P. Licciardo, A. Giordano, and L. Lania. 2000. Transcriptional activity of positive transcription elongation factor b kinase in vivo requires the C-terminal domain of RNA polymerase II. Gene 254:139 145.

Nechaev S, Adelman K: Promoter-proximal Pol II: when stalling speeds things up. Cell Cycle 2008, 7:1539-1544.

Nguyen, V. T., T. Kiss, et al. (2001). "7SK small nuclear RNA binds to and inhibits the activity of CDK9/cyclin T complexes." Nature 414(6861): 322-5.

Otero, G., J. Fellows, et al. (1999). "Elongator, a multisubunit component of a novel RNA polymerase II holoenzyme for transcriptional elongation." Mol Cell 3(1): 109-18.

Ott M, Schnolzer M, Garnica J, Fischle W, Emiliani S, Rackwitz HR, Verdin E: Acetylation of the HIV-1 Tat protein by p300 is important for its transcriptional activity. Curr Biol 1999, 9:1489-1492.

Patterson, G., Day, R. N. Piston, D. Fluorescent protein spectra. J. Cell Sci. 114, 837838 (2001).

Peng, J., Y. Zhu, et al. (1998). "Identification of multiple cyclin subunits of human P-TEFb." Genes Dev 12(5): 755-62.

Peterlin, B. M. and D. H. P (2006). "Controlling the elongation phase of transcription with P-TEFb." Mol Cell 23(3): 297-305.

Phair, R. D. and T. Misteli (2000). "High mobility of proteins in the mammalian cell nucleus." Nature 404(6778): 604-9.

Phair, R. D., S. A. Gorski, and T. Misteli. 2004. Measurement of dynamic protein binding to chromatin in vivo, using photobleaching microscopy. Methods Enzymol. 375:393414.

Ping YH, Rana TM: DSIF and NELF interact with RNA polymeraseII elongation complex and HIV-1 Tat stimulates P-TEFbmediated phosphorylation of RNA polymerase II and DSIF during transcription elongation. J Biol Chem 2001, 276:12951-12958.

Price DH. P-TEFb, a cyclin-dependent kinase controlling elongation by RNA polymerase II. Mol Cell Biol. 2000 Apr;20(8):2629-34.

Price DH. Poised polymerases: on your mark...get set...go! Mol Cell. 2008 Apr 11;30(1):7-10.

Rafalska-Metcalf IU, Janicki SM. Show and tell: visualizing gene expression in living cells. J Cell Sci. 2007 Jul 15;120(Pt 14):2301-7.

Reines, D., R. C. Conaway, and J. W. Conaway. 1999. Mechanism and regulation of transcriptional elongation by RNA polymerase II. Curr. Opin. Cell Biol. 11:342346.

Remillieux-Leschelle N, Santamaria P, Randsholt NB: Regulation of larval hematopoiesis in Drosophila melanogaster: a role for the multi sex combs gene. Genetics 2002, 162:1259-1274.

Redner S (2001) A Guide to First Passage Time Processes (Cambridge Univ Press, Cambridge, UK).

Reits EA, Neefjes JJ. From fixed to FRAP: measuring protein mobility and activity in living cells. Nat Cell Biol. 2001 Jun;3(6):E145-7.

Richter, P. H. Eigen, M. Biophys. Chem. 2, 255263 (1974).

Rice S (1985) Diffusion-Limited Reactions (Elsevier, Amsterdam).

Rigler, R. et al. Specific binding of proinsulin C-peptide to human cell membranes. Proc. Natl Acad. Sci. USA 96, 1331813323 (1999).

Robinett, C. et al. In vivo localization of DNA sequences and visualisation of large-scale chromatin organisation using lac operator/repressor recognition. J. Cell Biol. 135, 16851700 (1996).

Rougvie AE, Lis JT: The RNA polymerase II molecule at the 5' end of the uninduced hsp70 gene of D. melanogaster is transcriptionally engaged. Cell 1988, 54:795-804.

Qu, X., D. Wu, L. Mets, N. F. Scherer, Proc. Natl. Acad. Sci. U.S.A. 101, 11298 (2004).

Salerno D, Hasham MG, Marshall R, Garriga J, Tsygankov AY, Grana X (2007) Direct inhibition of CDK9 blocks HIV-1 replication without preventing T-cell activation in primary human peripheral blood lymphocytes. Gene 405: 6578

Sano, M., Abdellatif, M., Oh, H., Xie,M., Bagella, L., Giordano, A., Michael, L.H., DeMayo, F.J., and Schneider, M.D. (2002). Activation and function of cyclin T-Cdk9 (positive transcription elongation factor- b) in cardiac muscle-cell hypertrophy. Nat. Med. 8, 13101317.

Sano M, Schneider MD: Cyclin-dependent kinase-9: an RNAPII kinase at the nexus of cardiac growth and death cascades. Circ Res 2004, 95:867-876

Saunders A, Core LJ, Lis JT: Breaking barriers to transcription elongation. Nat Rev Mol Cell Biol 2006, 7:557-567.

Schuss, Z., Singer, A. Holcman, D. The narrow escape problem for diffusion in cellular microdomains. Proc. Natl Acad. Sci. USA 104, 1609816103 (2007).

Schutz, G. J., H. Schindler T. Schmidt, (1997) Singlemolecule microscopy on model membranes reveals anomalous diffusion. Biophys J 73: 10731080.

Senderowicz, A. M., and Sausville, E. A. (2000) J. Natl. Cancer Inst. 92, 376387

Serizawa, H., Conaway, R. C., and Conaway, J. W. (1992) Proc. Natl. Acad. Sci. U. S. A. 89, 74767480

Sims RJ 3rd, Mandal SS, Reinberg D: Recent highlights of RNApolymerase-II-mediated transcription. Curr Opin Cell Biol 2004,16:263-271.

Shav-Tal Y, Darzacq X, Shenoy SM, Fusco D, Janicki SM, et al. 2004. Dynamics of single mRNPs in nuclei of living cells. Science 304:1797800

Shim, E. Y., A. K. Walker, et al. (2002). "CDK-9/cyclin T (P-TEFb) is required in two postinitiation pathways for transcription in the C. elegans embryo." Genes Dev 16(16): 2135-46.

Shlesinger M (2007) First encounters. Nature 450:4041.

Shore SM, Byers SA, Maury W, Price DH: Identification of a novel isoform of Cdk9. Gene

2003, 307:175-182.

Slany RK: When epigenetics kills: MLL fusion proteins in leukemia. Hematol Oncol 2005, 23:1-9.

Slutsky, M. Mirny, L. A. Biophys. J. 87, 40214035 (2004).

Soumpasis, D. M. (1983). Theoretical analysis of fluorescence photobleaching recovery experiments. Biophys. J. 41, 9597.

Sprague, B. L., and McNally, J. G. (2005). FRAP analysis of binding: Proper and fitting. Trends Cell Biol. 15, 8491.

Sprague, B. L., Muller, F., Pego, R. L., Bungay, P. M., Stavreva, D. A., and McNally, J. G. (2006). Analysis of binding at a single spatially localized cluster of binding sites by fluorescence recovery after photobleaching. Biophys. J. 91, 11691191.

Sprague, B. L., Pego, R. L., Stavreva, D. A., and McNally, J.G. (2004). Analysis of binding reactions by fluorescence recovery after photobleaching. Biophys. J. 86, 34733495.

Stavreva, D. A., Muller, W. G., Hager, G. L., Smith, C. L., and McNally, J. G. (2004). Rapid glucocorticoid receptor exchange at a promoter is coupled to transcription and regulated by chaperones and proteasomes. Mol. Cell. Biol. 24, 26822697.

Stone B, Schummer M, Paley PJ, Thompson L, Stewart J, Ford M, Crawford M, Urban N, O'Briant K, Nelson BH: Serologic analysis of ovarian tumor antigens reveals a bias toward antigens encoded on 17q. Int J Cancer 2003, 104:73-84.

Taube, R., Lin, X., Irwin, D., Fujinaga, K., and Peterlin, B.M. (2002). Interaction between P-TEFb and the C-terminal domain of RNA polymerase II activates transcriptional elongation from sites upstream or downstream of target genes. Mol. Cell. Biol. 22, 321331.

Thompson, R.E., D. R. Larson, W. W. Webb, Biophys. J. 82, 2775 (2002).

Tsukamoto T, Hashiguchi N, Janicki SM, Tumbar T, Belmont AS, Spector DL. 2000. Visualization of gene activity in living cells. Nat. Cell Biol. 2:87178

Turano, M., Napolitano, G., Dulac, C., Majello, B., Bensaude, O., and Lania, L. (2006). Increased HEXIM1 expression during erythroleukemia and neuroblastoma cell differentiation. J. Cell. Physiol. 206, 603 610.

Van Herreweghe E et al. Dynamic remodelling of human 7SK snRNP controls the nuclear level of active P-TEFb. EMBO J. 2007 Aug 8;26(15):3570-80. Epub 2007 Jul 5.

Van Oijen, A. M., J. Kohler, J. Schmidt, M. Muller, G. J. Brackenhoff, J. Opt. Soc. Am. A 16, 909 (1999).

Vrljic, M., S. Y. Nishimura, S. Brasselet, W. E. Moerner H. M. McConnell, (2002) Transla-

tional diffusion of individual class II MHC membrane proteins in cells. Biophys J 83: 26812692.

Zeitlinger J, Stark A, Kellis M, Hong JW, Nechaev S, Adelman K, Levine M, Young RA: RNA polymerase stalling at developmental control genes in the Drosophila melanogaster embryo. Nat Genet 2007, 39:1512-1516.

Zhou M, Huang K, Jung KJ, Cho WK, Klase Z, Kashanchi F, Pise-Masison CA, Brady JN: Bromodomain protein Brd4 regulates human immunodeficiency virus transcription through phosphorylation of CDK9 at threonine 29. J Virol 2009, 83:1036-1044.

Zipfel WR, Williams RM, Webb WW. 2003. Nonlinear magic: multiphoton microscopy in the biosciences. Nat. Biotechnol. 21:136977

Yang Z, He N, Zhou Q: Brd4 recruits P-TEFb to chromosomes at late mitosis to promote G1 gene expression and cell cycle progression. Mol Cell Biol 2008, 28:967-976.

Yang, Z., Q. Zhu, et al. (2001). "The 7SK small nuclear RNA inhibits the CDK9/cyclin T1 kinase to control transcription." Nature 414(6861): 317-22.

Yao J, Munson KM, Webb WW, Lis JT. 2006. Dynamics of heat shock factor association with native gene loci in living cells. Nature 442:105053

Yildiz et al., Science 300, 2061 (2003); published online 5 June 2003 (10.1126/science.1084398).

Yik, J.H., Chen, R., Nishimura, R., Jennings, J.L., Link, A.J., and Zhou, Q. (2003). Inhibition of P-TEFb (CDK9/Cyclin T) kinase and RNA polymerase II transcription by the coordinated actions of HEXIM1 and 7SK snRNA. Mol. Cell 12, 971982.

Yik JH, Chen R, Pezda AC, Zhou Q: Compensatory contributions of HEXIM1 and HEXIM2 in maintaining the balance of active and inactive positive transcription elongation factor b complexes for control of transcription. J Biol Chem 2005, 280:16368-16376.

Yu J, Xiao J, Ren X, Lao K, Xie XS. 2006. Probing gene expression in live cells, one protein molecule at a time. Science 311:16003

Yuste SB, LindenbergK(2002) Subdiffusion-limited reactions.ChemPhys 284:169180.

Wachsmuth, M., Waldeck, W. Langowski, J. Anomalous diffusion of fluorescent probes inside living cell nuclei investigated by spatially-resolved fluorescence correlation spectroscopy. J. Mol. Biol. 298, 677689 (2000).

Waharte, F., Spriet, C. Heliot, L. Setup and characterization of a multiphoton FLIM instrument for protein-protein interactions measurements in live cells. cytometry (2006).

Wang, Y. M., Austin, R. H. Cox, E. C. Phys. Rev. Lett. 97, 048302 (2006).

Wang Y, Dow EC, Liang YY, Ramakrishnan R, Liu H, Sung TL, Lin X, Rice AP: Phosphatase PPM1A regulates phosphorylation of Thr-186 in the Cdk9 T-loop. J Biol Chem 2008, 283:33578-

33584.

Wen, Y. Shatkin, A. J. Transcription elongation factor hSPT5 stimulates mRNA capping. Genes Dev. 13, 17741779 (1999).

Willig, K.I., S. O. Rizzoli, V. Westphal, R. Jahn, S. W. Hell, Nature 440, 935 (2006).

Wimmer J, Fujinaga K, Taube R, Cujec TP, Zhu Y, Peng J, Price DH, Peterlin BM: Interactions between Tat and TAR and human immunodeficiency virus replication are facilitated by human cyclin T1 but not cyclins T2a or T2b. Virology 1999, 255:182-189.

Wittmann BM, Fujinaga K, Deng H, Ogba N, Montano MM: The breast cell growth inhibitor, estrogen down regulated gene 1, modulates a novel functional interaction between estrogen receptor alpha and transcriptional elongation factor cyclin T1. Oncogene 2005, 24:5576-5588.

Wittmann BM, Wang N, Montano MM: Identification of a novel inhibitor of breast cell growth that is down-regulated by estrogens and decreased in breast tumors. Cancer Res 2003, 63:5151-5158.

Part IX

Appendix

24 FLIP Imaging, Normalization and Background

The correction of bleach due to imaging in FLIP was conducted using a control cell. However, it is found that differences in the bleaching behaviour stem from different intensities of the nuclei bleached and control. This is why the normalization of FLIP is corrected additionally by fitting the first 100s of the FLIP without bleach to an exponential, and using the value to correct for the rest of the curve.
High noise levels likewise pose problems in FLIP results, since by bleaching the signal level of the bleached nucleus is overcome by the signal in the background and produce virtual stationary fractions of fluorophores at low transfection levels due to normalization artifacts. This is why cell line 10p rather than 19n was used in the experiments - it provided us with SNR ratio of $\sim$3, which enabled total depletion of the fluorescence without crashing extensively into the background signal.

24.1 Method of Accumulation Factor Measurement

The background is taken as the averaged intensity on the distance of 1500 - 3000nm from the calculated center of maximum accumulation. The signal is taken at distance 1-1000nm from the center. The maximum accumulation center is estimated from the LacI -CFP signal on the gene array.

25 Controls

CycT1-GFP with the fluorescent protein at the N-terminus was tested in FLIP experiments and gave unchanged results. An attempt was made to conduct FLIP on the Cdk9-GFP construct. This however, could not be analyzed efficiently due to fluorescence in the cytoplasm, which rendered it neccessary to include factors such as diffusion/trasport across the nuclear membrane; and hence, the results were incomparable.
With regards to other drugs/methods that inhibit transcripiton, ActD was tested, but being a

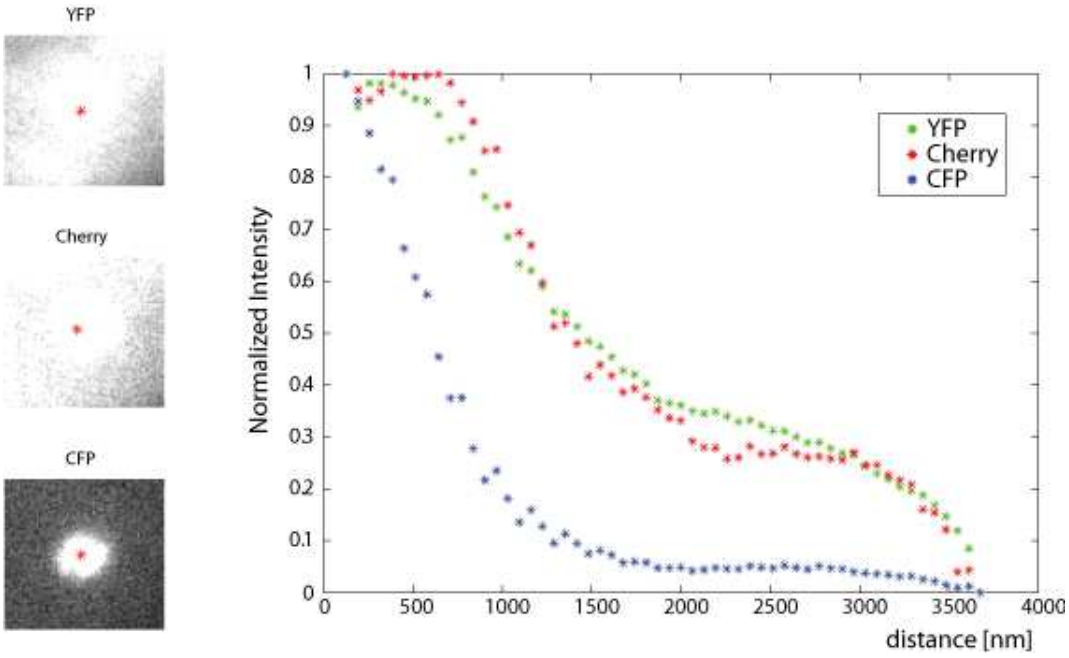

Figure 61: Method of accumulation factor measurement at the active gene array

strong intercalator, caused a visible change in the structure of the nucleus.
Tests of the system with flavopiridol surprisingly did not produce any effect, although the drug is known to break down the large complex with high efficiency. An explanation for this stems from the fact that flavopiridol, being a much more efficient and less specific inhibitor of transcription, causes RNA PolII to increase its mobility which was also found by FLIP experiments.

25.1 Overexpression Cell lines without DRB

25.2 Truncation CycT1 FLIP Experiments with out DRB

26 Error Estimations

To take into account cell variability and other factors contributing to the error within the FLIP curves, the bootstrap sampling method was utilized. The bootstrap is a resampling method for statistical inference used to estimate confidence intervals by taking each of the data points and randomly redistributing them in combination with others. In this way, all possibilities are

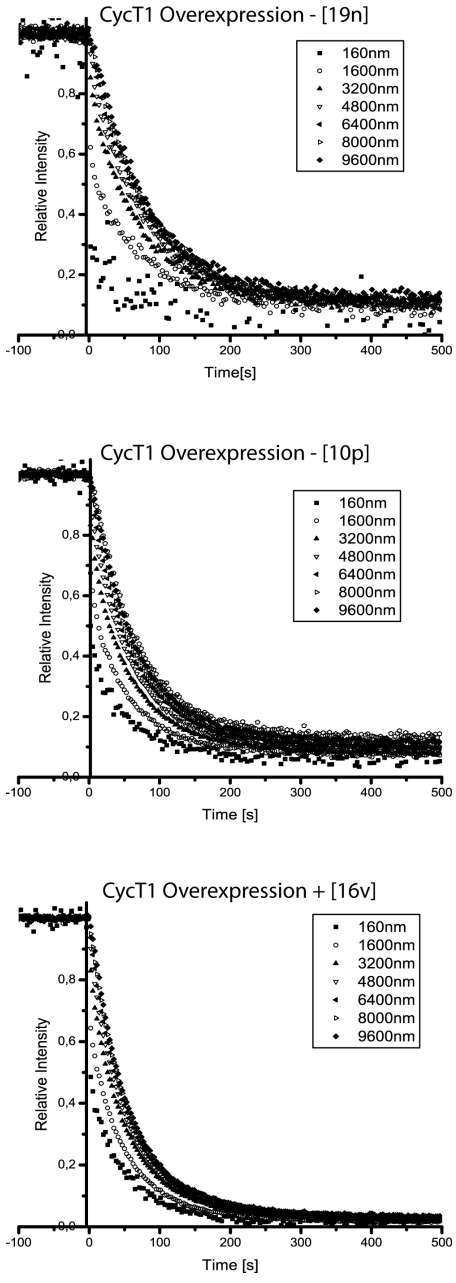

Figure 62: FLIP experiments conducted on cell lines with different expression levels of CycT1-GFP; untreated

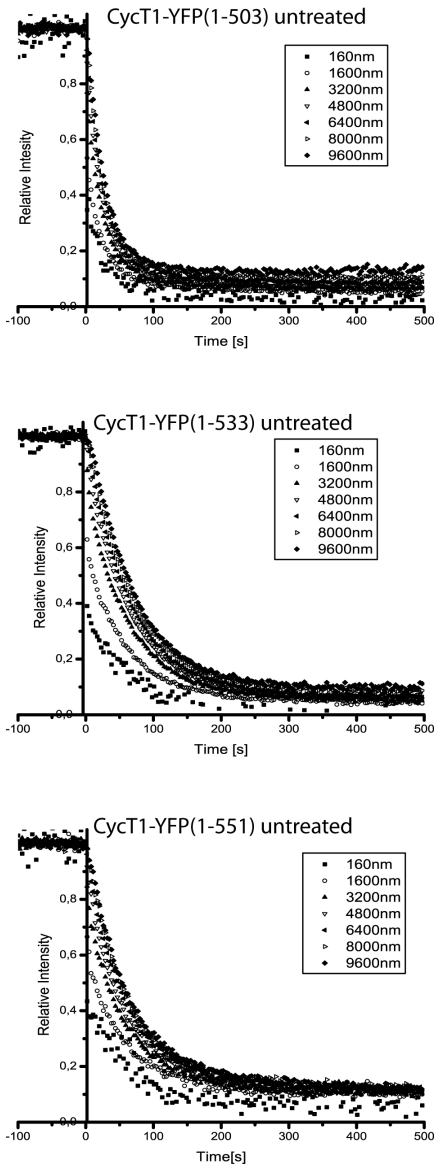

Figure 63: FLIP experiments conducted on transiently transfected cells with truncations of CycT1-YFP; untreated

probed and the mean value is taken as the one within the confidence interval. Herewith they were estimated to 95% and plotted on all FLIP curves. The bootstrap distribution $\hat{F}_b(x)$ is used to estimate bias, estimate a **standard error** (SE), or construct a confidence interval for the statistic of interest. The bootstrap estimates of bias B_b, and SE, s_B are the emperical estimates calculated from m bootstrap values:

$$B_b = \Sigma_{i=1}^{m}(\theta_i^B \hat{-} \hat{\theta})m$$

$$s_b = [\frac{\Sigma_{i=1}^{m}(\hat{\theta^B}_i - = \hat{\theta^B})^2}{m-1}]^{1/2}$$

[Philip M.Dixon, 'Bootstrap resampling']

FRAP curves were plotted with error bars from simple standard deviation of the total of ten curves.

27 Artefacts

The use of DMSO, as a solvent for DRB led to a mild increase in radial dispersion in the data when used at concentrations higher than 1000x. The delivery of DRB to cells herewith was not trivial since DMSO is also known to stick to plastic - effort was made to mix DRB evenly to obtain a homogeneous and direct immersion in the drug.